SLAC-R-640

A New Search for Elementary Particles with Fractional Electric Charge Using an Improved Millikan Technique

Nancy Marie Mar

Stanford Linear Accelerator Center, Stanford University, Stanford, CA 94309

Work supported by Department of Energy contract DE–AC03–76SF00515.

A NEW SEARCH FOR ELEMENTARY PARTICLES WITH FRACTIONAL ELECTRIC CHARGE USING AN IMPROVED MILLIKAN TECHNIQUE

A DISSERTATION
SUBMITTED TO THE DEPARTMENT OF PHYSICS
AND THE COMMITTEE ON GRADUATE STUDIES
OF STANFORD UNIVERSITY
IN PARTIAL FULFILLMENT OF THE REQUIREMENTS
FOR THE DEGREE OF
DOCTOR OF PHILOSOPHY

By
Nancy Marie Mar
April 1996

Abstract

We have devised and demonstrated the successful operation of a low cost, high mass throughput technique capable of performing bulk matter searches for fractionally charged particles based on an improved Millikan liquid drop method. The method uses a stroboscopic lamp and a CCD video camera to image the trajectories of silicone oil drops falling through air in the presence of a vertical, alternating electric field. The images of the trajectories are computer processed in real time, the electric charge on a drop being measured with an rms error of 0.025 of an electron charge. This error is dominated by Brownian motion. In the first use of this method, we have looked at 5,974,941 drops and found no evidence for fractional charges in 1.07 mg of oil. With 95% confidence, the concentration of isolated quarks with $\pm 1/3\,e$ or $\pm 2/3\,e$ in silicone oil is less than one per 2.14×10^{20} nucleons.

Acknowledgments

This experiment was much more complicated than anyone had anticipated and its success is due to the efforts of a great many people. I owe them all my gratitude and I would like to show my appreciation by naming them here.

I owe a great debt of gratitude, of course, to my adviser Martin Perl, whose wisdom and insights into physics contributed greatly to the understanding and analysis of the data and to the theory of the experiment. It was both a pleasure and a privilege to learn from him. He is the best adviser a student could have. He encouraged me with his words, his trust and his belief that I could learn. He forgave me my mistakes and made me learn from them. He has taught me to appreciate physics and to see its true beauty. My decision to study under Martin was the best one I made regarding my academic path.

I would also especially like to thank Eric Lee, our invaluable staff engineer, who provided a majority of the diagrams in this thesis and who had the patience to teach me the hands-on skills necessary to make me a contributing member of the group. His engineering prowess never ceases to amaze me.

The work Klaus Lackner has put into this project is also greatly appreciated. I thank him for all his input and guidance over the error analysis of the data. His suggestions for the thesis and the corresponding published paper were very welcome as well.

Thanks also goes to Helen Quinn who read the thesis in its earlier versions and made helpful suggestions on how to improve its contents. I am grateful for that.

I thank George Fleming for writing the data acquisition program. This experiment would have taken much longer without his excellent programming skills.

I also thank all our other collaborators: Brendan Casey, Edward Garwin, Charles Hendricks, and Gordon Shaw. Our group meetings were always full of information.

This experiment would not have existed at all, however, if it were not for the great technical support staff at SLAC. I would like to thank Ron Baggs, Bob Leonard, and Tom Nakashima for helping us build the apparatus and put together the electronic components specific to our experiment. I would also like to thank Jaime Davis, Sal Orlando, and Howard Rogers of the SLAC machine shop, who had the patience to teach me how to use the band saw, mill, lathe, and drill press. Finally, thanks goes to Jim Wahl, Terry Anderson and Sylvia MacBride of the publications department for all their work in getting my diagrams to me.

My years at Stanford would have been considerably less enjoyable were it not for the friendships I forged over the years. Thus, there are many friends I would like to thank, beginning with Judy Meo and Rose Forbes. Their very presence at SLAC would lighten a dark day. I enjoyed their company and appreciated all our little talks. I thank them for always listening to my problems and offering advice. I am grateful also for the friendship of Marcia Keating from the physics department for these same reasons.

Although they have all now graduated with their own doctorates, the following people were one time fellow graduate students who gave me encouragement, moral support and help when I needed them. I would like to thank these friends: Paolo Carini, Karl Ecklund, Robert Holtzapple, Tom Junk and Homer Neal.

I would also like to thank my family. I thank my parents and grandparents for believing in me and supporting me throughout my life. It is my sincerest wish that my mother had lived to see me get my doctorate, but I know that she is proud of me and smiling broadly in heaven. (May you rest in peace. I love you more than I can say.) I also thank my two sisters and brother. Like my parents, they believed in me and encouraged me. Thanks especially to Tom for always rushing to my side when things were bad. This is just one of the benefits of having a younger brother attend the same university. His companionship alone meant a lot to me. Indeed, the love of my entire family fills my life and makes me whole.

I thank my fiancé, Andrew, whose very existence and presence makes receiving

a doctoral degree the second most important thing in my life. His daily support, encouragement and help makes me constantly realize how blessed I am to have met him. I am grateful that we both decided to pursue our physics doctorates at Stanford.

Lastly and above all, I thank God. With Him, anything is possible. I firmly believe that He has always taken care of me and watched out for me. I thank God everyday for everything and everyone in my life.

I dedicate this thesis to God and my beloved family. Thank you all for everything.

Contents

List of Tables

List of Figures

Chapter 1

Introduction

We have conducted a search for elementary particles with fractional electric charge in silicone oil using an improved Millikan liquid drop method in which we automatically measure the charge on individual drops of about 7 μm in diameter. We have searched through 1.07 mg of oil and found no drops that contained a fractionally charged particle with $\pm\frac{1}{3}$ or $\pm\frac{2}{3}$ of an electron charge. Therefore, with 95% confidence, the concentration of isolated quarks with these charges in silicone oil is less than one per 2.14×10^{20} nucleons.

There has been much speculation but no confirmed evidence for the existence of isolated elementary particles with fractional electric charge. The most commonly proposed candidate for such a particle is an isolated quark that would have charge $\pm\frac{1}{3}\,e$ or $\pm\frac{2}{3}\,e$, where e is the magnitude of the electric charge of the electron. In this experiment, drops are produced with a nominal charge of $0\,e$, $\pm 1\,e$, $\pm 2\,e$, ... In the early part of the experiment, drops were produced with charges as large as $\pm 10\,e$, but in the remainder of the experiment, the drops were generally either neutral or had charges of $\pm 1\,e$, $\pm 2\,e$ or $\pm 3\,e$. The sensitivity of the experiment for an anomalous charge decreases when Q, the net electric charge on the drop, is close to Ne, N being an integer. Therefore, our conclusions are limited to the charge regions

$$0.2\,e \text{ to } 0.8\,e,\ 1.2\,e \text{ to } 1.8\,e,\ 2.2\,e \text{ to } 2.8\,e\ldots,$$

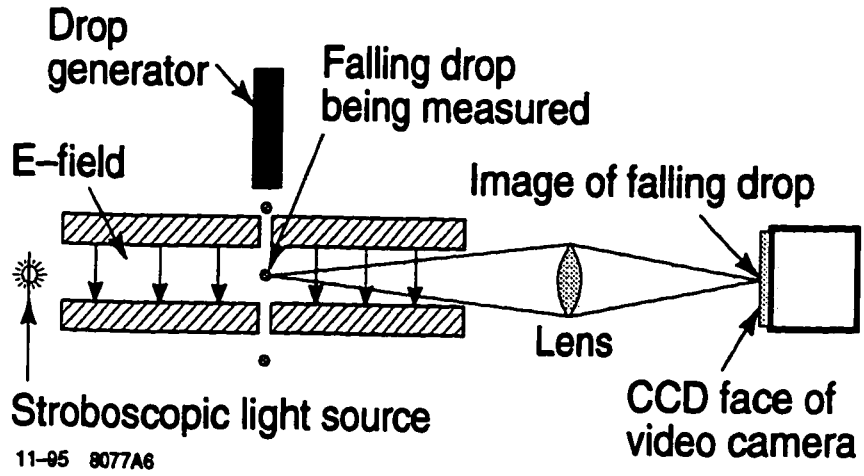

Figure 1.1: Schematic of the fractional charge search apparatus. Drawing is not to scale.

$$-0.2e \text{ to } -0.8e,\ -1.2e \text{ to } -1.8e,\ -2.2e \text{ to } -2.8e \ldots. \tag{1.1}$$

Our method is built upon the technique developed in fractional charge searches at San Francisco State University [1]–[4] and goes back to the original work of Millikan [5]–[7]. As shown schematically in Fig. 1.1, the mechanical part of the apparatus consists of two flat, circular, stainless steel plates separated by a distance small compared with the plate diameter, the ratio being on the order of 1:16. A device called a dropper produces on demand a spherical drop of silicone oil whose diameter is between 7 and 8 μm. Early in the experiment, we produced drops that were 7.6 μm in diameter. But 94% of the drops studied had a diameter of 7.1 μm. The data presented in the thesis is for both sizes, but for simplicity, the remainder of the discussion refers to the 7.1 μm drops.

The drops fall vertically through a small hole in the upper plate, through the space between the plates and then leave the apparatus through a small hole in the lower plate. The entire apparatus is in dry air at atmospheric pressure and room temperature. The frictional resistance of the air brings a 7.1 μm drop to terminal velocity within a few thousandths of a millimeter. The terminal velocity for a neutral

drop of this size is 1.35 mm/s. The frequency of drop production was set at 0.6 Hz. A 7.1 μm diameter drop of silicone oil has a mass of 1.71×10^{-4} μg and contains 1.03×10^{14} nucleons.

Between the plates there is a uniform, vertical electric field. The field strength changes in time with a square wave oscillation amplitude of 1.4×10^{6} V/m. If the drop has a non-zero charge, the terminal velocity differs according to whether the electric field reinforces or opposes the gravitational force. By the means described next, we measure the terminal velocity in both situations and use the theory described in Chapter 3 to calculate the charge on the drop and the mass of the drop.

Continuing to refer to Fig. 1.1, a stroboscopic lamp illuminates the drop twice for each electric-field orientation and a lens images the shadow of the drop onto a charge coupled device (CCD) video camera. Thus, the position of the shadow of the drop on the CCD surface measures the position of the drop in real space when the stroboscopic lamp flashes. A desktop computer uses the output of the CCD camera to calculate the drop's terminal velocities, diameter and charge. The computer also controls the experiment and stores the measurements.

The plan of the thesis is as follows: A historical overview of other quark searches is presented in Chapter 2. The theory of the experiment outlined above is presented in Chapter 3 [8]. The construction of the apparatus is described in Chapter 4. Collection, selection and presentation of data and errors are discussed in Chapters 5 and 6. Our results are summarized and compared with other measurements in Chapter 7. Proposed improvements and extensions of the experimental technique as laid out in [9] are discussed in Chapter 8.

Chapter 2

Historical Overview

Within the last thirty years, there have been many searches for free quarks. Searches have been conducted using particle accelerators and cosmic rays and they have been conducted in stable bulk matter using special techniques. These classes of searches will be discussed in detail and examples will be given because the results of these experiments are not directly comparable to our experiment or even to each other. Indeed, many of these searches require such specialized conditions for quark production and quark detection that they are of limited value. Furthermore, we believe that searches for fractionally charged particles in bulk matter of the type described in this thesis offers the best opportunity for finding free quarks, assuming that they exist as remnants from the early formation of the Universe.

In this thesis, remarks concerning the behavior of quarks are limited to a few paragraphs about the conventional field theory of quarks, namely Quantum Chromodynamics (QCD). This is done for two reasons. The main reason is that QCD is a description of the interactions amongst quarks and gluons and a generally assumed consequence of these interactions is confinement. Thus, conventional QCD has nothing to teach us about the possibility of finding free quarks or making them. The second reason is that we do not want this chapter to dominate the rest of the thesis in length.

The existence of elementary particles with fractional electric charge was first proposed by Gell-Mann [10] and Zweig [11] independently in 1964. These proposed particles were expected to follow the algebra of the group flavor SU(3) [12]. Since then many searches have been conducted to look for fractionally charged particles that exist in isolation. With the exception of LaRue's [13]–[17] experiment with niobium and McCusker's [18] search in cosmic rays, all searches conducted so far have yielded null results. The early negative findings led to the idea of quark confinement and the null results subsequent to the propounding of the confinement hypothesis have served to further support the idea.

Quark confinement states that particles such as quarks and gluons that have an associated quantum number called "color" cannot exist as free particles. According to this postulate, these particles can exist only in bound states that are color singlets [19]. Therefore, the particle states we observe in nature are color singlets.

A standard view of QCD is that the color force between quarks stays constant as their separation distance r increases, that is, the potential energy of the system is proportional to r. When a quark and antiquark separate, their color interaction does not weaken. Through the interaction of gluons with one another, the color field lines of force are squeezed into a tube-like region, as opposed to the Coulombic force where the field lines are allowed to spread out because there is no self-coupling of the photons to contain them. It is this lack of self-coupling amongst photons that enable two electrons, for example, to be isolated. However, as r increases between two quarks, the potential energy of the system increases until there is sufficient energy to create another quark-antiquark pair [19]. Theoretically, then, in conventional QCD, quarks and gluons can never be isolated.

Before turning to the history of searches for free quarks, a few comments will be made on theoretical speculations as to how QCD might be modified to allow the existence of free quarks. These speculations have an interesting history. Many, but not all of them, were published in a few year period around 1980 when the Fairbank group at Stanford University was making its strongest claims. When these claims were not confirmed by the middle of the 1980s, speculations on free quarks diminished. Many of these speculations involved placing conventional SU(3) into a larger group [20,

Strong Force	Weak Force	Comments
Y	Y	"Conventional" free quark.
N	Y	Fractionally charged lepton whose mass must be greater than $45\,\mathrm{GeV/c^2}$.
Y	N	See caption.
N	N	See caption.

Table 2.1: The mass constraint for fractionally charged leptons arises from the fact that accelerators studying Z^0 decays would have found these particles by now if their mass were less than $45\,\mathrm{GeV/c^2}$. Note that fractionally charged leptons that have the same weak interactions as the muon have a cross section of $\sigma(e^+e^- \longrightarrow Z^0 \longrightarrow \mu^+\mu^-)$ $\sim 1.4\,\mathrm{nb}$ [23]. If fractionally charged particles do not experience the weak force, the ratio $R_Q = \sigma(e^+e^- \longrightarrow l^{+Q}l^{-Q})/\sigma(e^+e^- \longrightarrow Z^0 \longrightarrow \mu^+\mu^-)$ defined by accelerator experiments, where l is a particle with charge $\pm 1/3\,e$ or $\pm 2/3\,e$, is $0.71 \times 10^{-2}\,Q^2$. Therefore, for $Q = \pm 1/3\,e$, this ratio is 0.8×10^{-3} and for $Q = \pm 2/3\,e$, it is 3.2×10^{-3}. Such values of R_Q are just below the limit of detection for Z^0 experiments done at CERN using LEP.

21]. Within the larger group, isolated fractionally charged particles, either quarks or composites of quarks and nucleons, would be allowed. A very illuminating paper is that of De Rújula [22]. The paper contains an interesting discussion of the relation amongst the possible existence of free fractionally charged particles, the range of the strong force and the effects of non-zero mass gluons.

Of course, there are other possibilities for the existence of isolated fractionally charged particles. The most general way to view this is to consider how a fractionally charged particle might partake of the known forces. Fractionally charged particles, by definition, must partake of the electromagnetic forces. Ignoring gravity because it is negligible with respect to the other forces, we make a table of the other possible forces that these particles might experience and make some general observations concerning these particles. The caption of Table 2.1 offers a more detailed discussion. We note,

however, that if fractionally charged particles were extremely massive (masses greater than hundreds of GeV/c^2), then they would not have been found anywhere.

Any theory of quark behavior that allows quarks to be isolated must include conventional QCD. To give an analogy, if there were a larger theory of quarks that allows them to be free, its relation to QCD is the same as that of special relativity to Newtonian mechanics.

2.1 Accelerator Searches

Searches for free quarks using accelerators involve two intrinsic uncertainties. First, the mass of the free quark is unknown. Therefore, we do not know how much energy is required to produce it. Since hadrons are bound by the strong force, the apparent mass of bound quarks are not a guide to the mass of the free quark. Second, we do not how know much energy is required in a collision to enable the separation of two bound quarks without first producing the expected standard products, none of which is a free quark. These remarks apply to all searches using e^+e^-, hadron-hadron and deep inelastic scattering techniques. An additional uncertainty in deep inelastic searches, however, is that we do not have a model of how a bound quark may be transformed to a free quark.

In the following discussion of accelerator searches, a few examples are given in order to illustrate the restrictions of the method.

2.1.1 Electron-Positron Annihilations

Quarks may be produced either exclusively or inclusively using e^+e^- colliders. The exclusive production of quark-antiquark pairs from the annihilation of colliding positrons and electrons ($e^+e^- \longrightarrow q\bar{q}$) leads to collinear two-prong events. This is a strong requirement and has the advantage of greatly simplifying the search for exclusively produced free quarks. The inclusive production of quarks, however, does not have such a simple experimental signature. This latter method produces quarks together with ordinary particles inside a jet of particles ($e^+e^- \longrightarrow q\bar{q}X$). No evidence for free

quarks has been found in e^+e^- annihilation experiments. In the following sections, a few typical searches are described in detail.

The JADE Collaboration Experiment

In 1980, the JADE collaboration at PETRA [24, 25] conducted both exclusive and inclusive searches for new particles with charge $Q = 2/3\,e, 1\,e, 4/3\,e,$ and $5/3\,e$ in the center-of-mass energy range of 27 to 35 GeV. No such particles were found. The limits found were based on an assumed mass and required an estimate of the efficiency for observing free quarks, which was obtained by assuming that the production of quarks of energy E is given by

$$E\frac{d^3\sigma}{dp^3} \propto e^{-3.5E}.$$

This was the distribution observed by the experimenters for pions, kaons, and protons in e^+e^- interactions.

Particles were identified by a simultaneous measurement of the mean energy loss $\left\langle \frac{dE}{dx} \right\rangle$ and the apparent momentum p/Q. Because $\left\langle \frac{dE}{dx} \right\rangle$ scales as Q^2, free particles with $|Q| = 1/3\,e$ have an expected ionization that is 1/9 that of free particles that have $|Q| = 1\,e$. Similarly, charge $|Q| = 2/3\,e$ particles have an expected ionization that is 4/9 that of $|Q| = 1\,e$ particles. Also, because the curvature of a particle in a magnetic field depends on Q, the apparent momentum will be larger than the true momentum by factors of 3 and 1.5 for $Q = 1/3\,e$ and $Q = 2/3\,e$ particles respectively. Therefore, these quantities are the natural choice to use as a means of particle identification.

In the JADE collaboration, these two quantities were obtained using the JADE-jet chamber, a cylindrical drift chamber surrounding the interaction point. The chamber was filled with an argon/methane/isobutane gas mixture pressurized to 4 atm and was operated in an axial magnetic field of strength 4.5 kG. A total of 48 points were measured along the track from the interaction point within a polar angle range of 34° to 146°. At each point, spatial coordinates (r, ϕ, z) and energy loss ΔE were determined. The r and ϕ components were given by the wire position and the drift time measurement, whereas z and ΔE were obtained from the signal amplitudes measured at the two ends of the wire.

In the search for exclusively produced free quarks, the trigger for a candidate event consisted of a twofold coincidence in the scintillation counter hodoscope surrounding the track detector. The two counters hit were required to be azimuthally separated by $180° \pm 30°$. Furthermore, the two tracks in the jet chamber had to be recognized by a hard-wired track-finding logic. For $Q = 2/3\,e$ particles, this trigger was 100% efficient. (The efficiency for $Q = 1/3\,e$ particles was too low to be considered for this analysis.) Off-line cuts required that the two tracks originating from the same interaction point be collinear to within 10° in space.

The corresponding search for inclusively produced quarks had different selection criteria [24]. Two types of triggers were used for multihadron events: the "charged particle trigger" and the "shower energy trigger". Over 95% of the multihadron events actually satisfied both triggers. The charged particle trigger required at least two of 42 time-of-flight counters to have fired, a total shower energy (sum of the barrel and end caps) greater than 1 GeV and at least one track recognized by the hard-wired track-finding logic based on the hit pattern of the track detector. The shower energy trigger, however, was based exclusively on the energy measurement of the lead glass counters and required a total energy greater than 4 GeV.

Off-line cuts were then made using the following criteria:

1. At least 2 tracks had to have passed through a fiducial volume around the interaction point of radius 3 cm and length ±40 cm. This volume was chosen to be considerably larger than the interaction region folded with the resolution.

2. Barrel shower energy had be greater than 2 GeV at a beam center-of-mass energy of 22 GeV and greater than 3 GeV at higher beam energies or both end cap shower energies had to be greater than 0.4 GeV.

Events surviving the off-line cuts were further inspected by hand for the correctness of pattern recognition and the existence of a vertex. Background arising from cosmic rays or showering e^+e^- or $e^+e^-\gamma$ events were subtracted. To further reduce the background, only events with at least four tracks were selected. This was done to minimize the $e^+e^- \longrightarrow \tau^+\tau^-$ background contribution, which was reduced even more by rejecting four-track events wherein three of the charged tracks were in opposite

direction to the fourth.

As candidates for tracks with an unusual energy loss, only those tracks with an ionization different from that of π, K, p, and e by more than 3.0 standard deviations were considered. Furthermore, tracks that had greater than minimum ionization were required to have had an energy loss of at least 17 keV/cm to eliminate background due to overlapping tracks.

Their limits were quoted in terms of the dimuon cross section $\sigma(e^+e^- \longrightarrow \mu^+\mu^-)$

$$R_Q = \frac{\sigma(e^+e^- \longrightarrow q\bar{q})}{\sigma(e^+e^- \longrightarrow \mu^+\mu^-)}.$$

For both the exclusive and inclusive quark production, this ratio was less than $\sim 10^{-2}$.

Searches performed by the JADE collaboration after 1980 [26], however, set other limits on quark production. These later experiments searched for the exclusive and inclusive production of fractionally charged particles of charge $Q = 1/3\,e$ and $Q = 2/3\,e$. The results for R_Q ranged from $10^{-2} \sim 10^{-1}$ for the exclusive production of quarks and was $\sim 10^{-3}$ for the inclusive production.

With R_Q ranging only from $10^{-3} - 10^{-1}$, this search is, unfortunately, not very significant. If quark production were simply a point particle process, R_Q would already range from $1/9 - 4/9$, but we know free quark production must be a very complicated process particularly given the uncertainties described in the beginning of Sec. 2.1. Therefore, we would expect very small R_Q values. Furthermore, we do not know the interaction cross section of quarks with matter. If this cross section were larger than the hadron-hadron cross section, then even smaller observed R_Qs would be obtained because the free quark might interact with the apparatus and not be detected.

The Mark II Experiment

In 1981, using MARK II at SPEAR [27], another inclusive free quark search was conducted. The center-of-mass energy in this case ranged from $3.9 - 7.4$ GeV. The trigger for this experiment required that one track register in the drift chambers and the appropriate one of 48 time-of-flight scintillators and a second track register in the inner layers of the drift chamber. For highly relativistic $Q = 2/3\,e$ particles,

the drift chambers and time-of-flight scintillators were fully efficient. Reconstructed tracks were required to be aimed toward the time-of-flight system while being 2 cm away from the counter edge and 5 cm away from a counter end. Also, the counter had to be intersected by only 1 reconstructed track. The z-position along the counter was determined by the time difference of the signals from the two photomultiplier tubes mounted one at each end of the counter and had to agree to ± 25 cm with the z-position acquired from the particle trajectory, which had been required to pass through all 16 layers of the drift chamber.

The pulse height measurements of the scintillators were used to obtain information on the ionization loss of each track. Tracks that showed a pulse height between 20% and 65% of the value expected for minimum ionizing $|Q| = 1\,e$ particles and an estimated particle mass greater than $0.85\,\mathrm{GeV/c^2}$ were retained for further studies. The number of tracks within $\pm 2\sigma$, where σ is the estimated, mass dependent mass resolution of typical quark mass regions were determined. For $Q = -2/3\,e$ particles with masses ranging from $1.0 - 3.0\,\mathrm{GeV/c^2}$, R_Q varied from 2.3×10^{-4} to 8.0×10^{-4}. These calculations were made at the 90% confidence level.

The MARK II group also conducted a search for exclusively produced free quarks. Candidate events were those wherein the two-track colinearity was better than 10° and the apparent momentum was greater than half the beam energy. The same pulse height cuts used for the inclusive search were imposed here. For $Q = 2/3\,e$ particles with a mass range of $1.0 - 2.8\,\mathrm{GeV/c^2}$, R_Q varied from 0.8×10^{-4} to 5.2×10^{-4}. Again, this was at a 90% confidence level.

Although MARK II has searched to significantly smaller R_Q values than the previously discussed experiment, the range of quark masses is quite limited. Once again, there is the uncertainty that a large quark-hadron cross section would substantially lower the observed R_Q.

The Free Quark Search (FQS) Experiment

A series of experiments designed to search for free quarks using the 29 GeV PEP ring at SLAC was conducted in the period from 1982 to 1984 [28]–[32]. Their method

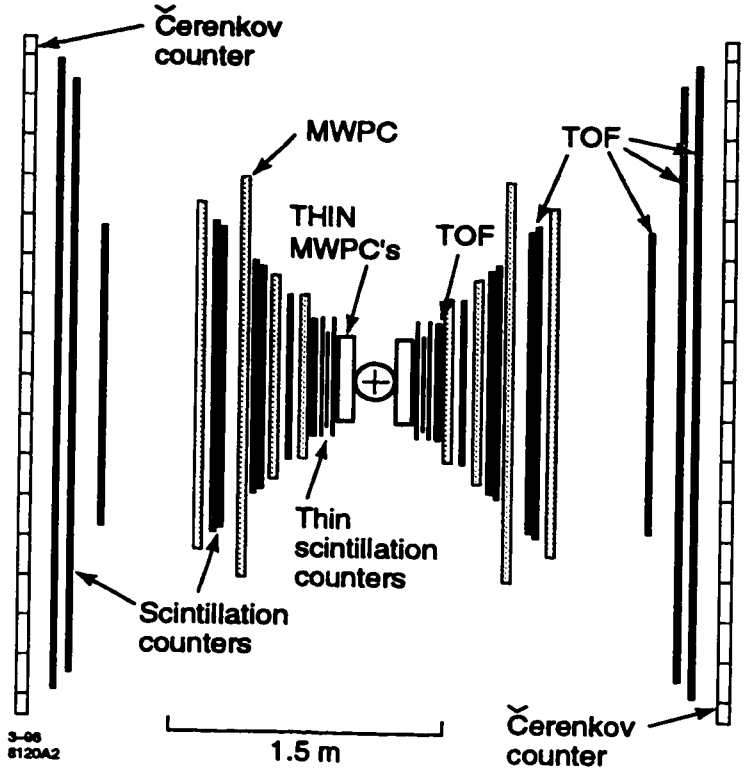

Figure 2.1: Schematic diagram of the detector used by the Free Quark Search group. The two identical arms each consisted of 9 multiwire proportional chambers, 12 scintillation counter hodoscopes and 1 lucite Čerenkov counter. The five scintillation layers labeled TOF at the right were equipped for time-of-flight measurements.

of particle identification differed slightly from the previous two experiments in that the charge of the detected particles were determined through $\langle dE/dx \rangle$ and velocity ($\beta = v/c$). As discussed above, JADE and MARK II used $\langle dE/dx \rangle$ and apparent momentum, which estimates charge based on an assumed mass.

The detector consisted of two symmetric arms orthogonal to the e^+e^- beams, each covering a face of a cube centered at the interaction region and subtending an angle of $4\pi/6$ (Fig. 2.1). Each arm was composed of nine multiwire proportional chambers (MWPC) used to define the trajectory of the particle ($\geq$ 97% efficient for $Q = 1/3\,e$ particles), twelve planes of of scintillation counter hodoscopes (the counters

were equipped with one photomultiplier tube at each end), and a single Čerenkov hodoscope. Five of the scintillation counter hodoscopes were equipped with time-of-flight electronics for measuring β. Another six planes (layers 9 through 17) consisted of ten counters arranged in roads projecting radially outward from the interaction region and was used as part of the trigger. The Čerenkov counter was used to verify the velocity measurement determined by the time-of-flight system.

In a search for exclusively produced quarks conducted in 1982 [28], the two tracks were required to be collinear within 8° in both the polar and azimuthal angles with respect to the the beam axis. Events were selected by requiring the track intercepts to be within 3σ of the interaction region, where σ was the resolution of the detector. The timing requirement was that the time on layer nine be within 10 ns of the beam crossing. Each track was then required to be associated with at least three time-of-flight measurements. A linear fit to the time versus path length of the particle was required to yield a χ^2 per degree of freedom less than 9. Cosmic ray background was elimininated by requiring the tracks to move outward from the interaction region.

Candidate events were required to have $Q < 0.8\,e$ in each arm. No such events were found. To extract an upper limit on quark production, the following factors were taken into consideration: trigger efficiency ($\sim$ 75% for lightly ionizing low mass quarks of $Q = 1/3\,e$, rising to $\sim$ 100% for masses around $8\,\mathrm{GeV/c^2}$), geometrical acceptance (taking into account the expected angular distribution of the produced quarks), radiative corrections, and a 5% loss of quark signal for particles with $Q = 2/3\,e$ because of the $Q < 0.8\,e$ requirement. The results were obtained at a 90% confidence level and are presented below

$$R_Q \leq 7.7 \times 10^{-3}, \quad m_Q \leq 13.8\,\mathrm{GeV/c^2}, \quad Q = \frac{2}{3}e,$$
$$R_Q \leq 9.7 \times 10^{-3}, \quad m_Q \leq 14.1\,\mathrm{GeV/c^2}, \quad Q = \frac{1}{3}e.$$

The upper limits on the mass range arose from the requirement that quarks had to have enough energy to penetrate to the outer part of the detector.

In the search for inclusively produced quarks conducted at PEP in 1982 [29], the apparatus was triggered when at least five of the six planes (layers 9 through 17)

were hit on at least one road in each arm and had pulse heights that were at least 5% of the expected value of $\langle dE/dx \rangle$ for a minimum ionizing particle of unit charge. Approximately 20% of the 1.5×10^6 triggers were due to beam-beam interactions while the remaining 80% were attributed to cosmic ray or single beam generated backgound. The multiprong beam-beam events were selected by the following criteria:

1. *Timing.* The average time to reach the innermost time-of-flight counters ($\sim$ 30 cm from the beam) was required to be within 7 ns of the beam crossing time. Also, to ensure that events progressed from the inside to the outside, the average arrival time in layers 18, 19 and 20 was required to follow that of the inner layers.

2. *3 or more good tracks.* Good tracks were defined as those that had at least 3 hits in the proportional chambers, had a linear fit with a χ^2 per degree of freedom less than 5.0 and that extrapolated back to a rectangular region centered around the interaction point. At least two of these three tracks were required to have $\langle dE/dx \rangle$ greater than 25% of the expected value for a minimum ionizing particle.

A charge calculation was then performed on tracks wherein at least 5 of the road counters had a signal above a threshold of 3% that of a minimum ionizing particle and two time-of-flight counters had valid hits. Using these criteria, they established a limit on R_Q on the order of $\sim 10^{-2}$.

At that point, however, none of the accelerator experiments had taken into account the interaction cross section of the quarks when they move through the length of the detector. Even if confinement were sometimes broken, free quarks may not have been detected in accelerator searches if the confining force causes the quarks to have interaction cross sections much larger than ordinary hadrons [22]. If that were the case, then these quarks would have interacted in the target, the beam pipe, or the surrounding apparatus before they even reached the detector. It was with this hypothesis in mind that the FQS group modified the detector to search for free quarks that had an interaction cross section with matter that was up to 100 times the geometric interaction cross section [30].

The detector was modified for this new search. A thinner beam pipe was used and

an additional detecting system composed of five thin multiwire proportional chambers whose thresholds were set at 2% of the expected energy loss for a minimum ionizing particle of unit charge and three 1.5 mm thick scintillators was placed in front of each spectrometer arm.

The trigger for the accepted events still required five hits in the six scintillation counter hodoscopes. With the modifications to the detector in place and for an exclusively produced quark, the five hits could only have been due to either the highly interacting quark itself or one of the secondaries produced by its interaction earlier in the spectrometer or in the beam pipe [26]. A total of 1.2×10^6 triggers were obtained.

Relativistic quarks were recognized by their energy loss in the five thin MWPCs. The value of $\langle dE/dx \rangle$ of the particle was taken to be the average of the four lowest pulse heights. Tracks were rejected if they satisfied any of the following criteria: had less than 4 measurements of pulse height, more than 1 overflow, an unlikely distribution of pulse height measurements, less than three pulse heights above 6% of the expected energy loss for a minimum ionizing particle of unit charge or were not well separated from neighboring hits.

Although there were 4600 events that had at least one track with an estimated $\langle dE/dx \rangle$ less than 60% of the expected pulse height, there were no two-prong events found in which both tracks had that energy loss. This established limits on the exclusive quark production of either charge $1/3\,e$ or $2/3\,e$. They were derived as functions of quark mass and assumed quark interaction cross section. At the 90% confidence level, their upper limits on R_Q ranged from 10^{-2} to 10^{-1}.

In the corresponding inclusive search, only $Q = 1/3\,e$ particles were studied. For this analysis, only one observable quark track with $\langle dE/dx \rangle$ less than 25% of the expected pulse height for a minimum ionizing particle was required. A further condition required that signals from at least 2 of 3 thin scintillator hodoscopes behind the MWPCs have pulse heights greater than 5% of that expected for a minimum ionizing particle. No fractional charge events were found. Again, at the 90% confidence level, their upper limits on R_Q ranged from 10^{-2} to 10^{-1}.

As noted above, this experiment seriously considered the problem of a large quark-hadron interaction cross section, but, unfortunately, they did not achieve small R_Q values.

The ALEPH Collaboration Experiment

More recent results have been reported from the LEP collider at CERN. Data taken during 1989 and 1990 were analyzed for unexpected mass and charge by measuring $\langle dE/dx \rangle$ of the charged tracks in the ALEPH Time Projection Chamber (TPC) [33]. The ALEPH detector consisted of an inner tracking chamber (ITC) comprised of eight concentric drift chamber layers close to the beam pipe that was used in both the track trigger and the track reconstruction. Surrounding the ITC was the TPC, a cylindrical, three-dimensional imaging drift chamber with 18 multiwire proportional chambers at each end. It had an axial electric field of magnitude 120 V/cm parallel or antiparallel to a magnetic field of strength 1.5 T. The electric field was of opposite direction in the two halves of the TPC, which was divided by a conducting membrane located at $z = 0$. Electrons arising from ionization drift to the end plates where they were detected by wire chambers with cathode planes that were segmented into concentric rows of pads. These cathode-pad rows provided up to 21 space points for charged particles. Charged particles within $|\cos\theta| < 0.96$ crossed all 8 layers of the ITC and at least 4 rows of the TPC. The TPC sense wires provided up to 330 measurements of $\langle dE/dx \rangle$ for each charged particle.

The ITC, TPC and the electromagnetic calorimeter (ECAL), a highly segmented sandwich of wires chambers and lead plates that covered a polar angle of $|\cos\theta| < 0.98$, were enclosed in a superconducting solenoid that provided an axial magnetic field of 1.5 T. The return yoke of the magnet was instrumented with one square centimeter streamer tubes to form the hadron calorimeter (HCAL) that covered an angular region given by $|\cos\theta| < 0.99$.

Events were selected when there was a charged trigger from the ITC and a particle penetrating the HCAL in the same azimuthal region as the ITC signal or an ECAL energy deposition greater than 0.2 GeV (1.3 GeV in 1989). The trigger efficiency for

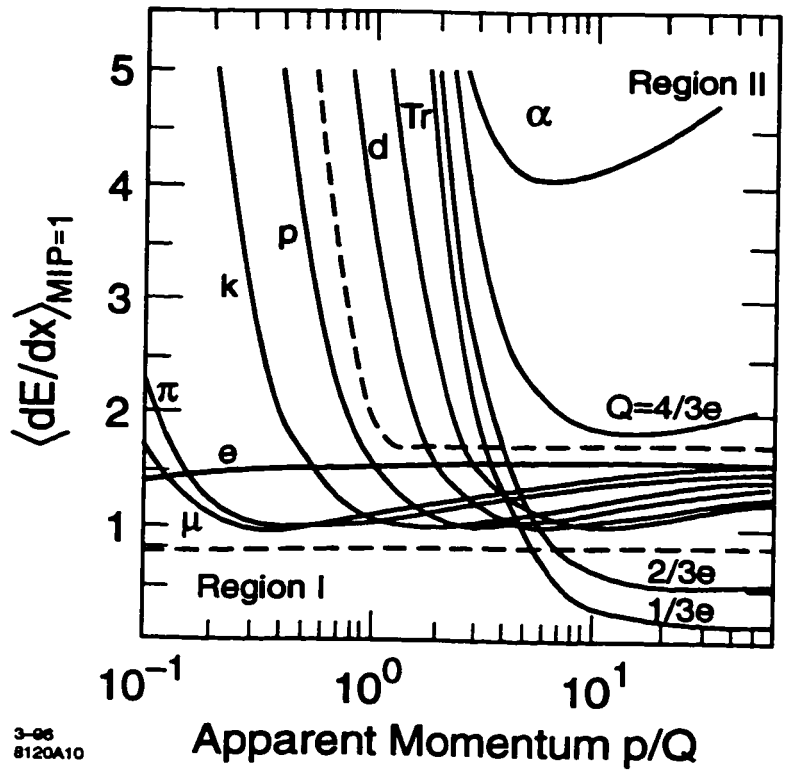

Figure 2.2: The expected ionization for different particle types. Those for fractional charges were for particles of mass $5\,\mathrm{GeV/c^2}$. An average resolution of the detector was assumed in determining the boundaries of the search regions.

an inclusive search was reported at 100% when the ionization of at least one track in the event gave an ITC trigger. For an exclusive search, the efficiency was assumed to be zero when the expected energy loss in the ITC was less than that of a minimum ionizing particle.

In Fig. 2.2, the expected curves for fractionally charged particles ($Q = \frac{1}{3}e$, $\frac{2}{3}e$, $\frac{4}{3}e$) of mass $5\,\mathrm{GeV/c^2}$ are shown as a function of apparent momentum, indicating the sensitive regions for the ALEPH analysis. The low ionization region I was bound from above by a line drawn 4σ below the mean ionization of the known $Q = 1\,e$ particles and from below by the detection efficiency of the detector. The high ionization region II was bound from below by a line 4σ above the mean ionization of the known $Q = 1\,e$

particles, from the left by the ionization curve of a mass $1.2\,\mathrm{GeV/c^2}$ and $Q = 1\,e$ particle and from above by the limits imposed by the dynamic range of the TPC electronics.

Tracks were considered candidates for region II if they had least 6 TPC and 4 ITC hits used for the helix fit. The χ^2 per degree of freedom for the helix fit was required to be less than 4. The $\langle dE/dx \rangle$ measurement was required to come from at least 150 wires, which gave at worst a 5.5% resolution. In order to eliminate δ rays and nuclear fragments arising from secondary interactions in the beam pipe and the walls of the tracking detectors, a cut forcing the minimum distance of the track helix to be less than 0.5 cm away from the main interaction vertex in a plane perpendicular to the beam and less than 5 cm away parallel to the beam was imposed.

In the low ionization region, less stringent cuts were imposed because the low ionization loss may have resulted in fewer and worse coordinate measurements and fewer $\langle dE/dx \rangle$ measurements in the tracking detectors. Therefore, only 4 TPC and as few as zero ITC hits were required. The χ^2 per degree of freedom in this case was required to be less than 9. The $\langle dE/dx \rangle$ was required to come from at least 80 wires. Lastly, the minimum distance of the track helix was required to be less than 2.0 cm away from the main interaction vertex in a plane perpendicular to the beam and less than 10 cm away parallel to the beam.

For either region, events were further rejected as beam gas events if

$$\frac{|E_+ - E_-|}{|E_+ + E_-|} > 0.95 \text{ and } E_{\mathrm{cal}} < 50\,\mathrm{GeV},$$

where E_+ (E_-) was the summed energy of charged tracks with $\cos\theta > 0$ ($\cos\theta < 0$) and E_{cal} was the total calorimetric energy of the event. Of 180,000 hadronic and leptonic events studied, only 9 candidates remained in region I and 35 in region II. A visual inspection of these candidates by the ALEPH collaboration confirmed that they had no accompanying signature that would distinguish them from normal hadronic or leptonic Z^0 events other than the high or low ionization of the one track. They also did not have unusual signatures in the calorimeter nor unusual energy flow patterns in the events. An isolation cut of 20° from the nearest neighbor with momentum

greater than 1 GeV/c rejected all these candidates. These events were attributed to background.

The ALEPH collaboration then proceeded to report upper limits for mass regions higher than $5\,\mathrm{GeV/c^2}$, where with the cuts applied, there were zero observed candidates. The upper limit on the mass range for these searches was $43\,\mathrm{GeV/c^2}$. The effect of the above cuts on the efficiency for detecting a particle with mass m and charge Q was dependent on the assumed model production. (The efficiency affected the ratio R_Q.) Two different hypotheses were used in this analysis. In model I, the momentum dependence was taken from a fit to the standard Bjorken variable distribution of hadrons in the ALEPH data and in model II, the momentum distribution for the produced particles was given by

$$E\frac{d^3\sigma}{dp^3} \sim \text{constant.}$$

The upper limits obtained for R_Q for the inclusive production of particles with charge of either $1/3\,e$ or $2/3\,e$, assuming particles distributed in momentum according to model I, ranged from $10^{-3} - 10^{-2}$ and were established at the 90% confidence level. For the inclusive production of quarks, assuming particles distributed in momentum according to model II, R_Q was between 10^{-3} and 10^{-2} for $Q = 1/3\,e$ particles and between 10^{-4} and 10^{-3} for $Q = 2/3\,e$ particles. A search for the inclusive and exclusive production of $Q = 4/3\,e$ particles established R_Q to be within the range of $10^{-4} - 10^{-3}$. Again, these limits were established at the 90% confidence level.

ALEPH also explicitly searched for exclusively and inclusively produced heavy, long-lived particles of charge $Q = 1\,e$. R_Q in both cases ranged from $10^{-4} - 10^{-2}$ at the 90% confidence level. The upper limit on the mass range for this search was $70\,\mathrm{GeV/c^2}$.

In some sense, this is the most interesting of the accelerator searches because it has the greatest mass range. Unfortunately, the R_Q values they obtained are not that stringent.

2.1.2 Deep Inelastic Scattering

According to the quark parton model, which is based on extensive experimental research, deep inelastic scattering of leptons occur via the exchange of virtual photons or intermediate vector bosons with the quarks (partons) in the target nucleons [26, 34]. The momentum given to the struck quark leads to the production of hadrons. However, the possibility that the quark might be liberated from the nucleon as a free particle has led researchers to use this technique to try to produce free quarks.

The European Muon Collaboration Experiment

A search was made in 1983 for long-lived fractionally charged particles produced by 200 GeV/c muons on a berrylium target using the CERN SPS muon beam [35] and beam line. The first part of the beam line was used as a source of high energy muons and the second part (after the target) as a spectrometer to measure the outgoing momenta. The spectrometer had a momentum acceptance of $\Delta p/p = \pm 10\%$ and a solid angle of $8\,\mu$sr. Although the solid angle was small, the experimenters asserted that the spectrometer, nevertheless, had good acceptance along the direction of the momentum of the struck quark. In addition, the $\left\langle \frac{dE}{dx} \right\rangle$ and time-of-flight of the produced secondary particles were measured.

The energy loss $\left\langle \frac{dE}{dx} \right\rangle$ was measured in six pairs of scintillators distributed over a length of 60 m in the beam line starting 330 m downstream of the Be target. Each pair consisted of a "big" (B) scintillator and a "small" (S) scintillator. They were set to accept positive and negative particles of unit charge with a momentum of 250 GeV/c and negative particles of unit charge with a momentum of 50 GeV/c. The trigger for a fractionally charged particle was defined by the six-fold coincidence of the S scintillators when a pulse height less than 60% of the expected pulse height from a minimum ionizing particle was observed in each of them. When the trigger conditions for the S counters were satisfied, the B counters were analyzed for their pulse heights. In no case did any of the tracks have more than one of these pulse heights less than 75% of minimum ionizing.

$Q(\times e)$	Momentum (GeV/c)	μ Flux ($\times 10^{11}$)	Acceptance	R_Q
$+\frac{2}{3}$	167 ± 17	4.6	20.4%	$< 1.2 \times 10^{-6}$
$+\frac{1}{3}$	83 ± 8	4.6	15.8%	$< 1.5 \times 10^{-6}$
$-\frac{2}{3}$	167 ± 17	1.6	20.4%	$< 3.5 \times 10^{-6}$
$-\frac{2}{3}$	33 ± 3	0.9	11.0%	$< 1.2 \times 10^{-5}$
$-\frac{1}{3}$	83 ± 8	1.6	15.8%	$< 4.5 \times 10^{-6}$
$-\frac{1}{3}$	17 ± 2	0.9	8.1%	$< 1.6 \times 10^{-5}$

Table 2.2: Summary of results obtained by the European Muon Collaboration.

To extract an upper limit for the quark cross section, they calculated the geometrical acceptance of the spectrometer and estimated a muon flux for the chosen momenta. Their upper limits were reported in terms of

$$R_Q = \frac{\sigma(\mu N \longrightarrow \mu q X)}{\sigma(\mu N \longrightarrow \mu X)}$$

and were valid for quarks with masses up to $9\,\mathrm{GeV/c^2}$ for $Q = 2/3\,e$ particles and $15\,\mathrm{GeV/c^2}$ for $Q = 1/3\,e$ particles because of production kinematics and timing requirements on the counters. The results are shown in Table 2.2. If quarks have lifetimes less than 10^{-8} s or have large absorption cross sections, these limits do not apply.

At first glance, these upper limits on R_Q of 10^{-6} are very impressive. But R_Q is simply the ratio of the upper limit on free quark production to the total cross section of μ-nucleon inelastic scattering, where the total μ-nucleon cross section used in this experiment required, on average, 4-momentum transfers on the order of a few $\mathrm{GeV^2}$. We have no reason to believe such relatively small 4-momentum transfers to be sufficient to produce free quarks. Therefore, this experiment has indeterminate significance.

The CHARM Experiment

Between 1983 and 1984 [36, 37], the CHARM collaboration conducted a search for fractionally charged particles produced in neutrino-nucleus and antineutrino-nucleus interactions using the CHARM neutrino detector at the CERN SPS. The neutrinos and antineutrinos used were predominantly ν_μ and $\bar{\nu}_\mu$. The detector consisted of a fine grain target calorimeter composed of 78 identical sub-units with a cross section of $3 \times 3\,\mathrm{m}^2$, surrounded by a magnetized iron frame and followed by a muon spectrometer. The calorimeter sub-unit comprised a 8 cm thick marble absorber plate, a 3 cm thick layer of twenty plastic scintillators and a layer of proportional tubes. The energy losses of tracks were determined by measuring pulse heights in the scintillation counters.

The average energy of the beam was 31 GeV for neutrinos and 21 GeV for antineutrinos. The trigger for this experiment required that at least four scintillator planes were hit and a total ionization energy larger than that produced by a 2 GeV shower. This trigger was 100% efficient for events with energy above 0.5 GeV. Potential candidate events were chosen based on the following criteria:

1. The primary interaction vertex had to be inside the fiducial volume defined by a $2.4 \times 2.4\,\mathrm{m}^2$ cross section and extending from plane 5 to plane 55 of the calorimeter.

2. The hadronic energy of the event had to be greater than 2 GeV.

3. The event had to not be a random superposition of two different events occurring in the time gate of the trigger. These events were rejected by comparing the event pattern in the proportional drift tube system with the one in the scintillator system.

There were approximately 2.64×10^3 neutrino events and 1.04×10^3 antineutrino events that passed these cuts.

Out of this sample, quarks were searched for in either the events that had a track emerging from the (anti)neutrino induced shower and producing a second shower ("bi-shower events") or the events that had a single track emerging from the (anti)neutrino

induced shower that was detected by the automatic pattern recognition in the proportional tube system ("mono-shower events"). The signals from the scintillators hit by these quark candidates were corrected for the track angles and attenuation in the counters. To distinguish $Q = \frac{1}{3}e$ and $Q = \frac{2}{3}e$ from $Q = 1\,e$ particles, a final cut was imposed. It was required that there were at least seven scintillators hit along the track, each with a mean pulse height less than 4.5 MeV. After this selection, no quark candidates remained.

The detection efficiency was obtained by a Monte Carlo method and depended on the quark mean-free-path (λ_Q), its mass and assumed fragmentation function, which describes the transition of quarks into hadrons. For this analysis, two different fragmentation functions were used: a constant one and one wherein the function was given by $e^z - 1$, where z is the fraction of the hadronic energy that the quark carries away. The produced quark was tracked through the calorimeter up to the secondary interaction point where it was allowed to either be absorbed (no re-interaction) or to interact again until it exhausted all its energy (re-interaction). The fragmentation function used to describe free quark production was also assumed to govern the hadronic interactions of the quark.

Results are shown in Table 2.3. It was assumed that only Cabibbo favored transitions ($d \longrightarrow u$ in neutrino induced events and $u \longrightarrow d$ in antineutrino events) can occur. Having observed zero events, the 90% confidence upper limits on free quark production were calculated with R_Q defined as

$$R_Q = \frac{\sigma(\bar{\nu}N \longrightarrow d\,X)}{\sigma(\bar{\nu}N \longrightarrow X)}$$

and

$$R_Q = \frac{\sigma(\nu N \longrightarrow u\,X)}{\sigma(\nu N \longrightarrow X)}.$$

The comments applied to the European Muon Collaboration results also apply to the CHARM results. We do not know what it means to have an upper limit on the neutrino production of quarks relative to the ν-nucleon interactions.

$Q(\times e)$	$M_Q = 1\,\mathrm{GeV/c^2}$		$M_Q = 10\,\mathrm{GeV/c^2}$	
$\lambda_Q/\lambda\pi =$	1	5	1	5
$\frac{2}{3}$ (reinteracting)	13	4	200	25
$\frac{2}{3}$ (not reinteracting)	60	5	400	30
$\frac{1}{3}$ (reinteracting)	16	4	300	50
$\frac{1}{3}$ (not reinteracting)	60	6	700	60

Table 2.3: Some of the results obtained by the CHARM collaboration on the production of ordinary quarks of mass M_Q in ν and $\bar{\nu}$ interactions [26]. Results are quoted at the 90% confidence level and are in units of 10^{-5} quarks per interaction. Charge $\frac{2}{3}e$ particles were sought in ν interactions and charge $\frac{1}{3}e$ particles were sought in $\bar{\nu}$ interactions.

2.1.3 Hadronic Production

The violent collisions of high energy hadrons might offer the best hope for the production of free quarks. There is more energy available for producing larger masses and perhaps more energy available for deviating from conventional QCD processes. Thus, because it is possible that quarks could be liberated in hadronic collisions of extremely high energy, the UA2 collaboration performed a relativistic free quark search using the CERN $p\bar{p}$ collider in 1982 [38]. The center-of-mass energy was 540 GeV.

The UA2 detector consisted of five drift chambers followed by 2 scintillation hodoscope planes separated by an iron plate and a telescope of five scintillation counters, $Q_1 - Q_5$. These last five were equipped with a phototube at each end and were used to determine the ionization of charged particles produced in $p\bar{p}$ collisions as well as detect events with abnormally low ionization. The scintillators of the front hodoscope, W_F, were also equipped with a phototube at each end, whereas the scintillators of the back hodoscope, W_B, were equipped with only one phototube located at the bottom end. These were used to acquire additional measurements of ionization. Two additional scintillation counters located behind the Q-telescope were used to reject particles that might simulate abnormally low ionization due to Čerenkov radiation in the light

guides of the telescope counters. This entire array was situated perpendicular to the $p\bar{p}$ beam direction.

The trigger for a fractionally charged particle consisted of requiring at least three out of the five signals obtained by linearly adding the amplified signals from the top and bottom phototubes of each counter Q_1 to Q_5 to exceed a threshold ionization of 5% of the ionization for a minimum ionizing particle of unit charge. An additional coincidence requirement was that both phototubes from either one of the two W_F counters give outputs above 3% of the ionization for a minimum ionizing particle. To suppress background from sources other than $p\bar{p}$ collisions, the trigger was also required to be coincident with a minimum bias event, defined as a signal from each of two scintillator arrays surrounding the vacuum chamber 10.3 m downstream of the interaction point and covering a pseudo-rapidity interval $\Delta\eta = 1.1$ around $\eta = \pm 4.7$.

In the analysis, events with zero pulse height in Q_1 or Q_5 were rejected to exclude particles leaving the Q-telescope through the sides. A particle had to traverse the entire thickness of the telescope to be considered. Events with signals from either veto counters or where the drift chambers showed that there were more than one track in the telescope were also rejected.

The pulse heights were corrected for attenuation along the scintillators and normalized so that their distributions peaked at 1.0. Ionization measurements were then defined for each of the W_F and Q_1 to Q_5 counters as the mean pulse height of the two phototubes. From the six ionization measurements obtained for each event, the most probable ionization was determined by using a maximum likelihood method. Tracks with too small a maximum likelihood were rejected as having inconsistent pulse height measurements. There were twenty-three events with an estimated ionization that was less than 70% of that expected for a minimum ionizing particle. Of these, fifteen were rejected because they had an abnormally low ionization in W_F or Q_5 only. None of the remaining eight events had a corresponding track in the drift chambers, five of which were assumed to be at least 50% efficient in producing hits in the drift chambers if they were genuine fractionally charged particles (all had an estimated ionization greater than 50% that of minimum ionizing). Therefore, they were rejected as spurious. The remaining three events were also rejected because in

each of them, there was an electromagnetic shower present in the lead glass blocks adjacent to the Q-telescope, which suggested that the low pulse heights were due to soft photons emerging from the lead glass that materialize or undergo Compton scattering in the counters. Therefore, no events were found with an ionization less than 70% of that expected for a minimum ionizing particle.

At the 90% confidence level, their null results yielded an upper limit on R_Q given by

$$2.3 = N_{MB}\alpha_Q R_Q,$$

where N_{MB} is the total number of minimum bias events, α_Q is the efficiency of the detector and R_Q is given by the ratio of quark yield around 90° to that of particles with unit electric charge detected at 90°. The detection efficiency was calculated using a Monte Carlo simulation program. It depended on the geometry of the detector, assumed quark mass and momentum spectrum (because of the detector thickness of $\sim 40\,\mathrm{g/cm^2}$ between the $p\bar{p}$ collision point and Q_5), and the deflection of the particle trajectories due to the magnetic field of the spectrometer. Quarks of various masses m_Q and charge $Q = \frac{1}{3}e$ and $\frac{2}{3}e$ were generated in the Monte Carlo simulation with a flat rapidity distribution around 90° and a transverse momentum distribution of the form $p_t e^{-5m_t}$, where m_t is the transverse mass.

For $Q = \frac{1}{3}e$ and $\frac{2}{3}e$, $R_Q \sim 2 \times 10^{-4}$ at low mass. The sensitivity of the measurement decreases with increasing quark masses, however, and for a mass about $2\,\mathrm{GeV/c^2}$, $R_Q \sim 2.5 \times 10^{-3}$ for $Q = \frac{2}{3}e$ and $\sim 10^{-3}$ for $Q = \frac{1}{3}e$.

However, most of the remarks applied to the e^+e^- searches also apply here: the mass range is small and the upper limits on R_Q are not that stringent.

Heavy-Ion Collisions

Within the last fifteen years, there have been several searches for free quarks produced in collisions of heavy ions on fixed targets. The idea here was that the environment in the immediate vicinity of an energetic heavy-ion collision would be more conducive for producing fractionally charged particles than an elementary particle interaction, where it is difficult to separate a quark from the remaining colored fragment [20, 39].

In the environment of a heavy-ion collision, a quark could be color shielded from these fragments by the quark-gluon sea and, therefore, liberated. Thus, heavy-ion collisions, in principle, are a good way to search for free quarks. However, we have no quantitative model on how a free quark might be produced in heavy-ion collisions and we do not know what the mass of the free quarks might be. Therefore, in the experiments described below, we do not offer an interpretation of the upper limits given.

In 1983, an experiment was conducted at the Bevalac wherein a beam of ^{56}Fe at 1.9 GeV/nucleon was incident on a predominantly lead target. Within a 30° cone behind the target were 26 five-gallon tanks of carbon tetrachloride, each of which contained a thin central wire maintained at a potential of ± 90 V with respect to its inside wall. These 26 wires included Au, In, Cu, Nb and W wires. Fractionally charged particles stopped in the tanks were thought to form fractionally charged atoms or molecules that drift to the wires within and become trapped there by their image charges since no subsequent reaction can make them neutral [3]. For the analysis, two of the forward tank wires were used. Each wire was passed twenty times through a drop of liquid mercury in a capillary tube to remove the surface layer of the wire. The two drops were then combined to form one sample. Another sample was made by dissolving the wires in some mercury taken from the target. These samples were then analyzed for fractional charge using the San Franciso State University Millikan apparatus [1]–[4]. Fewer than 5.0×10^{-7} fractionally charged particle were found per Fe-Pb collision at the 95% confidence level.

A similar experiment was conducted in 1987 at the Brookhaven National Laboratory (BNL) where 14.5 GeV/nucleon ^{16}O were incident on a mercury target [40]. In this experiment, the stopping tanks were filled with liquid argon and charged atoms were electrostatically collected on quartz fiber wires, each plated with about a 200 Å layer of gold. After the apparatus was exposed to 7×10^{12} relativistic ^{16}O for a period of several days, these gold layers were dissolved in mercury. The mercury was then analyzed using the San Francisco State University Millikan apparatus. No evidence for free quarks were found. An upper limit was established at the 90% confidence level at less than 1.0×10^{-9} quarks produced per O-Hg collision.

In 1989, another search was performed where a mercury target exposed to oxygen and sulfur beams at the CERN SPS was concentrated by distillation [41] and again analyzed using the San Francisco State University Millikan apparatus. No fractional charges were observed and an upper limit of $\sim 10^{-6}$ quarks per collisons was determined.

Other such experiments were performed, but we have only discussed a few. All yielded negative results. Limits were established between $\sim 10^{-10}$ and $\sim 10^{-6}$ [42]–[45]. The 10^{-10} limit was established by Matis *et al.* [44, 45] in 1988 and 1991. In 1988, the experiment consisted of searching for free quarks produced in collisions of 800 GeV/c protons with a heavy target at Fermilab. They acquired their mercury samples for analysis by the San Francisco State University apparatus via two different methods. In the first method, secondaries were stopped in mercury filled tanks. The mercury was then distilled for analysis. In the second method, secondaries were stopped in liquid nitrogen tanks and charged atoms were electrostatically collected on gold-coated electrodes. The gold coatings were dissolved in mercury. No evidence for the existence of free fractionally charged particles were found in either sample. In 1991, free quarks were sought in two separate experiments, one at BNL and the other at CERN, using ultra-relativistic beams. These two experiments were designed to trap quarks in mercury targets or liquid argon tanks located along the beam line. As before, the San Francisco State University apparatus was used for analyzing the mercury and the liquid argon. Again, no evidence for free quarks were found.

We note that in all the above accelerator searches, the upper limits were defined in various different ways or if they were defined the same way, they took into account different parameters of the experiment. This makes it difficult for us to directly compare one experiment to another even if they were both of the same type. For example, while the European Muon Collaboration and the CHARM collaboration both searched for free quarks using the deep inelastic scattering technique, one R_Q was defined in terms of the total μ-nucleon cross section while the other was defined in terms of the total ν-nucleon cross section. Given that the detectors were designed for different experiments, this disparity was to be expected. However, it makes it difficult

for true comparisons to be made. The upper limits these accelerator experiments established are not absolute and at best we can merely say that one experiment was more or less "sensitive" relative to another.

2.2 Cosmic Ray Searches

Although it is possible that primordial free quarks remaining from the Big Bang might eventually enter the Earth's atmosphere as a high energy cosmic ray, this is a highly speculative scenario. A more likely scenario is one where free quarks are produced in the interaction of cosmic ray particles and the Earth's atmosphere.

The integral energy flux [46] of all cosmic ray hadrons over the energy range $10 - 10^6$ GeV is given by

$$\phi(E > E_0) = 2.08\, E_0^{-1.67} \text{particles } (\text{cm}^2\,\text{sr}\,\text{sec})^{-1}. \tag{2.1}$$

In terms of the energy spectrum per nucleus, the primaries are about half protons and half He nuclei.

It is known that a cosmic ray particle, upon interacting with the Earth's atmosphere, will produce a shower of other particles that falls off at angles away from the zenith according to $e^{\frac{-z_0 \sec\theta}{\lambda}}$, where z_0 is the vertical depth in the atmosphere of a detector, λ is the primary proton attenuation mean-free-path in the atmosphere ($\sim 120\,\text{g/cm}^2$) and θ is the zenith angle. The dominant flux of cosmic ray particles at sea level are muons of a few hundred MeV/c momentum. This flux of relativistic muons provides both a primary background and a convenient source of calibration particles.

Many cosmic ray searches were performed because cosmic ray particles have higher energies than that available with accelerators. As published, the highest accelerator energy achieved by a $p\bar{p}$ accelerator was that of the UA2 experiment, where the center-of-mass energy was 540 GeV (see Sec. 2.1.3). They did not observe free quarks at this energy. To exceed 540 GeV, a cosmic ray proton colliding with a stationary proton in the atmosphere would have to have an energy in excess of 10^5 GeV. According to

Jones [46], the flux of particles with energies greater than a given energy E_0 is given by Eq. (2.1). Substituting the value $E_0 \approx 10^5\,\mathrm{GeV}$ into Eq. (2.1), we obtain a flux value of $\sim 10^{-9}\,(\mathrm{cm^2\,sr\,sec})^{-1}$. Therefore, if every collision of a cosmic ray particle of $E > E_0$ with a stationary atmospheric particle yields one free quark, there is an obvious upper limit on the quark flux of $\sim 10^{-9}\,(\mathrm{cm^2\,sr\,sec})^{-1}$ for $E_0 > 540\,\mathrm{GeV}$.

Of all the searches conducted, only McCusker claimed to have observed free quarks, but as tabulated by Jones in his review article [46], McCusker's claim was not consistent with more stringent determinations of quark flux from cosmic rays. More recent experiments have been conducted within the last decade and still no evidence of free quarks have been found. All of these experiments were conducted at or above sea level. Therefore, quarks that came in from the outside the atmosphere or quarks produced in the atmosphere must travel through the remaining atmosphere. This again brings up the problem of evaluating the effect of a large quark-hadron cross section.

We turn next to two recent cosmic ray searches that are critically affected by the magnitude of the quark-hadron cross section.

The Kamiokande II Experiment

A search for fractionally charged particles with $Q = \pm\frac{2}{3}e$ and $Q = \pm\frac{1}{3}e$ was conducted in 1991 using the Kamiokande II water Čerenkov detector located under 2700 m of water equivalent in the Kamioka mine approximately 300 km west of Tokyo, Japan [47]. A cylindrical steel tank contained 2400 tons of water viewed by 948 photomultiplier tubes (PMTs) covering 20% of the inner surface of the tank. This inner detector was surrounded by a 4π steradian water anticounter at least 1.2 m thick and viewed by 123 PMTs.

We note, however, that 2700 m of water equivalent is a substantial amount of rock. Cosmic ray hadrons, electrons and photons cannot penetrate this depth. The only particles that could reach this detector would be muons and neutrinos, which was the actual purpose of the detector and the reason for its location. Therefore, any fractionally charged particles detected by this experiment would have to have been

muons or neutrinos interacting in the material just above the detector. Thus, this search appears to be a variation of the deep inelastic scattering searches.

An alternative hypothesis is that quarks have an extremely small interaction cross section with hadrons. Such a small cross section would enable them to travel through the atmosphere without interacting with it and penetrate this depth. However, that possibility is very unlikely. Yet another hypothesis is that heavy ($> 45\,\mathrm{GeV/c^2}$) fractionally charged leptons exist, in which case Kamiokande II would have set a stringent limit.

The 90% confidence level upper limits on the fluxes were reported as

$$\Phi(|Q| = \frac{1}{3}e) = 2.1 \times 10^{-15}\,\mathrm{cm^{-2}s^{-1}sr^{-1}}$$

and

$$\Phi(|Q| = \frac{2}{3}e) = 2.3 \times 10^{-15}\,\mathrm{cm^{-2}s^{-1}sr^{-1}}.$$

Here the angular acceptance of the detector was taken was taken to be 4π.

The Kamiokande II collaboration further calculated an upper limit on the production cross section of quarks ($\sigma_{q_{production}}$) by cosmic ray protons given the primary proton spectrum and the upper limits on the fluxes they reported above. They find, with 90% confidence,

$$\sigma_{q_{production}} \leq 1.6 \times 10^{-40} \left(\frac{\Omega}{4\pi}\right)^{-1} M_q^{3.33}\,\mathrm{cm^2},$$

where M_q (GeV) is the quark mass, Ω is the angular acceptance related to the mountain shape and the quark survival probability between the production point and the detector site, which could not be calculated without knowledge of the interaction cross section with rock. The experimenters note that the limit is valid for the quark-mass range $M_q \leq 110\,(\Omega/4\pi)^{1/5.33}$ GeV, which was obtained from

$$M_q^{5.33} \leq 1.7 \times 10^{-4}\Phi^{-1} \left(\frac{\Omega}{4\pi}\right)\,\mathrm{cm^{-2}s^{-1}}.$$

The Mont Blanc LSD Experiment

The remarks noted above for the Kamiokande II experiment are applicable to another free quark search that was conducted in 1994 on data taken between December 1985 and February 1993 using the Mont Blanc LSD Scintillation Detector located under Mont Blanc at a slant depth of $500\,\mathrm{kg/cm^2}$ of standard rock [48].

At the 90% confidence level, the upper limits to the quark flux achieved by LSD were given as

$$\Phi(|Q| = \frac{1}{3}e) = 2.3 \times 10^{-13}\,\mathrm{cm^{-2}s^{-1}sr^{-1}}$$

and

$$\Phi(|Q| = \frac{2}{3}e) = 2.7 \times 10^{-13}\,\mathrm{cm^{-2}s^{-1}sr^{-1}}.$$

2.3 Bulk Matter Searches

We now consider the general subject of bulk matter searches. The basis for such searches is delineated in the following discussion.

There may have been a time in the very early history of the Universe when not all quarks were already bound in protons or neutrons, that is, a few quarks were left free and isolated. As the Universe evolved, these free quarks became attached to hydrogen or helium nuclei through electromagnetic or perhaps strong forces. Following the evolution further, some of the nuclei containing an extra quark remained in the intergalactic gas while others found themselves in galaxies and, ultimately, in stars. In the stars, the free quarks may transfer from hydrogen and helium nuclei to nuclei of heavier elements within the stars. If these stars then become supernovae, the heavier elements get expelled into space. Finally, some of the atoms containing quarks could conceivably end up in the solar system, in the vicinity of Earth, on the Earth itself, on the moon or in meteorites. Experiments that search for free quarks in bulk matter, then, have the challenge and the opportunity of securing the matter and searching through it for free quarks. An alternative hypothesis is that very energetic cosmic rays produce quarks that become lodged on the surfaces of the Earth or the moon.

What are the opportunities and limitations faced by experimenters who look for free quarks using bulk matter techniques? There are two obvious limitations: (1) there must be some residual free quarks left over from the Big Bang and (2) these quarks must have traveled through space and time to be within the experimenter's grasp. As to the opportunities, there are three obvious ones:

1. Given proper technology (we feel that we are developing a very good one), one could search through a very large quantity of material.

2. Bulk matter searches do not have to deal with the uncertainties of energy requirements as the accelerator searches do.

3. If free quarks were found in a given material or an upper limit on the density of free quarks were set in that material, then by understanding geochemistry and the chemistry of fractionally charged particles, we could estimate the density of free quarks in the Universe.

We note, however, one conceivable limitation in our specific bulk matter search in addition to the previously stated two. We use drops with a mass of $1.71 \times 10^{-4}\,\mu$g ($\sim 10^{14}\,\mathrm{GeV/c^2}$). If the free quark has a mass that is a substantial fraction of the mass of the drop, then the atom containing the free quark would be pulled to the core of the Earth because of its high density. For such a heavy quark, the gravitational force it experiences is equivalent to $\sim 10^5\,$V/cm acting on one electron. Therefore, we would not be able to measure it.

As stated above, fractionally charged particles might be found either in isolation or in association with particular nuclei. As discussed by Lackner and Zweig [49]–[51], the chemistry of atoms containing such nuclei is significantly different from the chemistry of their ordinary counterparts because the electronegativity of an element is substantially altered when its nuclear charge is changed by as little as $\frac{1}{3}$e. They also note that this change in electronegativity is of the same order of magnitude as typical electronegativity differences between ordinary atoms, which signifies drastic changes in the chemical behavior of "quarked atoms." Therefore, by considering quark chemistry, a material with a higher probability of containing quarks may be chosen as the test material. However, for this thesis, quark chemistry was not studied.

In this experiment, we used silicone oil in order to develop the method and make a preliminary search. We recognize that silicone oil does not offer the best opportunities of finding free quarks because it is a refined material[1].

The two techniques that have been employed by stable bulk matter searches are levitation and the Millikan liquid drop method. In the following sections, we discuss both techniques.

2.3.1 Magnetic Levitation

The most common levitation technique used in bulk matter searches is magnetic levitation. The charge on an object is measured by suspending that object with a magnetic field and then using an electric field to ascertain its charge. There are two types of magnetic levitation techniques: diamagnetic levitation and ferromagnetic levitation with feedback.

The former employs the property that diamagnetics are repelled by regions of nonuniform magnetic field. Therefore, a diamagnetic object falling under the influence of gravity in a nonuniform magnetic field can be suspended in such a field when the repulsive force is sufficient to counteract the gravitational force. Ferromagnetic materials, however, do not have a stable equilibrium position in a static magnetic field. To levitate ferromagnetic objects permanently, a feedback mechanism must be used. If the object tends to go up, the feedback "instantaneously" decreases the magnitude of the magnetic field so that the object will come back down. Likewise, if the object tends to go down, the magnetic field is increased so that the object will go back up. In practice, this feedback mechanism consists of a light source creating a shadow of the object on a photodetector. When the object falls (rises), the shadow covers a smaller (larger) fraction of the sensitive region of the photodetector and with an appropriate amplifier, the magnetic field is increased (decreased) [52].

To illustrate the use of this technique in searching for fractional charges, we consider an object levitated by a shaped magnetic field such that the object is located

[1]The refining process itself would remove quarked atoms from the sample because they would be considered impurities and taken out. Also, they may drift to the surfaces of the refining apparatus, particularly metal surfaces, and remain trapped there by their image charges.

at a local minimum of the field. Once the object is levitated, it can be forced to execute the motion of a harmonic oscillator with the introduction of a uniform (an assumption that will be discussed later), transverse, oscillating electric field into the system. The force equation for this object with charge Q is

$$m\ddot{x} + \alpha\dot{x} + \beta x = QEsin\,\omega t. \tag{2.2}$$

where α is the damping coefficient, β is the restoring force parameter and ω is the driving frequency of the system.

The steady state solution to Eq. (2.2) is given by

$$x = x_0 sin(\omega t - \phi),$$

where the amplitude of oscillation, x_0, is

$$x_0 = \frac{QE}{\sqrt{(\alpha\omega)^2 + (\beta - m\omega^2)^2}}. \tag{2.3}$$

At resonance, this amplitude becomes

$$x_0 = \frac{QE}{\alpha\omega}. \tag{2.4}$$

Since E, α, and ω are known parameters and x_0 is measured, we solve for Q to obtain

$$Q = \left(\frac{\alpha\omega}{E}\right) x_0. \tag{2.5}$$

If the object contained a fractionally charged particle, then $Q = (n \pm \frac{1}{3})\,e$, where n is an integer. Substituting this equation into Eq. (2.5), we see that for any value of n, x_0 would never pass through the value zero. On the other hand, if the object did not contain a free quark, then $Q = ne$ and x_0 would pass through zero. Therefore, measuring residual amplitude gives the residual charge according to Eq. (2.5).

A simplifying assumption made so far was that the electric field was uniform. In practice, this is not the case and the nonuniformity of the field has to be taken into

account because it can give rise to spurious residual charges. We consider the purely electric forces that may contribute to this spurious effect: 1) the polarization force 2) the patch force 3) the unbalance force and 4) the force due to the permanent electric dipole or higher multipole moments of the object.

Any object in a nonuniform electric field experiences a polarization force, F_{pol}, because the electric field induces a dipole moment on the object that interacts with the field gradient to produce a dipole force. For a conducting sphere of radius r, this force is

$$F_{pol} = \alpha E \frac{\partial E}{\partial x}, \tag{2.6}$$

where α, the polarizability, is given by $4\pi\epsilon_0 r^3$. Substituting the applied electric field E_a for E, we see that F_{pol} is quadratic in E_a and would, therefore, produce a motion at twice the frequency of E_a. If the detection system is sensitive only to the resonance frequency either because this frequency is enhanced or because frequencies different from the resonance frequency are filtered out, then F_{pol} is irrelevant and no spurious charge effects arise from the polarization force.

However, contaminants deposited on the field plates or local irregularities in the Fermi level of the plates (patches) could lead to static field contribution, E_s, to the total field, which can be expressed as

$$E = E_a + E_s. \tag{2.7}$$

The potential differences corresponding to the patch fields have typical values of tens of millivolts and while these fields are small with respect to the applied field, they make a non-negligible contribution to the residual charge calculation. Substituting Eq. (2.7) into Eq. (2.6) and neglecting the terms quadratic in E_a and E_s because they are negligible, we are then left with the two cross terms

$$F_s = \alpha \left(E_s \frac{\partial E_a}{\partial x} + E_a \frac{\partial E_s}{\partial x} \right).$$

But the first term is negligible with respect to the second and so

$$F_s \cong \alpha E_a \frac{\partial E_s}{\partial x}.$$

Adding this force to the electric force QE_a, we obtain for the total force

$$F_{tot} = \left(Q + \alpha \frac{\partial E_s}{\partial x}\right) E_a.$$

Clearly, this second term simulates a residual charge. Therefore, the apparent residual charge must be determined and subtracted from the measured value of Q to ascertain the true charge on the object. This is done by taking balls with the same radius and measuring them successively in conditions where the patches do not change. If one ball contains a quark and the subsequent one does not, then the difference in their residual charge must be $\pm\frac{1}{3}e$. Then these runs, where different balls of the same radius are compared, are intermixed with runs on balls of a different radius. Because the residual charge depends on r^3, this information confirms the normalization of the patch effect.

Another force that gives a spurious fractional charge, is the "unbalance force". If the square wave oscillation of the electric field were perfect, the average potential difference of each plate with respect to the walls of the levitation chamber should vanish. In practice, however, asymmetries due to a difference in the switching times of the plates may be present. If a non-zero average occurs, this is equivalent to having a time independent potential above zero applied to the plate in question, which produces a gradient, $\partial E_u/\partial x$, at the position of levitation because of edge effects. This yields an unbalance force given by

$$F_u = \alpha E_a \frac{\partial E_u}{\partial x}.$$

However, this gradient is negligible if the plates have a large diameter and a small separation. Therefore, its contribution to a pseudo-fractional charge can be ignored.

Lastly, the permanent electric dipole moment of the ball couples to the field gradient in a nonuniform field to yield the dipole force

$$F_{dipole} = p_x \frac{\partial E_a}{\partial x}.$$

Because this is also linear in E_a, it would simulate a fractional charge. This force can be estimated by measuring the permanent electric dipole moment of the ball. This is done by creating a known gradient of the applied electric field at the position of the ball and measuring the corresponding change in the force acting on the ball. However, this is also unimportant if the plates are flat and parallel. The same conclusion is true for the higher multipole moments.

We conclude this section on the magnetic levitometer technique by describing the Stanford experiments from 1977 to 1981 [13]–[17] and the Smith [53] experiment in 1985 on niobium balls.

The Stanford Experiments

A series of experiments from 1977 to 1981 [13]–[17] were conducted at Stanford University using superconducting niobium spheres heat-treated on a tungsten substrate and levitated by a magnetic field. Positive evidence for the existence of fractional charge in matter was found.

The apparatus was kept at 4.2° K and consisted of a suspended niobium ball of mass $\sim 9 \times 10^{-5}$ g that oscillated vertically at a frequency of ~ 0.8 Hz in the magnetic field. The ball was levitated between two horizontal capacitor plates and its position was sensed by a SQUID (superconducting quantum interference device) magnetometer. The charge on the ball was changeable at will with movable β^+ or β^- emitters. A loading mechanism allowed the balls to be inserted or removed from the measurement region. The plates were movable with respect to the ball while a fixed separation was maintained between them.

The alternating force on the ball in the vertical z direction was given by

$$F_A = (Q_r + ne)E_A + \vec{P}_A \cdot \nabla E_s + \vec{P}_s \cdot \nabla E_A + F_M + F_q, \tag{2.8}$$

where Q_r is the residual charge, n is the integer charge number, E_A and E_s are the z-components of the applied, alternating electric field and static electric field arising from the patch effect respectively, P_s and P_A are the permanent and induced electric dipole moments on the ball, F_q is the force due to an electric quadrupole and F_M is the force due to the tilting of the magnetic moment by the torque $\vec{P}_s \times \vec{E}_A$.

To determine the residual charge on the ball from the residual force F_A^r, defined as the value of F_A for $n = 0$ in Eq. (2.8), the background forces had to be determined accurately and taken into account. LaRue *et al.* [13]–[17] asserted that all background forces were negligible at z_0 where $\partial E_A/\partial z = 0$ except for the one arising from the patch effect. Therefore, the residual alternating force was given by

$$F_A^r(z) = Q_r E_A + P_{A,z}\frac{\partial E_s(z)}{\partial z} + P_{s,z}\frac{\partial E_A(z)}{\partial z},$$

where $\frac{\partial E_A(z)}{\partial z}$ was measured experimentally by adding a constant voltage to E_A.

As indicated in the introduction to this section, the patch effect was determined by taking balls of the same radius and measuring them succesively under the same conditions and comparing them with each other to determine their residual charge. The Stanford experimenters asserted that almost all patch changes occurred between levitations and that they could measure the residual force to $\sim 0.01\, eE_A$. Figure 2.3 shows the results of the samples analyzed in 1981.

The Smith Experiment

The niobium spheres analyzed by Smith [53] were 0.28 mm in diameter and were coated with 0.01 mm of iron to allow ferromagnetic levitation at room temperature. The samples were levitated in vacuum (so that its charge would not change frequently due to the presence of ions) by a horizontal magnetic field distribution produced by the poles of an electromagnet shaped and positioned to maximize the working volume. Two additional field shaping blocks were positioned to convert the shallow double maximum in the magnetic field (in the x-direction) into a single maximum at the mid-plane. A given sample was situated at the mid-plane, where it was stable with respect to displacements in the x- and z-directions, but unstable in the y-direction

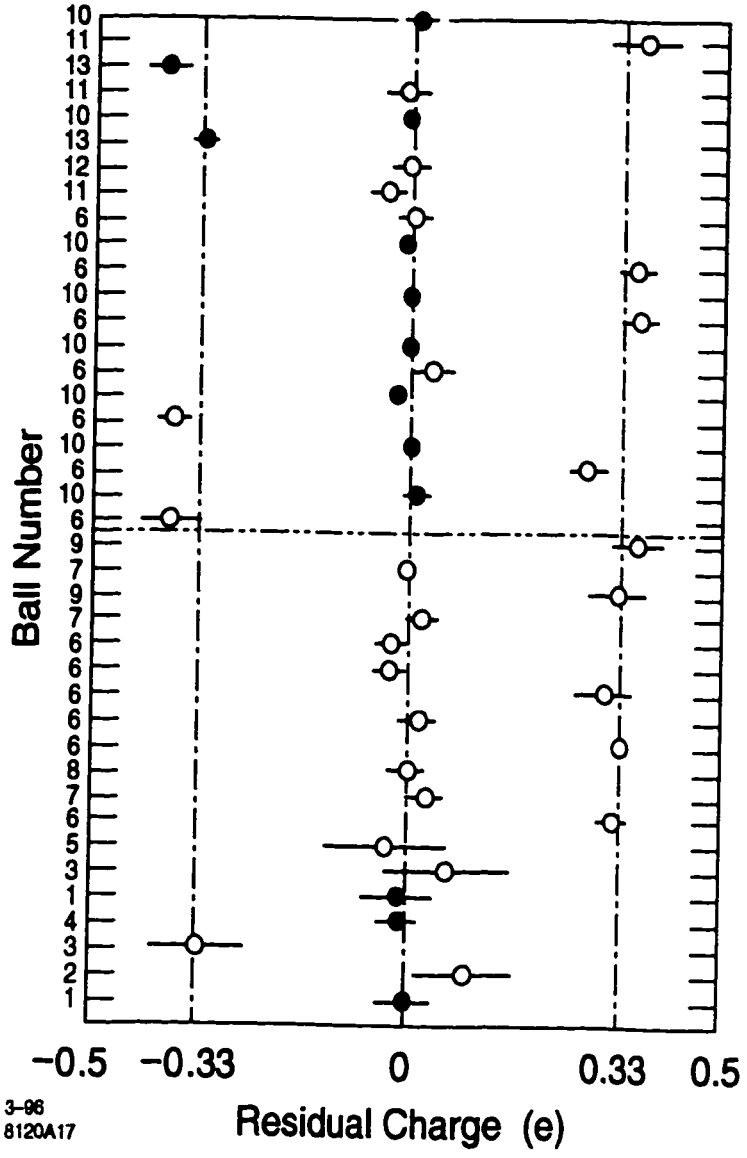

Figure 2.3: Data obtained by the Stanford experiment. Because of these results, the Stanford group claimed to have found evidence for the existence of fractionally charged particles in niobium.

(vertical). The vertical motion was stabilized by feedback control of the levitation field.

A $\pm 2.5\,\mathrm{kV}$ alternating electric field[2] in the x-direction was applied at a frequency adjusted for each sample to the resonant frequency of the x-motion. Typically this was about 1.9 Hz. The plates were capable of sliding in the z-direction, relative to the fixed levitation position, to allow investigation of patch effect variations if required. For charge measurements, however, they were always centrally located. Small damping coils outside the plates provided a magnetic restoring force proportional to dx/dt that limited the resonant oscillations to an amplitude proportional to the AC electric force and, therefore, proportional to the charge on the sample. The z-motion was also damped so that further instabilities were minimized. A weak alternating magnetic field spinned the sample at $1 - 2\,\mathrm{Hz}$ about the x-axis to average out any surface irregularities and any non-axial components of the intrinsic electric and magnetic dipole moments on the sample.

The transverse magnetic field configuration, parallel to the electric field, was chosen to avoid the additional error that arises when the induced electric and magnetic dipole moments are orthogonal [52] and to minimize the noise in the measurements of the ball motion (noise is minimized when measurements of the ball motion are made in a direction perpendicular to the direction of stabilization).

The ball motion was measured by means of three laser beams.[3] The shadow of the ball from each were imaged onto a split photodiode to provide separate voltage signals proportional to the displacement in the x-, y- and z-directions. The ball was inserted into the levitation position by an externally controlled removable cup. Pulses of ultraviolet light of adjustable intensity and duration neutralized the ball from an initial value of $Q \approx -10^6\,e$ to the required starting value of $Q \approx -6\,e$, and then changed the charge on the ball in unit steps to a final value of $Q \approx +6\,e$. Beginning

[2]The balance between positive and negative high voltage supplies was maintained to better than $\pm 2\,\mathrm{V}$ and, thus, contributed less than $0.01\,e$ error.

[3]The possibility that the heating of the sample by the laser beams in the initial stages of levitation may evaporate any quark ions in the sample was considered by Smith *et al.*. The temperature rise in the Smith samples was about 200° C over a period of two hours, which they asserted was better for the samples than the 1800° C over 17 hours used in heat-treating the Stanford samples.

at $-6\,e$, a maximum of twelve 4-min blocks of data were recorded at each charge level, after which short pulses of UV light were fired until the computer detected a charge change. This process was repeated until the charge reached $+6\,e$. In practice, one test would take between two and twelve hours, depending on whether there were any spontaneous charge changes.

The photodiode signals corresponding to the x-coordinate of the ball were processed by a lock-in amplifier and the voltage V corresponding to the oscillation amplitude at the driving frequency were recorded every $4\mu s$ by computer. Every 4 min the data was averaged and the phase of the electric-field square wave was shifted by 180° to eliminate a small zero shift arising from stray coupling affects. To minimize vibrational noise, data was acquired at night.

The apparent residual charge, Q_r, on a ball was obtained from a least squares fit to the expression $V = k(Q_i + Q_r)$, where Q_i is an integral multiple of e. Fits to second and third order polynomials were also made to check the validity of the linearity assumption. Runs were rejected if spontaneous charge changes prevented the accumulation of sufficient data at each charge level or sufficient number of charge levels to obtain a least squares fit with a statistical error less than $0.05\,e$. In normal runs, the data had a standard deviation of $0.2\,e$ after 4 min and $0.02\,e$ after 400 min. Smith *et al.* also observed that the patch effect appeared to decrease with time. An initial non-zero bias of $0.1\,e - 0.2\,e$ was present, but disappeared after a conditioning period of about two weeks, leaving results centered close to zero with a spread of $0.05\,e$. A total of 64 measurements on 46 different samples showed no evidence of a fractionally charged particle. This corresponds to an upper limit of 600 quarks/g or 10^{-21} quark/nucleon at the 95% confidence level. Despite the greater amount of niobium searched in this experiment than in the Stanford experiments with niobium, Smith *et al.* did not confirm the Stanford findings.

2.3.2 Millikan Liquid Drop Technique

The principle behind Millikan-type searches is very straightforward. A potential difference is applied between the parallel plates of a capacitor. A charged drop is injected between the plates and observed with an optical setup (different optical

setups were used for different experiments). The charge on the drop is determined either by suspending the drop in the electric field or using the terminal velocities of the drop as the electric field switches between two states. The experiment we describe below used the latter method of charge determination.

From 1981-1985, San Francisco State University used a piezoelectric drop ejector to produce single drops of mercury (native or refined) or water (from a variety of sources) on demand [1]–[4]. The dropper was made from a capillary tube of soft glass that had been sealed off at the end by heating, thereby forming a sharp conical tip. A hole was then opened by grinding off the glass with fine-grained sandpaper under a microscope, making orifices on the order of $4\,\mu$m. The drop sizes ranged from $3.5\,\mu$m to $6.5\,\mu$m. The drops were ejected into dry air at atmospheric pressure.

A falling drop was illuminated by an argon laser and its image was formed on a plane of 92 horizontal slits. As the image of the drop passed over the slits, pulses of light were detected by three photomultiplier tubes. The first and third tubes monitored pairs of guard slits located at the beginning and the end of the slit pattern. They were used to reject data taken when two drops passed through the chamber at the same time. Measuring the time between pulses from adjacent slits enabled the experimenters to calculate the velocity of the drop. The signals from the three photomultiplier tubes were sent to a hardware peak detector and to an on-line computer that digitized the signal.

When the image of the drop passed over the third slit, 10 kV was applied across the plates. After the drop passed through slit 39 with velocity v_1, the voltage was reversed. After the drop crossed the next 35 slits with velocity v_2, the voltage was reversed again. The drops crossed the remaing slits with velocity v_3. Assuming that the drop was spherical and using Stokes' Law, the radius r and the charge Q were given by

$$r^2 = \frac{9\eta(v_1 + v_2)}{4\rho g} \text{ and } Q = \frac{3\pi\eta r(v_1 - v_2)}{E}.$$

(The equations for radius and charge in our experiment is given by Eqs. (3.5) and (3.6).) Drops were rejected if they were too highly charged to be measured well since they may reverse their direction when the field was switched. About 30% of

Group	Material	Mass (mg)	Method
LaRue *et al.* [13]–[17]	niobium	1.1	levitometer
Marinelli *et al.* [76]	iron	3.7	levitometer
Liebowitz *et al.* [54]	iron	0.72	levitometer
Smith *et al.* [53]	niobium	4.7	levitometer
Jones *et al.* [55]	meteorite	2.8	levitometer
Hodges *et al.* [1]	refined, native mercury	0.06, 0.115	Millikan
Joyce *et al.* [2]	sea water	0.051	Millikan
Lindgren *et al.* [3]	mercury	0.5	Millikan
Savage *et al.* [4]	native mercury	2.0	Millikan

Table 2.4: Summary of stable bulk matter searches. Only LaRue *et al.* [13]–[17] claimed to have observed fractionally charged particles. Subsequent experiments all yielded null results. The last four entries are from the San Francisco State University apparatus.

the drops were rejected for this reason. Charge changes during measurement was also a potential source of error for this experiment. They identified such drops by comparing v_3 with v_0, the velocity of the drop as determined from the first 10 slits after the voltage was turned on. The charge change dQ was given by

$$dQ = \frac{3\pi\eta r(v_3 - v_0)}{E}.$$

This quantity was calculated for each drop and drops for which dQ was not consistent with zero were rejected. Under good running conditions, the experimenters detected about one charge change per 1000 drops. In addition to rejecting single events under the above criteria, entire runs, which consisted of about 4000 drops, were rejected if they failed any one of the following preset run criteria. These criteria were that there be no more than four charge changes per one thousand events and that the measuring error for Q be less than $0.045\,e$. About a third of the runs were so rejected.

The results of the San Francisco State experiments are summarized in Table 2.4

along with other bulk matter searches. Currently, the most recent San Francisco State experiment [4] gives the most stringent upper limit on the abundance of free quarks obtained via the Millikan technique.

Chapter 3

Theory of the SLAC Experiment

Consider a drop falling under the influence of gravity and a vertical electric field that switches between two discrete states, up and down. By Stokes' Law we have the two equations

$$mg + QE_{\text{down}} = 6\pi\eta r v_{E_{\text{down}}}, \tag{3.1}$$

$$mg - QE_{\text{up}} = 6\pi\eta r v_{E_{\text{up}}}, \tag{3.2}$$

where g is the acceleration due to gravity, Q is the net electric charge on the drop, $E_{\text{up,down}}$ is the magnitude of the applied electric field depending on whether the field points up or down respectively, η is the dynamic viscosity of air, $v_{E_{\text{up}}}$ and $v_{E_{\text{down}}}$ are the terminal velocities of the drop corresponding to $E_{\text{up,down}}$, r is the radius of the drop, and m is the effective mass of the drop. The effective mass is given by $m = 4/3\ \pi r^3(\rho_{\text{oil}} - \rho_{\text{air}})$, where ρ_{oil} is equal to $913\,\text{kg/m}^3$. Taking the sum of and the difference between Eqs. (3.1) and (3.2), we obtain the following two equations

$$2mg + Q(E_{\text{down}} - E_{\text{up}}) = 6\pi\eta r(v_{E_{\text{down}}} + v_{E_{\text{up}}}), \tag{3.3}$$

$$Q = 6\pi\eta r\left(\frac{v_{E_{\text{down}}} - v_{E_{\text{up}}}}{E_{\text{down}} + E_{\text{up}}}\right). \tag{3.4}$$

Substituting Eq. (3.4) into (3.3) gives an equation for the radius of the drop

$$r = 3\sqrt{\frac{\eta}{2g(\rho_{\text{oil}} - \rho_{\text{air}})}}\left(\frac{v_{E_{\text{up}}}V_{\text{down}} + v_{E_{\text{down}}}V_{\text{up}}}{V_{\text{down}} + V_{\text{up}}}\right)^{\frac{1}{2}}. \tag{3.5}$$

Here we have substituted $E_{\text{down}} = V_{\text{down}}/d$ and $E_{\text{up}} = V_{\text{up}}/d$, where $V_{\text{up,down}}$ is the applied voltage and d denotes the separation between the electric-field plates[1]. Substituting Eq. (3.5) into Eq. (3.4) yields the charge equation

$$Q = 9\pi d\sqrt{\frac{2\eta^3}{g(\rho_{\text{oil}} - \rho_{\text{air}})}}\left(\frac{v_{E_{\text{down}}} - v_{E_{\text{up}}}}{V_{\text{down}} + V_{\text{up}}}\right)\sqrt{\frac{v_{E_{\text{up}}}V_{\text{down}} + v_{E_{\text{down}}}V_{\text{up}}}{V_{\text{down}} + V_{\text{up}}}}. \tag{3.6}$$

To improve the precision and accuracy of our measurements, we explicitly include the dependence of η and ρ_{air} on ambient temperature and pressure. We define the following function

$$F(T,P) = \sqrt{\frac{2}{g(\rho_{\text{oil}} - \rho_{\text{air}})}}\,\eta^{\frac{3}{2}} = \sqrt{\frac{2}{g(\rho_{\text{oil}} - c\frac{P}{T})}}\left(\frac{aT^{\frac{3}{2}}}{b+T}\right)^{\frac{3}{2}}, \tag{3.7}$$

where $\rho_{\text{air}} = c\frac{P}{T}$ and $\eta = \frac{aT^{\frac{3}{2}}}{b+T}$ and parameters are given as $a = 1.485 \times 10^{-6}\,\frac{\text{kg}}{\text{m sec}\sqrt{^\circ\text{K}}}$, $b = 110.4^\circ$K, and $c = 3.489 \times 10^{-3}\,\frac{\text{kg}\,^\circ\text{K}}{\text{m}^3\text{Pa}}$. The parameters P and T denote the ambient air pressure (Pa) and the ambient temperature (°K) respectively. Equation (3.6) becomes

$$Q = 9\pi d\ F(T,P)\left(\frac{v_{E_{\text{down}}} - v_{E_{\text{up}}}}{V_{\text{down}} + V_{\text{up}}}\right)\sqrt{\frac{v_{E_{\text{up}}}V_{\text{down}} + v_{E_{\text{down}}}V_{\text{up}}}{V_{\text{down}} + V_{\text{up}}}}. \tag{3.8}$$

Equation (3.8) clearly shows that the charge on a drop can be calculated by measuring terminal velocities alone. All other parameters are entered into the acquisition program.

[1] $V_{\text{up,down}} = \pm 13\,\text{kV}$ and $d = 9.4\,\text{mm}$

Chapter 4

Apparatus

4.1 Drop Generator

The part of the apparatus that has required the most development is the generator for producing small and uniform size oil drops. The design of the oil drop generator, called the dropper for the sake of brevity, is based on a combination of ideas for fluid drop ejectors originally developed at San Francisco State University [1]–[4] and Lawrence Livermore Laboratories. Nevertheless, we have had to make many improvements.

As shown in Fig. 4.1, the dropper consists of a brass tube with an inside diameter of 4.8 mm, wall thickness 1.6 mm and length 6.4 cm. An annular piezoelectric transducer disk made from lead zirconate titanate with an inside diameter of 6.4 mm, outside diameter 25.4 mm, and thickness 2.5 mm is attached around the lower portion of the tube with epoxy. A 9.5 mm diameter stainless steel orifice plate of 0.4 mm thickness with an 8 μm diameter concentric hole is affixed to the bottom of the dropper also with epoxy. The 8 μm diameter hole fixes approximately the diameter of the drop. The exact diameter depends on the voltage with which we pulse the transducer.

The dropper is filled with silicone oil and placed under a low-grade vacuum for about one and a half hours. This is done so that air bubbles acquired during the filling process are removed. A plastic tube with an inner diameter of 4.8 mm and approximately 30 cm long is placed over the opening of the dropper and is likewise

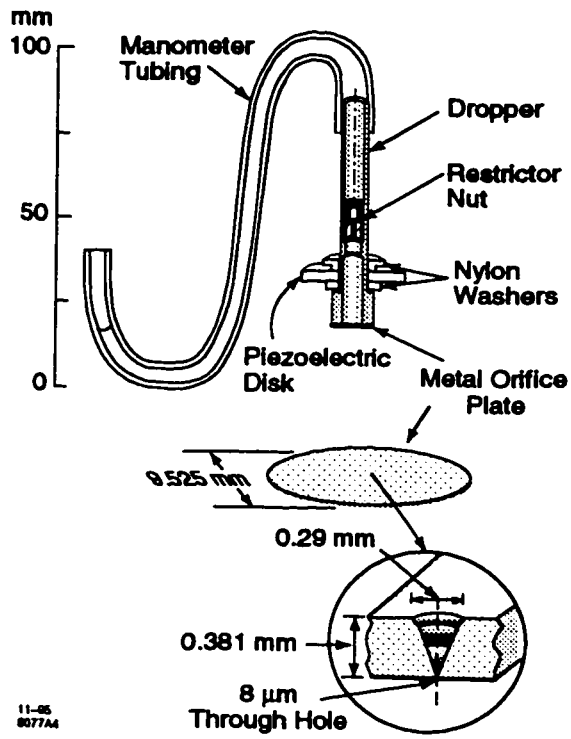

Figure 4.1: Drawing of the dropper and of the orifice plate affixed to the bottom of the dropper. A cross section of the orifice plate is pictured at the lower right. It shows the conical features of the 8 μm hole that determines approximately the size of the drops. Dimensions for the orifice plate were obtained by studying the plate under an electron microscope. The slope of the conical sides of the orifice changes from approximately 32° from the vertical near the top to 20° from the vertical and finally to 18° from vertical. At the very bottom of the plate, the orifice is cylindrical.

filled with oil. The end of the tube is varied in height relative to the bottom of the dropper to control the amount of relative pressure at the fluid meniscus of the ejection orifice (Fig. 4.1). The dropper holds approximately 6 g of oil that was changed about every 2 million drops.

Drop ejection is initiated when the piezoelectric transducer contracts radially upon receiving an electrical pulse from the high-voltage pulse amplifier [57]. This contraction squeezes the dropper and forces drop ejection. In our case, the transducer is pulsed at a driving voltage ranging from 130 to 160 V with a pulse width ranging from 0.85 to 1.2 μs. A restrictor nut sits inside the dropper so that there is a node for the pressure wave arising from the transducer pulse. The transducer then relaxes to its rest state until the next electrical pulse. The negative pressure wave caused by the relaxation of the piezoelectric material to its equilibrium state retracts the fluid into the dropper. The fluid column retraction takes place in the long conical column of the orifice hole, thus preventing air from being drawn into the main fluid chamber (Fig. 4.1). Capillary action then restores the meniscus, so that upon the next electrical pulse, drop ejection is once again initiated. A slightly negative manometer pressure is necessary to prevent excessive surface wetting of the orifice and fluid leakage during the equilibrium state. Empirically, it has also been observed that a slightly negative manometer pressure gives more reliable single drop production. (For a general introduction to drop-on-demand systems, see [58] and the references therein.)

4.2 Charge Inducer Mechanism and Charge Separator

The dropper is situated in a 2.5 cm diameter Delrin holder with a 0.28 mm thick concentric steel charge inducer plate located parallel to the ejection orifice with a 1 mm separation (Fig. 4.2). The inducer plate has a 100 μm through hole. No electrical contact is made between the dropper, which is grounded, and the inducer plate, which is held at a positive or negative voltage, depending on whether we wanted to induce

net positive or negative charge on the drops. However, because we preferred to work with neutral or close to neutral drops, the charge inducer was very rarely used.

The dropper and holder are placed inside a 2.5 cm hole in a 12.7 mm thick sheet of transparent acrylic. The acrylic sheet is attached to an x-y stage used for aligning the dropper to the charge separator. The base of the x-y stage is mechanically connected to a 6.4 mm thick sheet of transparent acrylic that has a 2.5 cm hole that holds the separator. The charge separator consists of two small, flat electrode plates about 0.25 mm thick, 8 mm wide and 1.2 mm high inserted along two diametrically opposite grooves milled into a 3 cm high Delrin rod. A transverse electric field is set up between the two electrodes. During the troubleshooting phase of the experiment, we used the charge separator to spatially separate the charged drops. A typical value of the magnitude of this field would be 2×10^4 V/m. The actual field, however, depended on the tests we were running. The charge separator was not used during data acquisition.

4.3 The Electric-Field Plates

The stainless steel electric-field plates are 15.24 cm in diameter and have 0.79 mm concentric holes through which the drops fall. The dropper, holder, and charge separator ensemble is placed in a 2.5 cm through hole in a 22.9 cm $\times$ 30.5 cm nylon platform, which is attached to the top electric-field plate with screws. The bottom plate is likewise attached to a second nylon platform with the same dimensions as the first. In addition to attaching the electric-field plates to the nylon platforms, the screws have the added benefit of enabling us to adjust the parallelism of the plates. The two platforms are connected by pillars at the four corners. Since the drops used are 7.1 μm in diameter, they are extremely sensitive to air currents. Therefore, it is necessary to provide shielding against convection and other air currents by isolating the electric-field region. Thus, the remaining four faces of the box are covered with 6.35 mm thick transparent acrylic. This material was chosen so that we can illuminate and view the falling drops. The entire assembly is located within another chamber with 9.5 mm thick transparent acrylic walls because we had observed that a single air

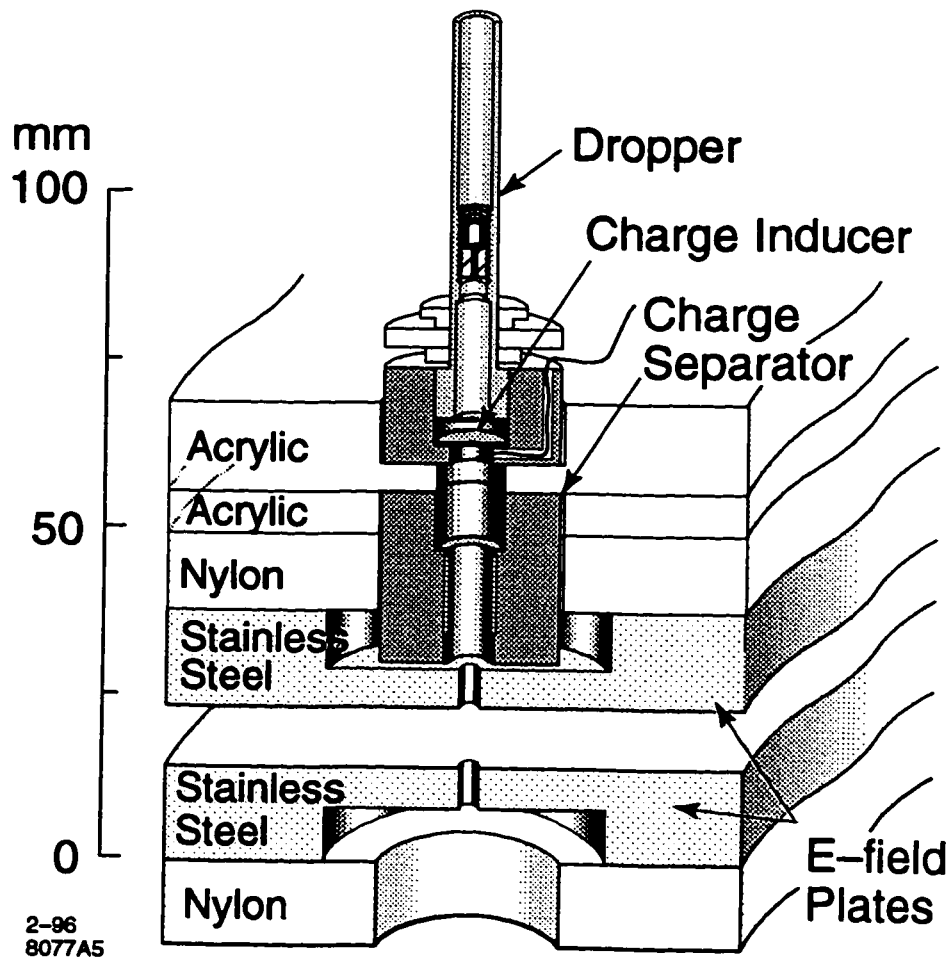

Figure 4.2: Cross sectional view of the entire dropper ensemble. The dropper is situated in a Delrin holder placed in a sheet of transparent acrylic that is attached to an x-y stage used to align the dropper to the charge separator. The second acrylic sheet holds the charge separator and is fastened to the nylon platforms. The electric-field plates are attached to the nylon platforms.

current shielding box was insufficient (Fig. 4.3).

4.4 Drop Velocity Measurement Method

The drops are backlit by a stroboscopic source [59] flashing at 9.99 Hz (Fig. 4.4). A 210 mm focal length thick lens, 30 cm away from the dropper, focuses the image of the drop's shadow as it falls between the two electric-field plates onto a CCD video camera 106 cm away from the lens. The RS-170 (US black and white television) analog signals from the CCD camera are converted to a digital image by a video capture card installed in a 90 MHz Pentium desktop computer. The data acquisition program analyzes the image and locates the position of the drop. Two captured images are required for one velocity measurement. The time between image captures is 100.1 ms. After one velocity measurement is completed, the electric field switches direction and two more images are captured for another velocity measurement. In this way multiple velocity measurements are made per drop. For every two velocity measurements, one charge calculation is generated according to Eq. (3.8).

Since our charge measurements are determined by measuring velocities, determining the time intervals between drop measurements and the position of the drops has to be performed with high precision. The clock pulses coming from the CCD camera are separated by 100.1001 ms with a variation of approximately 0.5 μs. The electric-field switching time was verified on an oscilloscope using an internal 1000:1 voltage divider. It was ascertained that the switching time was sufficiently short that the electric field is able to settle to its final value before the next measurement cycle begins. This switching time constant was measured to be approximately 4.7 ms. The position precision of the drops is discussed in the following sections.

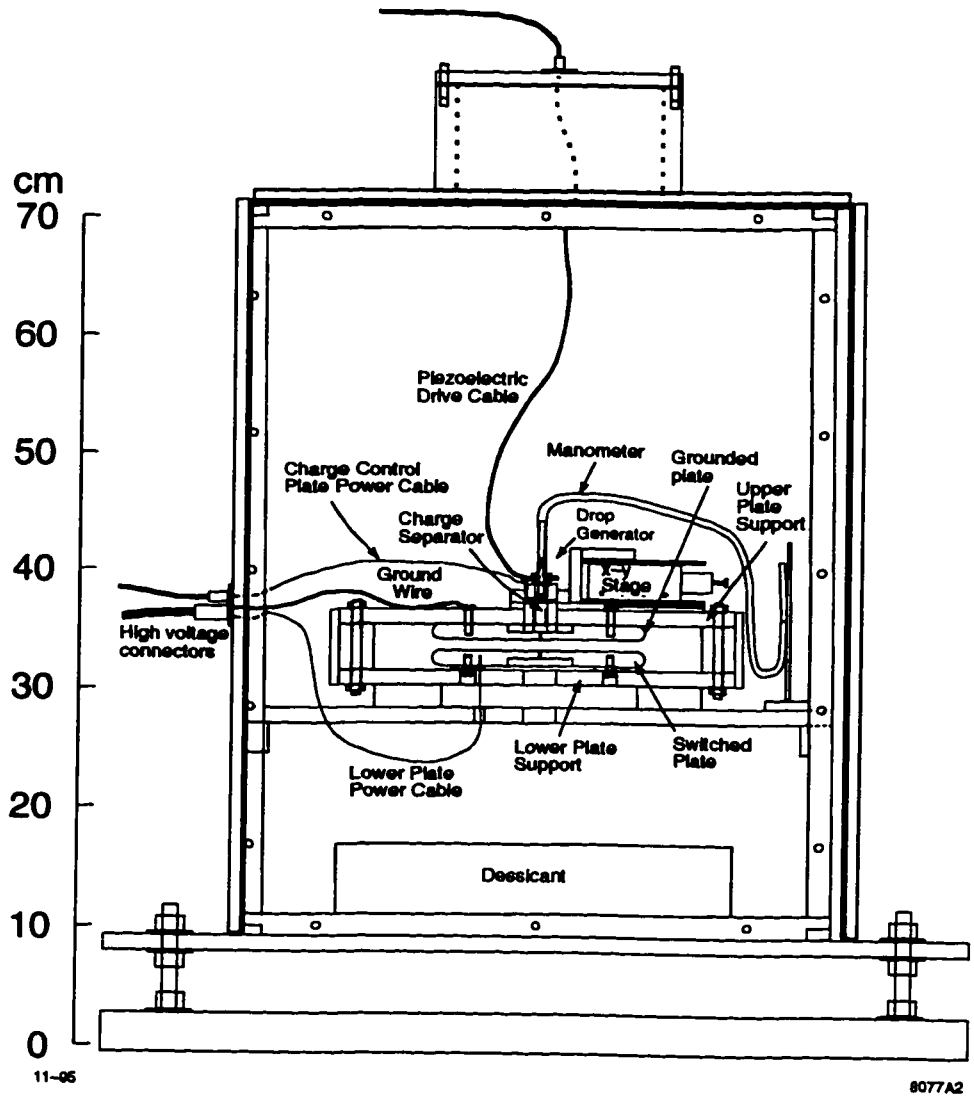

Figure 4.3: Diagram of the experimental chamber.

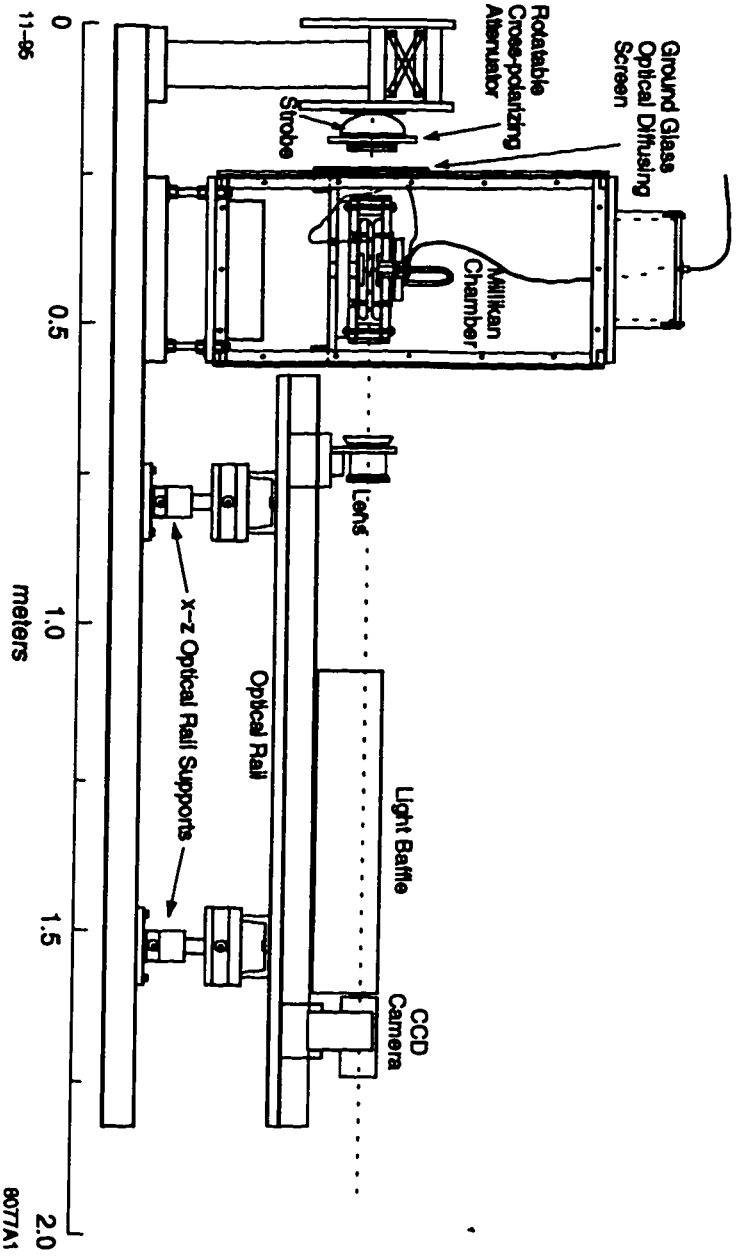

Figure 4.4: Diagram of the experiment showing the stroboscopic source at the far left, the apparatus, lens and CCD camera.

4.5 Camera, Image Digitization Card, and Drop Position Precision

The drops are imaged with a standard RS-170 output commercial grade CCD video camera [60]. The active region of the CCD sensor is a rectangular region that is 6.4 mm by 4.8 mm, divided into 182,710 (755 by 242) pixels. The strobe flash illuminates the active region of the CCD camera for 4 μs and the entire active region is read out and encoded in each RS-170 field. The dimensions of a pixel are 8.5 μm along the 6.4 mm dimension and 19.5 μm along the 4.8 mm dimension. Within the 4.8 mm, there are 242 pixels; an internal pseudo-interlacing procedure involving intensity averaging over alternate vertical pixels generates the 484 scan lines required by the RS-170 video standard. The CCD chip uses full frame transfer technology that gives a theoretical 100% fill factor for the photosensitive regions. The camera is rotated 90° from the usual orientation so that the 6.4 mm direction is parallel to the path of the falling drops. This gives higher measurement resolution and avoids the image position distortion caused by the internal pseudo-interlacing procedure.

The optical system images from the drop plane to the camera focal plane with a magnification of about 4.0. Thus, each CCD camera pixel images an area of 2.1 μm high by 4.9 μm wide in the real space of the falling drops. Recall that the drops are 7.1 μm in diameter. The rms vertical positional accuracy with which the drops could be located in the real space of the falling drops was less than $\sigma_z = 0.35\,\mu$m, which corresponds to 17% of the vertical pixel dimension.

The charges on the 755 by 242 CCD pixels are transmitted via RS-170 standard video signal to a video image capture device, a monitor and a video cassette recorder. This video image capture device is an ImageNation Cortex-I, 8 bit (256 gray scale) resolution, memory buffering image capture card. CCD imaging systems that do a direct transfer of digitized CCD image to computer memory are available, but are generally an order of magnitude more expensive than standard RS-170 analog output cameras.

Each horizontal video line (vertical real space) is digitized internally by the capture card into 512 memory mapped pixels representing 3.1 μm in real space in the image

plane of the falling drops. Since RS-170 signals are internally dual-interlaced and a strobed image produces illumination over only one of the two internally overlapping fields, the camera vertical line resolution (horizontal real space) is only 242 lines. This is not an important loss of data because the lateral velocities of the drops are near zero and are not used to determine the electric charge on the drops. The reduction of real space vertical pixel resolution from the 755 CCD pixels per scan line to an internally represented 512 pixels also does not represent a significant loss in position information because the horizontal modulation transfer function of the camera goes to zero past the 550 horizontal lines due to electrical bandwidth limitations.

4.6 Drop Position Algorithm

The essence of the drop position algorithm is to repeatedly find the real space position of a single drop image by computing the weighted centroid of the pixel intensities of the drop image. Since the drop is backlit, the shadow is darker than the background illumination, so the pixel gray scale values are inverted (*i. e.* 255 minus gray scale value) before weighing to ensure that the darker pixels receive more weight. Based on the available computational power, the algorithm design philosophy is to locate and track the position of a single drop image in a single pass of the image without performing detailed (and computationally intensive) image analysis and without storing any image data. In order to do this within 100 ms, the algorithm had to be simple and concise. However, the simplicity required of the algorithm to meet the 100 ms time budget introduced the possibility of false triggers due to multiple drop images in the same field of view. Therefore, it was necessary to add real time cuts to the data.

The algorithm consists of two steps: search and track. In the search step, no valid drop images were located in the previous frame and any previous track histories were written to disk and no longer available. Each subsequent frame is examined using a two-level trigger to locate a drop image in the frame. The first level searches the frame by examining every other pixel of every other row for any pixels that are darker than some threshold value. If at least one dark pixel is found, a coarse centroid of all dark pixels is passed to the second level trigger. If there are two or more drops, the

centroid is computed with pixels from both. The ideal algorithm would compute the distances between various dark pixels so that clusters can be detected and multiple coarse centroids computed. In practice, however, such an algorithm proved to be too computationally intensive to use in a real time search.

Since the algorithm is designed to measure the charge of only one drop at a time, the second level trigger was designed to eliminate the case where two drops are in the field of view at the same time or there was sufficient nonuniformity in background illumination to cause one or more background pixels to fall below the threshold. However, as discussed in Sec. 6.2.1, double drops still posed a problem. Using the coarse centroid of dark pixels passed from the first level trigger, the second level trigger examines the 11×11 pixel subframe centered on the coarse centroid. In a single pass, it computes an average of the four corner pixels to determine the level of the background illumination, sorts the remaining 117 pixels and computes a refined centroid using only the twenty darkest pixels after subtracting the mean background illumination. If the mean weight per pixel of the twenty darkest pixels (assumed to be part of the drop image) is more than two below the mean background, then the trigger passes the refined centroid to the tracking routine as a valid drop position.

If the first level falsely triggers on random fluctuations in the background illumination, the second level trigger should reject the event since the rms fluctuation of the background illumination has consistently been observed to be less than two levels of gray scale from the mean value when averaged over an 11×11 subframe. If the first level triggers on two drop images in the field of view, then, if the drop centroids are separated by more than $50\,\mu$m in real space and are of equivalent darkness, the coarse centroid will fall in the region between the drops. If the drops are much closer, then the second level trigger will pass this detection as a valid drop, leaving the final rejection to the tracking algorithm.

The tracking algorithm uses the same two level trigger as the search algorithm and maintains a stack of at most four drop positions at any given time, since this is all that is required for a single charge measurement. When a track has been started and a frame fails to pass the search trigger, all track data is written to disk and the algorithm returns to search mode. Additionally, if there is a drop image that was

near the bottom of the field of view in one frame and there is another image near the top of the field of view in the next frame, the tracker assumes that one drop exited and a new one entered and writes all past track data to disk and starts a new track.

Two positions are recorded for each orientation of the field to determine $v_{E_{\text{up}}}$ and $v_{E_{\text{down}}}$. If the drop moves in a direction opposite the field orientation, then the velocity is signed negative. The horizontal velocities are also calculated and used to reject drop trajectories that have a sudden increase in horizontal velocity. This is the first cut on a multiple drop event, since a heavy, fast-moving drop may overtake a slower drop for one or two frames, which pulls the centroid to one side and causes a large horizontal velocity. When one velocity for each field orientation is measured, the tracker computes the charge. We can see from the Eq.(3.8) that it might be possible to compute an imaginary result. Physically, this can never happen. Therefore, this becomes the second cut on multidrop events.

Chapter 5

Development and Operation of the Experiment

5.1 Development of the Experiment

Our goal in the experiment was to search for isolated fractional electric charge in about 1 mg of Dow-Corning 200, 5 centistoke silicone oil. In the beginning of the experiment, we knew that we required drops with diameters of 10 μm or less to obtain sufficiently good charge measurement precision. However, there were many questions that could only be answered by experimentation. Among these were: How uniform would be the drop size? At what rate could we make the drops? What drop size would give the best precision? How rapidly could a PC-type desktop computer with a video image capture board determine and record the drop charge in real time?

Therefore, when we began operating the experiment in February 1995, we mixed periods of data acquisition with periods of apparatus testing, apparatus improvement, computer program improvement and troubleshooting. By April 1995, we were able to devote most of the experimental time to data acquisition. The experiment had to be interrupted for about two months in the early summer of 1995 when a five-month long renovation of the roof and air-conditioning system of the building forced us to move the apparatus to a seismically quieter location. The experiment was resumed

in July 1995 and ended in September 1995.

During the entire experiment, we saved the position-time trajectory measurements of every drop produced during a data acquisition run on the hard drive of the acquisition computer. When the hard drive reached maximum capacity, we transferred all the data for all the runs on the hard drive to back-up data cartridges and then proceeded to purge the hard drive.

In the early stages of the experiment, we found that the precision of the drop charge measurement improved as the drop diameter decreased. The principal reason is that smaller drops have smaller gravitational terminal velocities, as shown in the following equation

$$v_{g,\text{terminal}} = \frac{2r^2(\rho_{\text{oil}} - \rho_{\text{air}})g}{9\eta} \tag{5.1}$$

Drop charge measurement precision improves as the ratio $v_{E,\text{terminal}}/v_{g,\text{terminal}}$ increases, $v_{E,\text{terminal}}$ being the component of velocity produced by the QE force (Eqs. (3.1) and (3.2)). On the other hand, since the goal of the experiment was set at 1 mg total of drop masses, the smaller the drop, the larger the number of drops that must be studied. We compromised with a drop diameter of 7.1 μm. Figure 5.1 shows the size uniformity of the drops produced.

We found that two factors placed an upper limit on the rate at which drops could be generated and their charge measured. First, the algorithm for finding the drop position failed if the image captured more than one drop (Sec. 4.6). Second, for reasons we did not understand, as the drop generation rate increased above 1 Hz, drop production became irregular until two or more drops are produced simultaneously. This led to unreliable data as discussed in Chapter 6. Therefore, for clean, consistent data we set the drop generation at 0.6 Hz. As discussed in Chapter 8, our goal for the next experiment is to considerably increase the drop generation rate. Since the end of the experiment, we have found a way to operate the dropper with a frequency greater than 100 Hz.

The drop position detection algorithm was also determined to be sensitive to nonuniformity in the light field illumination. By affixing a ground glass screen on the side of the experimental chamber facing the strobe, we were able to diffuse the

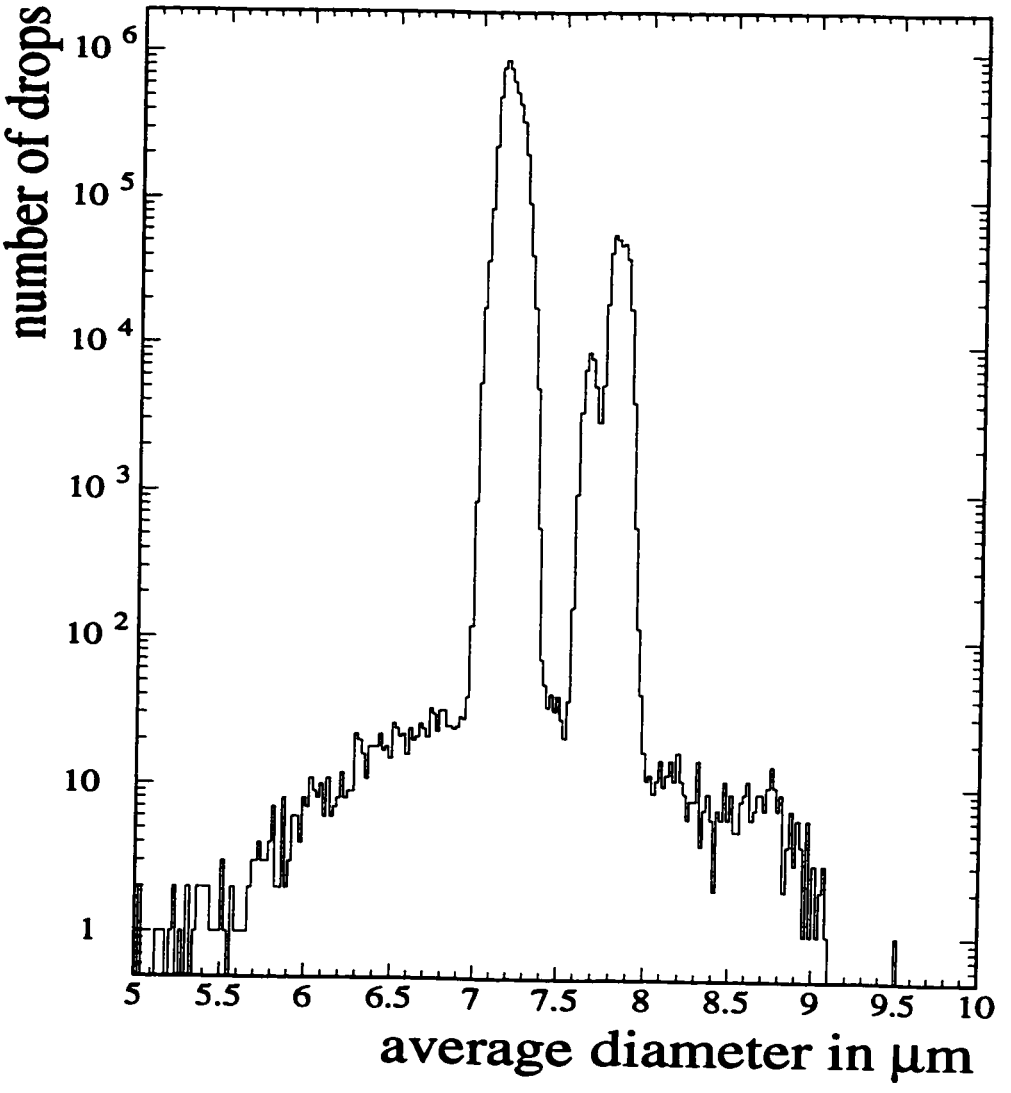

Figure 5.1: Histogram of the average diameter of the drops produced. The initial stage of data acquisition utilized 7.6 μm drops. The remainder of the experiment used 7.1 μm drops.

light from the stroboscopic source and thereby improve the uniformity of the light field illumination (see Fig. 4.4). We also found that the light distribution from the stroboscope changed slightly as the bulb aged. Therefore, we periodically readjusted the bulb position slightly and we replaced it once.

As the experiment went along, a phenomenon occurred and recurred which we do not yet understand. As already mentioned above, except for the first stage of operation, we did not attempt to induce any charge on the drop; the charge induction voltage was set to zero. Then most of the drops had zero charge with a few drops having charge $\pm 1\,e$ and rarely $\pm 2\,e$. After a few months of operation, we noticed the charge distribution spreading to $\pm 3\,e$, $\pm 4\,e$, and even $\pm 5\,e$ with fewer drops having zero charge. We preferred to have $0\,e$, $\pm 1\,e$, or $\pm 2\,e$ because the precision of the charge measurement is better when the drop charge is small (see Appendix B); and a large charge spread leads to more drop measurements not meeting the criteria outlined in Sec. 6.2. The only way we found to reduce the charge distribution spread was to remove the old oil in the dropper and fill the dropper with new oil, the new oil being taken from the same storage container as the old oil. Then over a period of several months, the limits of the charge distribution once again spread from $\pm 2\,e$ to $\pm 5\,e$. Our speculation is that ions form in the oil either due to chemical interaction of the oil with the dropper material or due to diffusion of contaminants that appear because the manometer is open to the atmosphere. We have no evidence for this speculation.

5.2 Operation of the Experiment

During periods of data acquisition, we operated the experiment continuously, 24 hours per day and 7 days per week. Table 5.1 illustrates the data and calculations recorded for each drop on the computer hard disk. The data acquisition was divided into runs about 9 hours long, each run containing about 10 Mb of data. The data from each run was put through a data analysis program to look for any free fractional electric charges and to make sure the apparatus was working properly. If the data showed unusual properties, such as an abnormally high drop rejection rate, data acquisition

was stopped until a solution was found. When about 600 Mb accumulated on the hard disk, the data was transferred to a back-up data cartridge.

drop no.	polarity	row_1	column_1	row_2	column_2	v_x	v	Q/e
1	−1	180.971	38.341	181.366	84.301	0.0093	1.3830	—
1	+1	181.696	129.739	181.972	174.972	0.0065	1.3611	0.0605
1	−1	182.710	220.573	183.127	266.399	0.0098	1.3789	0.0493
1	+1	183.432	311.861	183.499	357.009	0.0016	1.3585	0.0564
1	−1	184.369	402.686	184.353	447.772	-0.0004	1.3566	−0.0052

Table 5.1: Sample of data taken for a typical drop. The drop is identified by a tag number shown in the first column. The field direction is given by the polarity. A polarity of −1 indicates that the electric field is pointing down and a polarity of +1 indicates that the field is pointing up. The values under the columns entitled row_1, $column_1$, row_2, and $column_2$ locate the centroid of the drop in terms of pixels at two different times separated by 100.1 ms. (The pixel positions are shown to three decimal places for convenience in performing calculations, but the measurement precision is about one decimal place.) The horizontal velocities of the drop are shown in the column entitled v_x and the vertical velocities of the drop are given in the adjacent column, both in mm/s. The last column shows the net charge on the drop.

Chapter 6

Data Analysis

During the course of the experiment, we measured the charge on 6,161,651 drops. Using the criteria for acceptance of drop charge measurement discussed in Sec. 6.2, there are 5,974,941 drops in the accepted charge measurement category. Thus, approximately 3% of the drops were rejected. The accepted drops have a total mass of 1.07 mg and comprise a total of 6.41×10^{20} nucleons.

6.1 Presentation of Data

Figure 6.1 is a histogram of the accepted charge measurements for the 5,974,941 accepted drops. The distribution shows that most drops have a charge Q in the range between $\pm 5\,e$ with the $0\,e$ peak dominant. As discussed in Appendix B, neutral drops led to slightly higher precision charge measurements.

In analyzing the data, we define N_c as the signed integer closest to Q/e. Then

$$q = \frac{Q}{e} - N_c \tag{6.1}$$

is the signed deviation of the measured charge from the closest integer charge. Figure 6.2 is a histogram of q for the entire experiment. This histogram is approximated by a Gaussian distribution with

$$\sigma_q = 0.025. \tag{6.2}$$

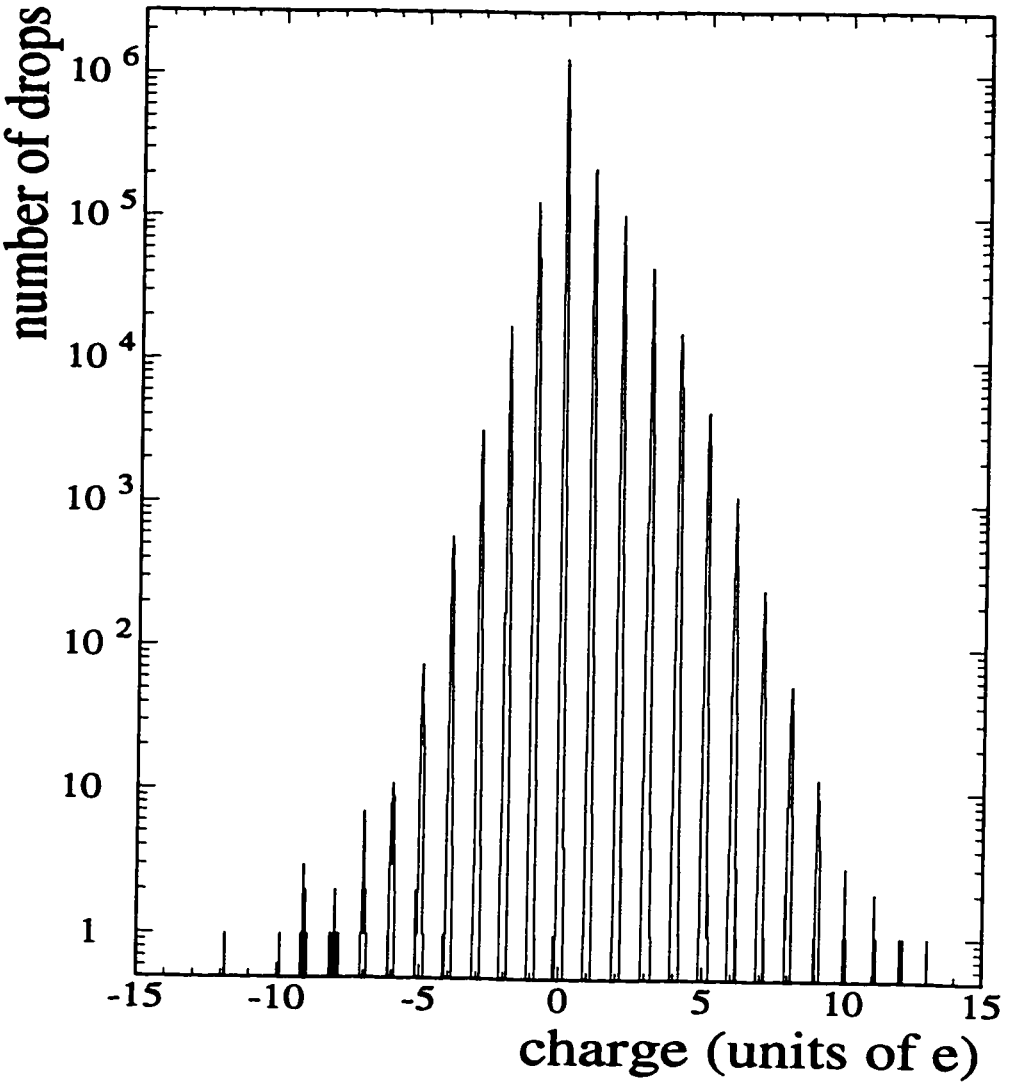

Figure 6.1: Histogram showing the distribution of the charge on the 5,974,941 accepted drops. Note that a majority of the drops are neutral or are close to neutral.

This fit has a χ^2 per degree of freedom of about 1.5. This is the experimental precision of the drop charge measurement. We are pleased with this small σ_q. In Sec. 6.3, we discuss the factors that may be preventing an even smaller σ_q.

Figure 6.3 is another presentation of the data shown in Fig. 6.2. We define N_s as the largest non-negative integer less than $|Q|/e$ and then define

$$q_s = \frac{|Q|}{e} - N_s. \tag{6.3}$$

This is the histogram that we use to search for fractional charge, hence the subscript s for search. Figure 6.3 also shows the search range to which q_s is sensitive. During the experiment, we looked at the data as it was produced in the presentation of Fig. 6.3. Our provisional criterion for possible fractional charge events was that

$$0.2 < q_s < 0.8. \tag{6.4}$$

Such a drop would have a charge differing by more than 8 standard deviations from an integer charge and its charge should be measured with the same precision as the other drops. From Fig. 6.3, we see that there are no fractionally charged particles with a charge of $\pm\frac{1}{3}e$ or $\pm\frac{2}{3}e$. We note that there is one event that shows an absolute charge greater than $0.2e$. The charge on that drop was $-0.2045\,e$. Therefore, that event is merely part of the tail. (We also note at this point that fractionally charged particles with measured charge within $0.2\,e$ of integer charge is indistinguishable from our measurement spread unless a significantly large peak were found that rose above the tail.) The final criteria for the fractional charge search are discussed in Sec. 6.2.

6.2 Criteria for Acceptance of a Charge Measurement

As discussed in Chapter 3, the determination of the charge and radius of a drop requires two velocity measurements, $v_{E_{\rm up}}$ and $v_{E_{\rm down}}$. The first velocity measurement

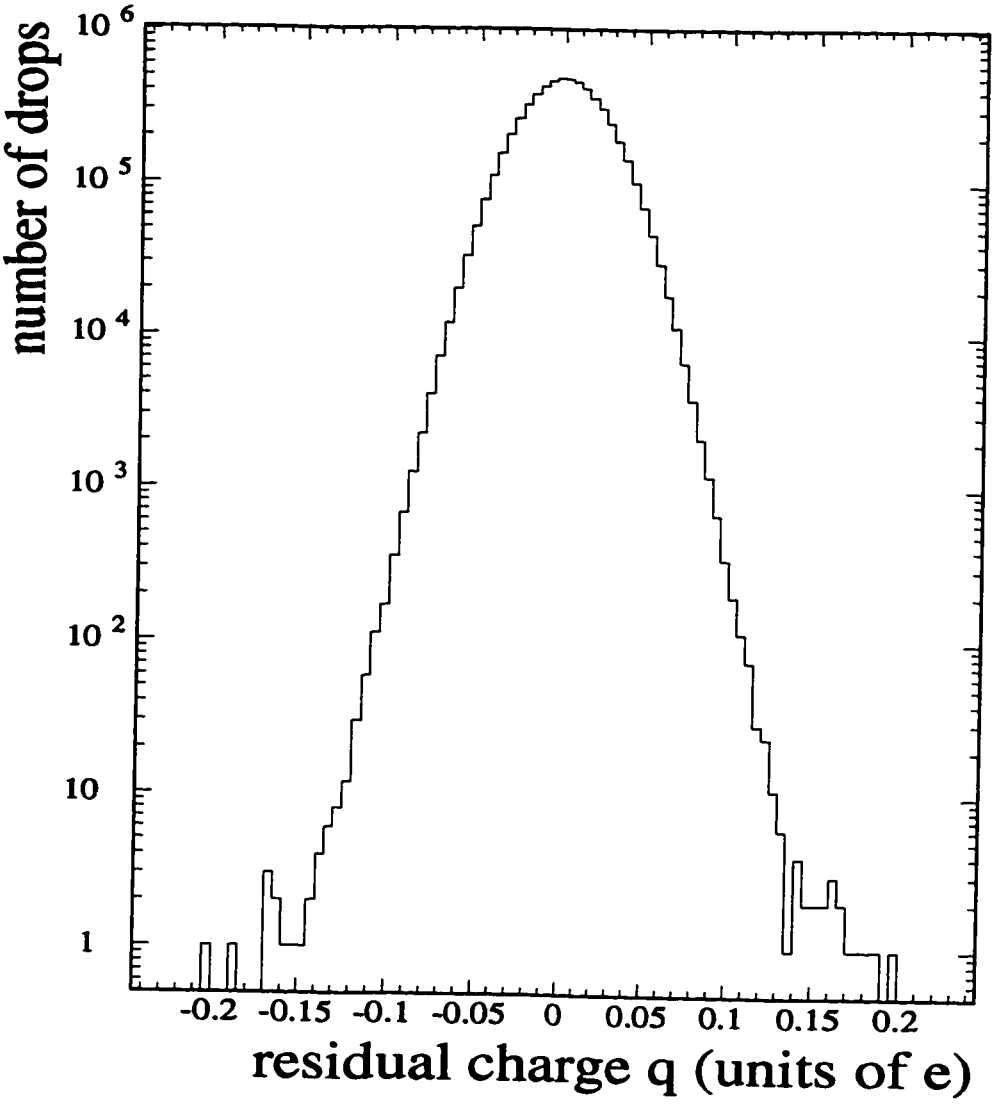

Figure 6.2: Histogram showing the residual charge on the 5,974,941 drops. The residual charge is defined by $q = \frac{Q}{e} - N_c$. A Gaussian fit yields $\sigma_q = 0.025$.

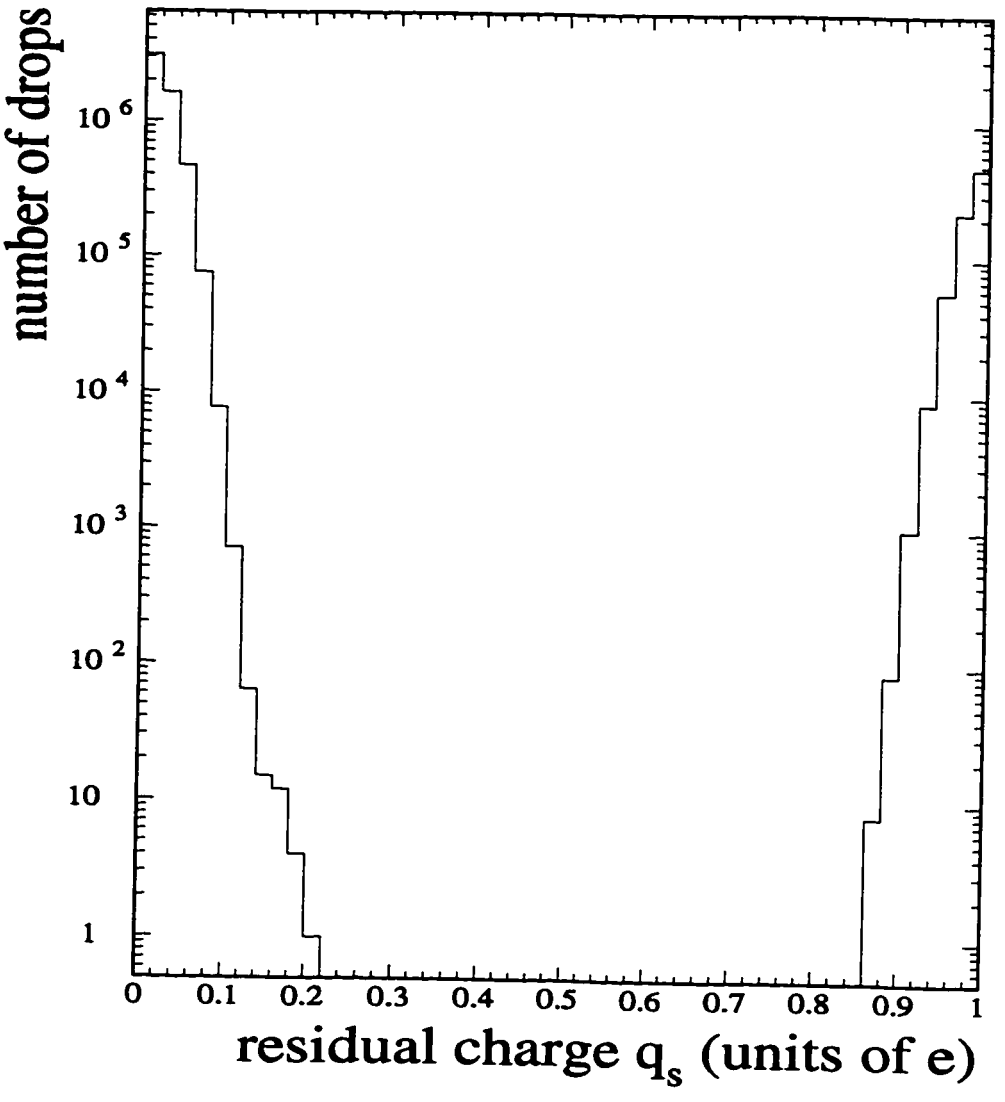

Figure 6.3: Another representation of the data presented in Fig. 6.2 showing the residual charge. Here, residual charge is defined by $q_s = \frac{|Q|}{e} - N_s$. Histograms of this type were viewed for the individual runs to look for anomalous events.

requires two vertical position measurements, z_a and z_b; the second velocity measurement likewise requires two vertical position measurements, z_c and z_d. If the charge on the drop changes at any position between z_a and z_d, a false fractional charge would be measured. The charge would change if a free ion or electron attaches itself to the drop or if the drop is hit by a cosmic ray. Therefore, a single measurement of the charge on a drop cannot be used for a fractional charge search.

Two measurements of charge, Q_1 and Q_2, on a given drop would allow a test for charge change by considering the difference $\Delta Q = Q_2 - Q_1$. However, we felt more confident with requiring at least three measurements of charge per drop as it falls between the electric-field plates. This criterion of at least three charge measurements requires at least four different velocity measurements, which, in turn, require at least 8 different position measurements along the trajectory of the drop. This means that the first and the third measurement of charge on a given drop are completely independent. Thus, the first criterion of an acceptable drop charge measurement is

$$\textit{criterion 1: 3 or more charge measurements.} \tag{6.5}$$

We use the arithmetic average

$$Q = \frac{Q_1 + \ldots + Q_n}{n}, \text{ where } n = 3,\ 4,\ \text{or } 5, \tag{6.6}$$

to define the charge Q on the drop. To eliminate measurements that contain a charge change, we define

$$Q_{\min} = \min(Q_1, \ldots, Q_n), \tag{6.7}$$

$$Q_{\max} = \max(Q_1, \ldots, Q_n), \tag{6.8}$$

$$\Delta Q = Q_{\max} - Q_{\min}. \tag{6.9}$$

We then require

$$\textit{criterion 2:}\quad \Delta Q < \Delta_{\text{crit}} \tag{6.10}$$

for the charge measurement on a drop to be called acceptable. The majority of all

drops, 87.7%, have four charge measurements, 5.9% have three and 6.4% have five. Our final choice for Δ_{crit} is outlined in the following subsection.

These two criteria were originally developed to eliminate drop charge measurements that contained a charge change, but they turned out to be crucial in the elimination of two instrumention effects. The first instrumentation effect is that the drop position algorithm depends upon uniform light field illumination of the falling drop. This uniformity was checked frequently by the experimenters and adjusted when necessary, but these adjustments had to be done by hand. Furthermore, the performance of the stroboscope bulb deteriorated with age and was affected by the line voltage of the building. We found that deviations from illumination uniformity could interfere with precise Q measurement by introducing noise in the target window. This noise appears as darkened pixels that would be taken by the drop finding algorithm as part of the drop centroid it is locating. This would give an erroneous position of the drop and, therefore, an erroneous charge measurement.

The second instrumentation effect eliminated by the two criteria is the inability of the drop finding algorithm to analyze events with more than one drop per video frame. Multiple drops might appear in a frame for two reasons. First the dropper occasionally produced two drops simultaneously. Second, drops produced at the rate of 0.6 Hz might occasionally appear in the same frame. As an illustrative example, consider two drops, one positively charged and the other neutral. Assume that the neutral drop emerges from the dropper first. The positively charged drop then is initially only 1.67 s behind. But before either drop enters the active imaging area, they are affected by the electric field leaking through the 0.79 mm hole in the upper electric-field plate. The electric field always starts negative and field switching begins only after a drop enters the measurement region. Therefore, a drop experiences a negative field on average. The negative electric field leaking through this hole will accelerate the positively charged drop so that the spacing between the neutral drop and the positive drop will be diminished. Both drops reach terminal velocity, however, before they enter the measurement region of the electric field and on average the charged drop falls with the same velocity as the neutral drop during the time of measurement; therefore, the diminished spacing between the drops remains and they

may appear in the same video frame.

6.2.1 Determining the Final Value for Δ_{crit}

As a preliminary analysis of the data, we considered in detail all drops for which

$$0.2 < q_s < 0.8 \tag{6.11}$$

and

$$\Delta Q < 0.4\, e. \tag{6.12}$$

We called such drops anomalous.

At first we simply looked at the three separate charge calculations and the velocities from which the charges are derived. Then about one third of the way through the experiment, we began to record on cassette tape the video image of the falling drops. We then looked back after each run at the video image of the anomalous drops if there were any. Initially we videotaped 16 hours per day; eventually going to 24 hours per day when the videotaping system was upgraded. Taking into account that our videotaping was incomplete, as just explained, we found that about 43% of the anomalous drops videotaped actually consisted of two close together drops. Such a configuration leads to errors in the calculation of the drop position because the centroid found by the drop finding algorithm is not the true centroid of either drop. We visually inspected over 10^3 drop images wherein the drops had

$$0.0 < q_s < 0.2 \quad \text{or} \quad 0.8 < q_s < 1.0$$

and none of the viewed drops showed a double drop in the video image.

Returning to the anomalous drops defined by Eqs. (6.11) and (6.12), we found a total of 31 drops divided as follows:

10 drops: no video image,

12 drops: video images show 1 drop per image,

9 drops: video images show 2 drops per image.

As we mentioned earlier, we used the the inequality, $\Delta Q < \Delta_{\rm crit}$, as a criterion to reject charge measurements in which there was a charge change during the measurement, and we used $\Delta_{\rm crit} = 0.4\,e$ during the data acquisition period in order to study the tails of the ΔQ distribution. However, approximately 97% of all charge measurements have $\Delta Q < 0.15\,e$ (Fig. 6.4). Since we expect the ΔQ distribution will be the same for drops with non-integer charge as for drops with integer charge, our final ΔQ acceptance criterion is

$$\Delta Q < 0.15\,e. \tag{6.13}$$

Our final criteria for non-integer charge events are then

$$\begin{aligned} 0.2 < q_s < 0.8, \\ \Delta Q < 0.15\,e. \end{aligned} \tag{6.14}$$

These are the criteria for the data shown in Fig. 6.3.

6.3 Limitations on the Precision of Charge Measurement

We have considered, and where possible, calculated or measured, the following phenomena which may limit the precision of the drop charge measurement:

1. Brownian motion of the drop in air.
2. Change in mass of the drop by evaporation during fall.
3. Force on the drop due to the induced dipole moment.
4. Precision of drop position measurement.
5. Apparatus vibration.
6. Air currents in the Millikan chamber.

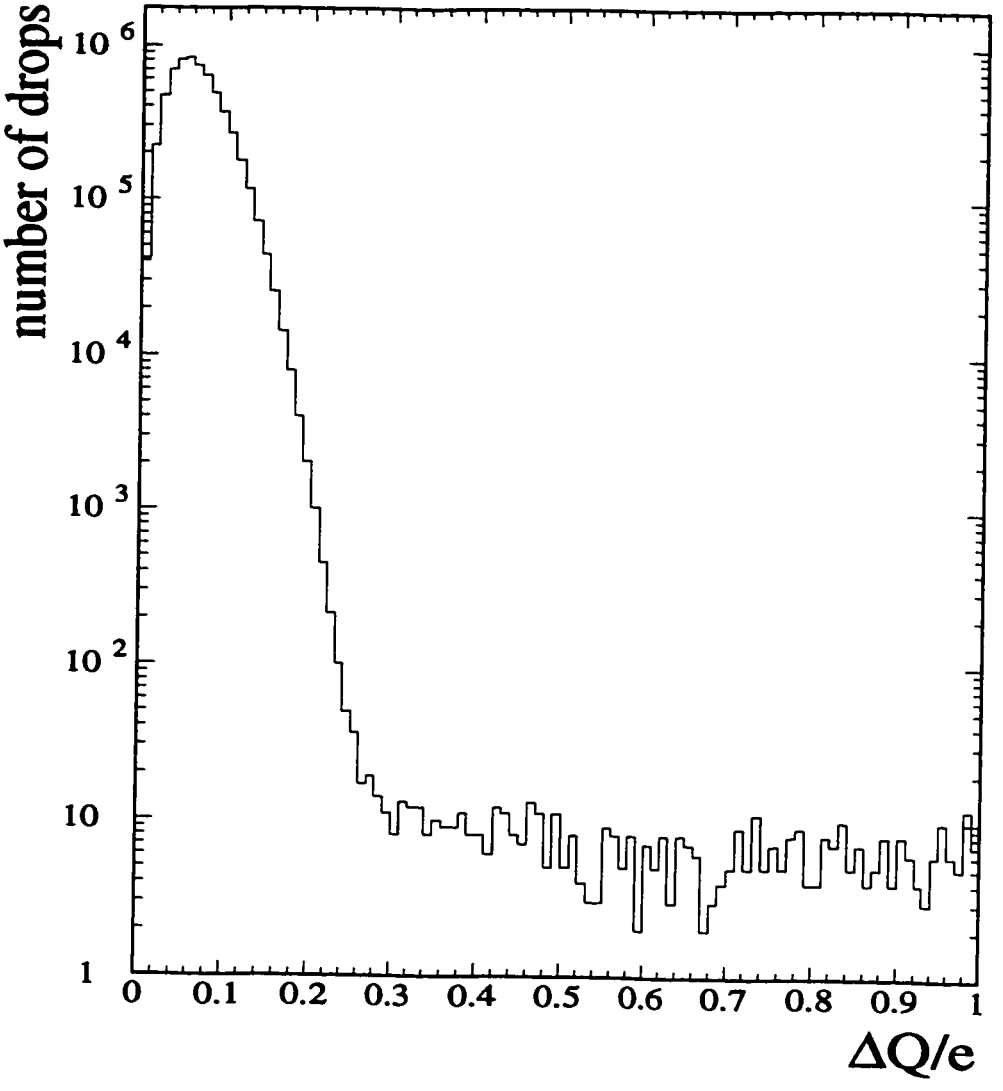

Figure 6.4: Histogram showing that about 97% of the data has $\Delta Q < 0.15\,e$. From the tail of the distribution we calculate that the upper limit to the number of drops that undergo a charge change during measurement is less than 0.02%.

7. Nonuniformity of the electric field.

8. Time variation of the temperature in the Millikan chamber.

6.3.1 Brownian Motion of the Drop in Air

The impact of air molecules colliding with the drop causes a fluctuation in the vertical velocity of the drop given by

$$v_{\text{Brownian}} = \sqrt{\frac{kT}{m}}, \tag{6.15}$$

where T is the air temperature and m is the mass of the drop. This leads to

$$\sigma_{q,\text{Brownian}} = 0.021, \tag{6.16}$$

the square of which is about 70% of the measured precision of σ_q^2. For a fixed drop mass m, $\sigma_{q,\text{Brownian}}$ is the lower limit on the attainable charge measurement precision. Appendix A gives a detailed derivation of this value.

6.3.2 Change in Drop Mass Due to Evaporation

Another factor that contributes to σ_q is the evaporation of the drop as it falls. The change in the mass of the drop has an effect on the charge measurement because a mass change causes a velocity change and, therefore, an apparent charge change (Eq. (3.8)). In the initial stages of the experiment, we actually started with water as our test fluid. However, evaporation of the water drops was not a problem we could overcome to our satisfaction. To test whether the Dow Corning fluids also demonstrated a high evaporation rate, we conducted bulk studies of the 5 cS silicone oil and empirically compared its evaporation rate with those of the 1 cS and 2 cS fluids. Although the bulk studies showed negligible evaporation of the 5 cS fluid, evaporation is, in fact, observable in our experiment because of the small drop size.

We measured the average value $(\partial v/\partial z)_{\text{evaporation}}$ by taking a run with the electric field off, that is, with zero electric field, and for each drop, considering the four or more sequential velocity measurements: v_a, v_b, v_c, v_d, ... Let z_a be the average position

during the determination of v_a and so forth. We then calculate $(\partial v/\partial z)_{\text{evaporation}}$ by averaging over the quantities $(v_b - v_a)/(z_b - z_a)$, $(v_d - v_c)/(z_d - z_c)$ ...and over all the drops. We find

$$(\partial v/\partial z)_{\text{evaporation}} = -3.03 \times 10^{-6}\,\text{mm/s}/\mu\text{m}. \tag{6.17}$$

Therefore, over one charge measurement cycle wherein the drop traverses approximately 287 μm, this velocity gradient leads to an error in the velocity measurement of 8.75×10^{-4} mm/s. This provides an upper limit to the average error in q of

$$\delta_{q,\text{evaporation}} = 2 \times 10^{-3}. \tag{6.18}$$

However, evaporation affects all drops similiarly and presumably this error does not fluctuate from measurement to measurement. The average effect is taken into account in the calibration (see Sec. 6.4). Any errors arising from evaporation is, therefore, negligible in comparison to $\sigma_q = 0.025$.

6.3.3 Force on Drop Due to Induced Dipole Moment

The vertical electric field of 1.4×10^6 V/m induces an electric dipole moment in the drop. If the electric field were spatially uniform, that is, E_z = constant, there would be no net force on the drop due to the induced dipole, but the holes in the centers of the electric-field plates break the uniformity. Along the vertical symmetry axis of the plates, the field is smaller near the holes and has a maximium halfway between the plates. Therefore, $\partial E_z/\partial z$ is not zero and the interaction of the induced dipole with $\partial E_z/\partial z$ produces a dipole force on the drop proportional to $\partial E_z/\partial z$. By Stokes' law, this dipole force changes the terminal velocity by an amount v_{dipole} that is proportional to the dipole force. We denote by $v_{g,E}$ the terminal velocity of the drop caused by the gravitational and electric force so that the total velocity of a drop is given by $v = v_{g,E} + v_{\text{dipole}}$. Both $v_{g,E}$ and v_{dipole} are given a positive sign when they are in the downward vertical direction. Near the top plate, $v_{\text{dipole}}(\text{top})$ is positive, that is,

downward and

$$v = v_{g,E} + v_{\text{dipole}}(\text{top}) > v_{g,E}. \tag{6.19}$$

As the drop continues to travel, v_{dipole} decreases in magnitude but remains directionally the same. At the center, the velocity of the drop is given by

$$v = v_{g,E} \tag{6.20}$$

since $v_{\text{dipole}}(\text{center}) = 0$. When the drop passes the center, v_{dipole} changes direction and is then upwards. Therefore, $v_{\text{dipole}}(\text{bottom}) < 0$ and

$$v = v_{g,E} + v_{\text{dipole}}(\text{bottom}) < v_{g,E}. \tag{6.21}$$

Thus, the field nonuniformity has the overall effect of monotonically reducing v as the drop falls, giving a non-zero $\partial v/\partial z$. However, we make our measurements in the central 1.6 mm between the electric-field plates where $\partial v/\partial z$ is negligible (see Sec. 6.3.7).

Using a method similar to the one described in the previous section for finding $(\partial v/\partial z)_{\text{evaporation}}$, we measured the average value $(\partial v/\partial z)_{\text{dipole}}$ by taking a typical run and selecting the charge zero drops. Again, for each drop, we considered the four or more sequential velocity measurements: v_a, v_b, v_c, v_d, ...and calculated $(\partial v/\partial z)_{\text{dipole}}$ by averaging over the quantities $(v_b - v_a)/(z_b - z_a)$, $(v_d - v_c)/(z_d - z_c)$ ...and over all the drops. Subtracting the effect due to evaporation, we find

$$(\partial v/\partial z)_{\text{dipole}} = -1.73 \times 10^{-6}\,\text{mm/s}/\mu\text{m}. \tag{6.22}$$

Again, over one charge measurement cycle, this leads to an average error in q of

$$\delta_{q,\text{dipole}} = 1 \times 10^{-3}. \tag{6.23}$$

Compared with $\sigma_q = 0.025$, $\delta_{q,\text{dipole}}$ is negligible.

6.3.4 Precision of Drop Position Measurement

There is a lower limit set on the precision with which the z-position of a drop can be measured, the limit arising from the non-zero size of the CCD pixel and defects in the drop position algorithm. We have not found a way to measure this precision. All we can do is find an upper limit on σ_z by assuming that the major components of σ_q are $\sigma_{q,\text{Brownian}}$ and σ_z. Then we find

$$\sigma_z \leq 0.35\,\mu\text{m} \tag{6.24}$$

in real space, which is 17% of a pixel.

6.3.5 Apparatus Vibration

When we began the experiment, we found that some part of the initial σ_q was caused by vibrations of parts of the apparatus. These vibrations, in turn, arise from the vibrations in the walls and floor of the building. Therefore, the apparatus was built on a wooden table that was stiffened with two I-beams. Weights were placed on the table to further dampen residual resonances. We also moved the entire assembly to that part of our laboratory room with the smallest wall and floor vibrations. The effect of residual vibrations on σ_q is included in σ_z.

6.3.6 Air Currents in the Millikan Chamber

We have eliminated observable air currents in the Millikan chamber by enclosing the chamber in double walls and by operating the experiment in a temperature controlled room. Unobservable air currents may contribute to σ_q since

$$v_{\text{measured}} = v_{g,E} + v_{z,\text{air}}, \tag{6.25}$$

where $v_{z,\text{air}}$ is the z-component of the air velocity. We have not found a method to measure $v_{z,\text{air}}$. We can, however, set an upper limit on the average horizontal component of the air velocity, $v_{x,\text{air}}$, by looking at the measurements of the horizontal

position of a drop as it falls. By taking the root mean square of the lateral velocities of each drop and then taking the root mean square of that value, we obtain

$$|v_{x,\text{air}}| \leq 0.013\,\text{mm/s}. \tag{6.26}$$

Of course, $v_{z,\text{air}}$ can easily be larger. Therefore, $v_{z,\text{air}}$ may contribute to σ_q.

6.3.7 Nonuniform Electric Field

Figure 6.5 shows a numerical calculation of $\partial_z E_z$ along the z-axis. The calculation used a computer relaxation method that generates the value of the electric field by calculating the charge distribution on the plates.

As mentioned earlier, E_z is smaller at the plates because of the holes in the plates. The variation in the center region is very small. We use the central 1.6 mm of the vertical distance for viewing the drops, thus taking measurements where E_z is most uniform. The calculation shows that

$$\frac{E_z(0) - E_z(z)}{E_z(0)} \sim \mathcal{O}(10^{-4}) \tag{6.27}$$

in the region of interest (Fig. 6.6). The charge measurement is affected by the same negligible factor.

The same calculation also provides an estimate of the dipole force which is given by

$$F_{\text{dipole}} = P_z \frac{\partial E_z}{\partial z}, \tag{6.28}$$

where P_z is the z-component of the induced dipole moment on the drop

$$P_z = 4\pi\epsilon_0 \frac{\epsilon - 1}{\epsilon + 2} r^3 E_z. \tag{6.29}$$

For silicone oil $\epsilon \sim 2.7$ [61], which implies $P_z = 1.46\,e\,\text{cm}$. The gradient $\partial_z E_z$ in the central region varies from about $-11\,\text{V/cm}^2$ to $11\,\text{V/cm}^2$ which leads to variations in the apparent charge of about $\pm 1.2 \times 10^{-3} e$. Since this is the maximum variation, this result is in good agreement with the experimentally observed fluctuation of $\pm 1 \times 10^{-3} e$.

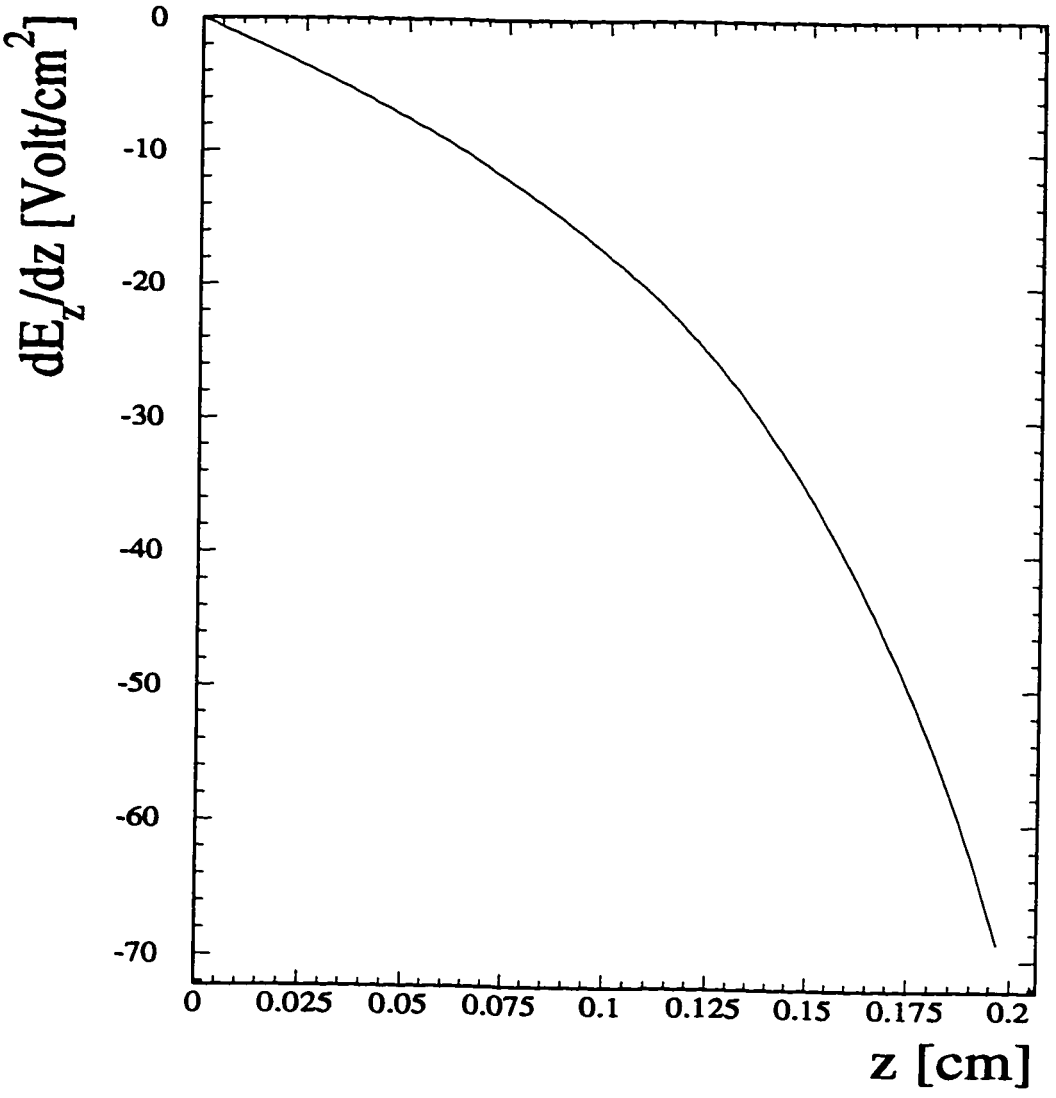

Figure 6.5: Numerical calculation of the gradient of the electric field. z is zero halfway between the plates.

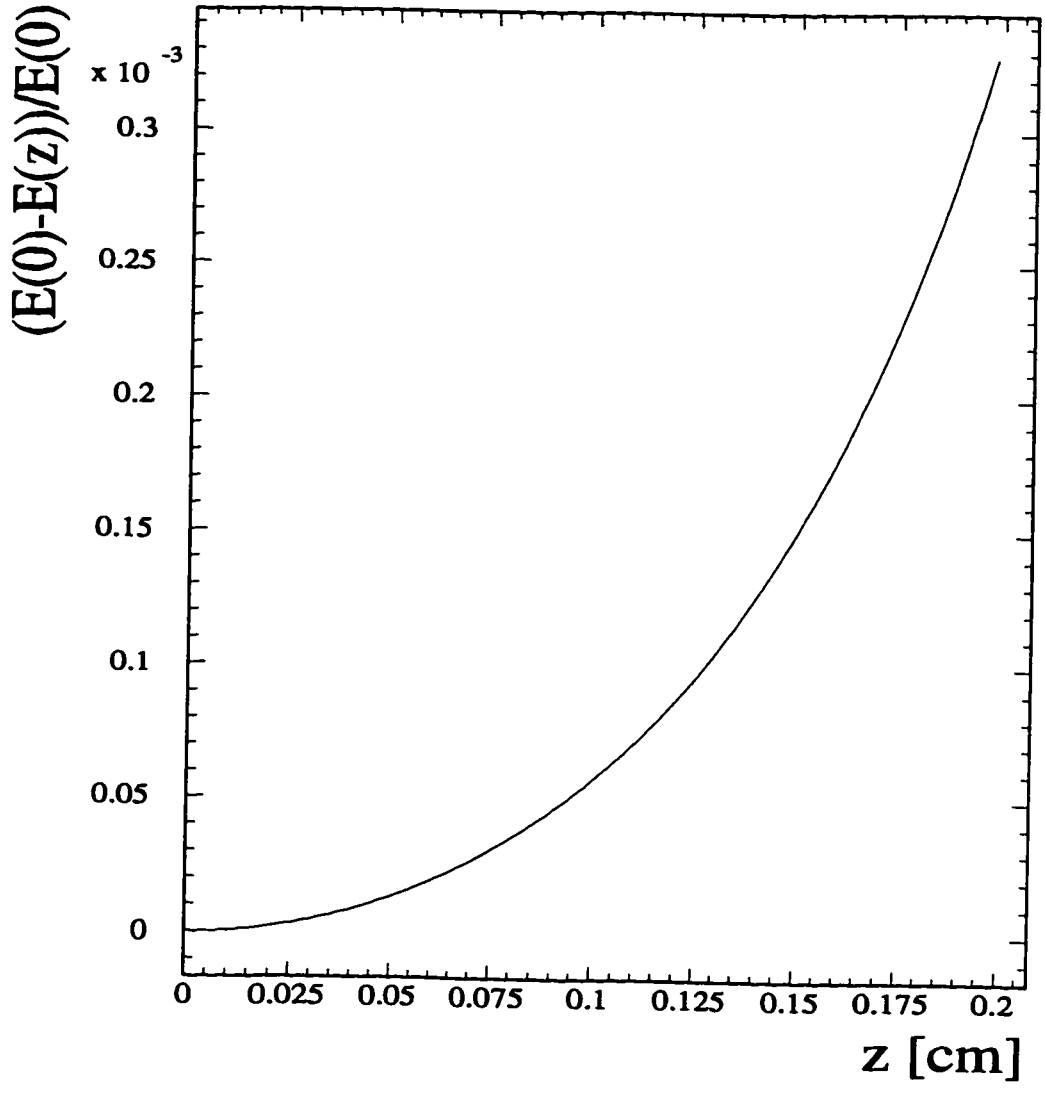

Figure 6.6: Numerical calculation of the electric field. Shown is the relative deviation of the z-component of the electric field from its value at the center between the plates.

6.3.8 Time Variation of Temperature in Millikan Chamber

As previously discussed, to minimize the effects of temperature on the data, the experiment is conducted in a temperature controlled room and thermometers in the measurement chamber enable us to enter temperature as a parameter in our data acquisition program. As yet, however, the instantaneous temperature is not directly supplied to the charge calculation code in the computer and must be entered manually. We have observed temperature fluctuations of up $\pm 2.5°C$ per day.

The temperature dependence of the charge equation (Eq. (3.8)), comes in two places, the viscosity and density of air. The correction arising from the latter is small compared with that from the viscosity of air. A $\pm 2.5°C$ change in temperature causes a variation in the viscosity of air of $\pm 0.65\%$. This in turn leads to a variation of the calculated drop charge of

$$|\delta_{q,\mathrm{temp}}| \leq 0.01. \tag{6.30}$$

This may be an important contribution to $\sigma_q = 0.025$. We regret that we did not directly supply the instantaneous temperature of the Millikan chamber to the charge calculation code. Our analysis is based on an average temperature of $22.0°C$.

6.4 Calibration

We conclude this chapter with a short discussion on the limitations of the absolute charge measurement. Since the goal of this experiment was to detect fractional charges, great care has been taken to eliminate fluctuations in individual charge measurements. However, there was no need to optimize the accuracy of the absolute measurement. Instead the integer spacing of the drop charges has been used to calibrate the measurement apparatus. Deviations from integer spacing have been absorbed into the empirically determined magnification factor of the optical system. This magnification had to be readjusted only when the oil was changed (because this necessitated removing the dropper from the system and then replacing it) and can absorb an overall adjustment of about three percent. As a consequence, it was not necessary to include corrections for the slight nonsphericity of the drops due to air

drag and interaction with the electric field, nor have we included the small-radius corrections to Stokes' law that Millikan applied. For the drop size considered here, these effects are very small and since they affect all drops equally, they are simply absorbed in the calibration.

Chapter 7

Conclusion

As shown in Fig. 6.3, once the measured charge is within $0.2\,e$ of integer charge and the measured charge approaches that integer, the sensitivity of the search rapidly decreases. Therefore, our main conclusions are for charges which are at least $0.2\,e$ distant from an integer charge, namely the regions

$$0.2\,e \text{ to } 0.8\,e, 1.2\,e \text{ to } 1.8\,e, 2.2\,e \text{ to } 2.8\,e\ldots,$$
$$-0.2\,e \text{ to } -0.8\,e, -1.2\,e \text{ to } -1.8\,e, -2.2\,e \text{ to } -2.8\,e\ldots.$$

In 1.07 mg of silicone oil we have not found any accepted drops with fractional charges in these regions. This 1.07 mg contains 6.41×10^{20} nucleons. Therefore, with 95% confidence the concentration of particles with charges in these charge regions in silicone oil is less than one per 2.14×10^{20} nucleons. This result, of course, applies to the specific case of searches for isolated quarks with the charge taken to be $\pm 1/3\,e$ or $\pm 2/3\,e$.

Table 7.1 lists the results of other published bulk matter searches for isolated quarks with charge $\pm 1/3\,e$ or $\pm 2/3\,e$. Ignoring the differences in the material examined, we see that our null result agrees with the null results found by all the experiments except LaRue *et al.* at Stanford. These null experiments range from being about 5 times more sensitive than our search to being about 1/20 as sensitive. Our experiment is the first one using an organic material, but we do not consider this

Group	Material	Mass (mg)	σ_q
LaRue *et al.* [13]–[17]	niobium	1.1	0.010-0.093
Marinelli *et al.* [76]	iron	3.7	0.013-0.129
Liebowitz *et al.* [54]	iron	0.72	~ 0.001
Smith *et al.* [53]	niobium	4.87	0.02–0.05
Jones *et al.* [55]	meteorite	2.8	0.03–0.07
Hodges *et al.* [1]	refined, native mercury	0.06, 0.115	0.035-0.040
Joyce *et al.* [2]	sea water	0.05	0.037
Lindgren *et al.* [3]	mercury	0.5	0.035
Savage *et al.* [4]	native mercury	2.0	0.040
This experiment	silicone oil	1.07	0.025

Table 7.1: Summary of results obtained in bulk matter searches.

important.

We have developed a reliable method of searching for fractional electric charge in bulk material. As discussed in the next chapter, we know how to greatly increase the rate at which we produce and examine drops. Therefore, we know how to examine samples up to 100 mg in mass, ultimately perhaps 1000 mg. Also, while oil is the most convenient material for our present experiments, we believe that our method can be extended not only to other liquids, but to suspensions of small particulates in liquids.

Our overall goal is to search for isolated fractionally charged particles in such materials as minerals from the surface of the Earth or the surface of the moon, meteorites and perhaps some metals. As has been discussed by Lackner and Zweig [49]–[51], there are substances that are much preferred as carriers of free quarks produced in the early evolution of the Universe. The strength of our method is that we can select these materials and study them in sample sizes ranging from a milligram to hundreds of milligrams. If there were free quarks or other fractionally charged particles in such samples, we would find them. If there were not, we can set, by far, the most

meaningful upper limits on the density of such objects in the Universe.

By pursuing the bulk matter search method, we avoid many of the uncertainties inherent in attempts to find fractionally charged particles using accelerators or cosmic rays. We do not have to concern ourselves with questions on how free quarks or fractionally charged objects are produced in collisions and in a broader sense, we do not have to concern ourselves with the mass of the free quark. We are then left with just two uncertainties: whether fractionally charged particles exist and whether they can travel through time and space to be within our grasp.

Chapter 8

Proposed Improvements and Future Extensions

The goal of our next experiment is to increase, by at least a factor of 100, the rate at which we produce drops and measure their charges. While the charge measurement precision and the reliability of the experiment are adequate, some improvements are required. The computer system, including the video digitization card, must be able to find drop positions, calculate drop velocities, calculate drop charge and mass and record at a rate of at least 100 Hz. The algorithms for finding drop positions and calculating drop velocities must be able to distinguish the trajectories of many drops whose images are in the same video frame. We have been developing programs to attain these goals and with a faster computer and video digitization card, it is straightforward to make this improvement.

Another required improvement is to generate drops at a much greater rate. For the next phase of the experiment we have already created a prototype system wherein we are capable of producing a two dimensional array of drops while pulsing the dropper at 100 to 150 Hz. The size of the drops produced is about 7 to 9 μm. We can control the size of the drops and the rate at which we can produce them consistently. This significantly increased rate will enable us to search through at least $\sim$ 1 mg of material a day. A magnetic levitometer experiment such as the one used by Smith [53]

would take over a month to search through 10 mg of material, whereas it would take our next generation system less than two weeks. Furthermore, in addition to being considerably faster than the levitometer technique, our improved Millikan method is considerably less expensive.

In closing, we note that in the previous paper delineating this experiment [9], we discussed the value of levitating a drop after charge measurement if it is a fractional charge candidate. Then the charge can be measured again. This was to be accomplished in [9] by always producing drops with large charges, $10\,e$ to $20\,e$. However, in this experiment, we have found that we get the best precision and more consistent overall operation if the drops have zero or close to zero charge. Therefore, we are developing a method for putting a large charge on a drop after its initial charge has been measured and the drop is considered a fractional candidate. However, this is under continuing investigation.

Appendix A

The Error due to Brownian Motion

The thermal velocity of the drop leads to a random walk with the thermal velocity and a stepsize that is roughly the stopping distance due to viscous drag. For times Δt much longer than the stopping time, the variation in position is given by [62, 63]

$$\Delta z^2 = \frac{2kT}{6\pi\eta r}\Delta t.$$

Thus, a velocity measurement, given by two position measurements Δt apart, has an uncertainty due to Brownian motion of

$$\Delta v = \sqrt{\frac{kT}{3\pi\eta r\Delta t}} = 8.1 \times 10^{-3}\,\mathrm{mm/s}\,.$$

This uncertainty in velocity arising from Brownian motion propagates as an uncertainty in the charge calculations according to the equation

$$\begin{aligned}\sigma_q \;=\; \sigma_v c_1 \Bigg[(c_2 v_{E_{\mathrm{down}}} + c_3 v_{E_{\mathrm{up}}}) \Bigg(2 + (c_2 - c_3) \left[\frac{v_{E_{\mathrm{down}}} - v_{E_{\mathrm{up}}}}{c_2 v_{E_{\mathrm{down}}} + c_3 v_{E_{\mathrm{up}}}} \right] + \\ (c_2^2 + c_3^2) \left[\frac{v_{E_{\mathrm{down}}} - v_{E_{\mathrm{up}}}}{2(c_2 v_{E_{\mathrm{down}}} + c_3 v_{E_{\mathrm{up}}})} \right]^2 \Bigg) \Bigg]^{\frac{1}{2}}, \end{aligned} \tag{A.1}$$

where we have defined $c_1 = \frac{9\pi d}{e}\left(\frac{1}{V_{\text{down}}+V_{\text{up}}}\right)F(T,P)$, $c_2 = \frac{V_{\text{up}}}{V_{\text{up}}+V_{\text{down}}}$, and $c_3 = \frac{V_{\text{down}}}{V_{\text{up}}+V_{\text{down}}}$ for convenience and clarity. Since $V_{\text{up}} = V_{\text{down}}$, our equation for the error in charge becomes, upon neglecting the much smaller quadratic term,

$$\sigma_q = \sigma_v c_1 \sqrt{2v_g}. \tag{A.2}$$

Because not all the charge measurements are independent, it was necessary to estimate the error arising from related charge measurements. The first charge measurement is obtained from two independent measurements of velocity v_a and v_b. The second measurement is taken from v_b and v_c and so on with the third and fourth charge measurements. We can calculate an average charge using

$$Q_{\text{ave}} = \frac{1}{4}\left(Q(v_a,v_b) + Q(v_c,v_b) + Q(v_c,v_d) + Q(v_e,v_d)\right).$$

We assume that each measurement of the velocities has the same error δ. This yields

$$\Delta Q_{\text{ave}} = \delta\sqrt{\left(\frac{\partial Q_{\text{ave}}}{\partial v_a}\right)^2 + \left(\frac{\partial Q_{\text{ave}}}{\partial v_b}\right)^2 + \left(\frac{\partial Q_{\text{ave}}}{\partial v_c}\right)^2 + \left(\frac{\partial Q_{\text{ave}}}{\partial v_d}\right)^2 + \left(\frac{\partial Q_{\text{ave}}}{\partial v_e}\right)^2}. \tag{A.3}$$

The partial derivatives can be expressed in terms of those of Q and we find

$$\begin{aligned}
\frac{\partial Q_{\text{ave}}}{\partial v_a} &= \frac{1}{4}\left(\frac{\partial Q(v_a,v_b)}{\partial v_a}\right),\\
\frac{\partial Q_{\text{ave}}}{\partial v_b} &= \frac{1}{4}\left(\frac{\partial Q(v_a,v_b)}{\partial v_b} + \frac{\partial Q(v_c,v_b)}{\partial v_b}\right),\\
\frac{\partial Q_{\text{ave}}}{\partial v_c} &= \frac{1}{4}\left(\frac{\partial Q(v_c,v_b)}{\partial v_c} + \frac{\partial Q(v_c,v_d)}{\partial v_c}\right),\\
\frac{\partial Q_{\text{ave}}}{\partial v_d} &= \frac{1}{4}\left(\frac{\partial Q(v_c,v_d)}{\partial v_d} + \frac{\partial Q(v_e,v_d)}{\partial v_d}\right),\\
\frac{\partial Q_{\text{ave}}}{\partial v_e} &= \frac{1}{4}\left(\frac{\partial Q(v_e,v_d)}{\partial v_e}\right).
\end{aligned}$$

If we make the additional simplifying assumption that the variations in the velocity measurements are sufficiently small (independent of the direction of the electric field),

we can evaluate the derivatives at the average values. We obtain

$$\Delta Q_{\text{ave}} = \frac{\delta}{4}\sqrt{(\partial_{v_a}Q)^2 + 4(\partial_{v_b}Q)^2 + 4(\partial_{v_c}Q)^2 + 4(\partial_{v_d}Q)^2 + (\partial_{v_e}Q)^2}. \tag{A.4}$$

We note at this point that $v_a \approx v_c \approx v_e = v_{E_{\text{down}}}$ and $v_b \approx v_d = v_{E_{\text{up}}}$. Therefore, substituting $v_{E_{\text{down}}}$ and $v_{E_{\text{up}}}$ for v_a, v_b, v_c, v_d and v_e where appropriate, Eq. (A.4) becomes

$$\begin{aligned}
\Delta Q_{\text{ave}} &= \frac{\delta}{4}\sqrt{6(\partial_{v_{E_{\text{down}}}}Q)^2 + 8(\partial_{v_{E_{\text{up}}}}Q)^2} \\
&= \frac{\delta}{4}\sqrt{7\left((\partial_{v_{E_{\text{down}}}}Q)^2 + (\partial_{v_{E_{\text{up}}}}Q)^2\right)} \times \\
&\quad \sqrt{1 - \frac{(\partial_{v_{E_{\text{down}}}}Q)^2 - (\partial_{v_{E_{\text{up}}}}Q)^2}{7((\partial_{v_{E_{\text{down}}}}Q)^2 + (\partial_{v_{E_{\text{up}}}}Q)^2)}}.
\end{aligned} \tag{A.5}$$

We assert, however, that the second term in the radicand is negligible since $(\partial_{v_{E_{\text{down}}}}Q)^2 - (\partial_{v_{E_{\text{up}}}}Q)^2 \ll (\partial_{v_{E_{\text{down}}}}Q)^2 + (\partial_{v_{E_{\text{up}}}}Q)^2$. This is due to the fact that $(\partial_{v_{E_{\text{down}}}}Q)^2 \propto v_{E_{\text{down}}}$, $(\partial_{v_{E_{\text{up}}}}Q)^2 \propto v_{E_{\text{up}}}$ and $v_{E_{\text{down}}} - v_{E_{\text{up}}} \ll v_{E_{\text{down}}} + v_{E_{\text{up}}}$. Equation (A.5) then becomes

$$\begin{aligned}
\Delta Q_{\text{ave}} &= \frac{\delta}{4}\sqrt{7\left((\partial_{v_{E_{\text{down}}}}Q)^2 + (\partial_{v_{E_{\text{up}}}}Q)^2\right)} \\
&= \frac{\sqrt{7}\delta}{4}\sqrt{\left((\partial_{v_{E_{\text{down}}}}Q)^2 + (\partial_{v_{E_{\text{up}}}}Q)^2\right)}.
\end{aligned} \tag{A.6}$$

Similar derivations for the cases where the number of charge measurements is three and five yield factors of $\sqrt{5}/3$ and $\sqrt{9}/5$ respectively. To determine the overall multiplicative factor in our error estimate we add these three factors together in quadrature with their appropriate weights. (Recall that 87.7% of the total number of drops have four charge measurements, 5.9% have three and 6.4% have five.) The σ_v used in Eq. (A.2) has this multiplicative factor taken into account. This gives us an error of 0.021 for a 7.1 μm drop from Brownian motion. Because our errors add in quadrature, Brownian motion accounts for about 70% of our σ_q^2.

Appendix B

The Effect of Q on Charge Measurement

Using the definitions for c_1, c_2, and c_3 described in the previous appendix, we note that Eq. (3.8) can be written as follows

$$Q = c_1\, e\, \left(v_{E_{\text{down}}} - v_{E_{\text{up}}}\right) \sqrt{c_2 v_{E_{\text{down}}} + c_3 v_{E_{\text{up}}}}. \tag{B.1}$$

Solving for the quantitiy $v_{E_{\text{down}}} - v_{E_{\text{up}}}$ and substituting this quantity into the error equation, Eq. (A.1) becomes

$$\sigma_q = \sigma_v c_1 \left[\left(c_2 v_{E_{\text{down}}} + c_3 v_{E_{\text{up}}}\right) \left(2 + (c_2 - c_3) \left[\frac{Q}{c_1\, e\, \left(c_2 v_{E_{\text{down}}} + c_3 v_{E_{\text{up}}}\right)^{\frac{3}{2}}} \right] + \right.\right.$$
$$\left.\left. (c_2^2 + c_3^2) \left[\frac{Q}{2c_1\, e\, \left(c_2 v_{E_{\text{down}}} + c_3 v_{E_{\text{up}}}\right)^{\frac{3}{2}}} \right]^2 \right) \right]^{\frac{1}{2}}. \tag{B.2}$$

Since $c_2 = c_3 = 1/2$ in this experiment, the above equation can be simplified

$$\sigma_q = \sigma_v c_1 \sqrt{v_g \left(2 + \left[\frac{Q}{8c_1 e v_g^{\frac{3}{2}}}\right]^2\right)} \tag{B.3}$$

$$= \sigma_v c_1 \sqrt{v_g \left(2 + \left[\frac{Q}{30.4\, e}\right]^2\right)} \tag{B.4}$$

Equation (B.4) clearly shows that higher charged drops lead to a greater σ_q.

Appendix C

Electronic Configuration of the Experiment

As discussed earlier, the piezoelectric transducer is pulsed using a high-voltage pulse amplifier with a driving voltage ranging from 130 to 160 V and a pulse width ranging from 0.85 to 1.2 μs[1]. The input to the high-voltage pulse amplifier is a signal from a pulse generator [64] that is asynchronous with the 60 Hz signal from the CCD camera (Fig. C.1). Although synchronizing the pulse generator with the camera using a frequency divider that receives its timing signals from the camera is a built-in option, it is not necessary to do so to acquire data. We exercised this option only in the early stages of the experiment when we wanted to conduct studies on the meniscus and the drop ejection process. The stroboscopic light source, however, is synchronized to the camera as shown in Fig. C.1. The synchronicity of the strobe and the CCD camera enables us to study the ejection process under controlled time intervals. Also shown in Fig. C.1 is the connection of the polarity switcher to the electric-field plates. The polarity switcher uses a vacuum tube switch that switches from negative to positive

[1]Drop ejection was not always achieved at these specifications with other ejection orifices or other identical droppers. These values are applicable to the 10 μm ejection orifice used in the oil dropper presently residing in the experimental chamber, but were not applicable to other ejection orifices epoxied to the same dropper.

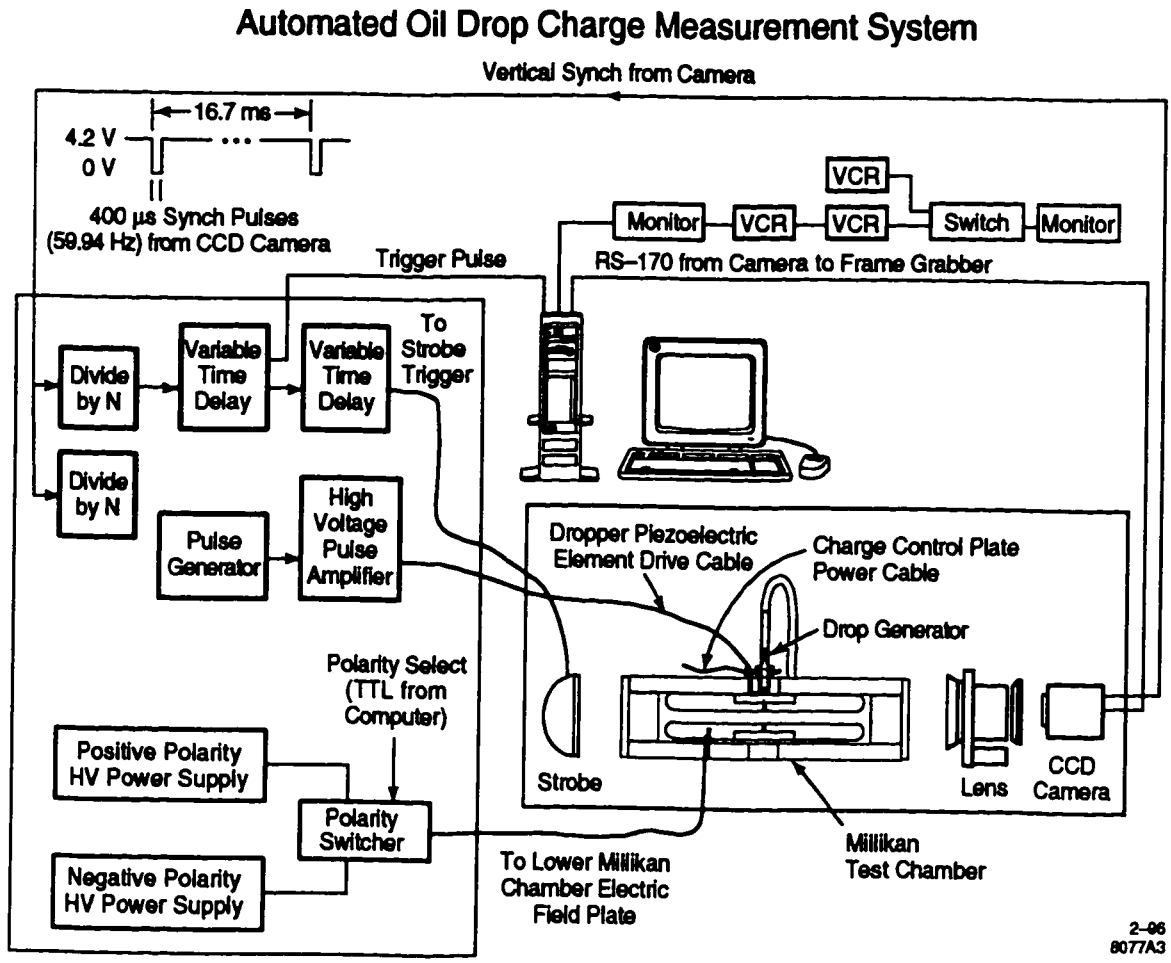

Figure C.1: A schematic of the electronics used in the experiment.

polarity and is computer controlled. The vacuum tube fails at voltages greater than $\pm 13\,\mathrm{kV}$, however, and so we were required to operate at that voltage.

Appendix D

The Water Phase of the Experiment

As mentioned in Chapter 3, we initially attempted this experiment using distilled water as the test fluid. But the inherent problems associated with this choice of fluids were never rectified to our satisfaction and the apparatus itself was complicated and difficult to maintain. In this appendix, we give a brief description of the original dropper and discuss the difficulties we encountered.

Figure D.1 shows the water dropper assembly. The dropper consisted of a cylindrical piezoelectric element (lead zirconate titanate) mounted between two circular, stainless steel endcaps 5.1 cm in diameter. The piezoelectric cylinder was 6.4 mm in length and had an outer diameter of 1.4 cm, an inner diameter of 0.7 cm and a thickness of 0.3 mm. A 2.5 cm diameter detachable orifice plate holder, also composed of stainless steel, was attached to the bottom endcap. A neoprene O-ring provided an air seal between the tapered nozzle located at the center of the lower endcap and the 9.5 mm orifice plate. The two endcaps were connected by four threaded rods. The upper endcap was mechanically attached to the circular top plate of the experimental chamber. The length of the dropper ensemble, from the top of the upper endcap to the bottom of the lower endcap, was approximately 10 cm.

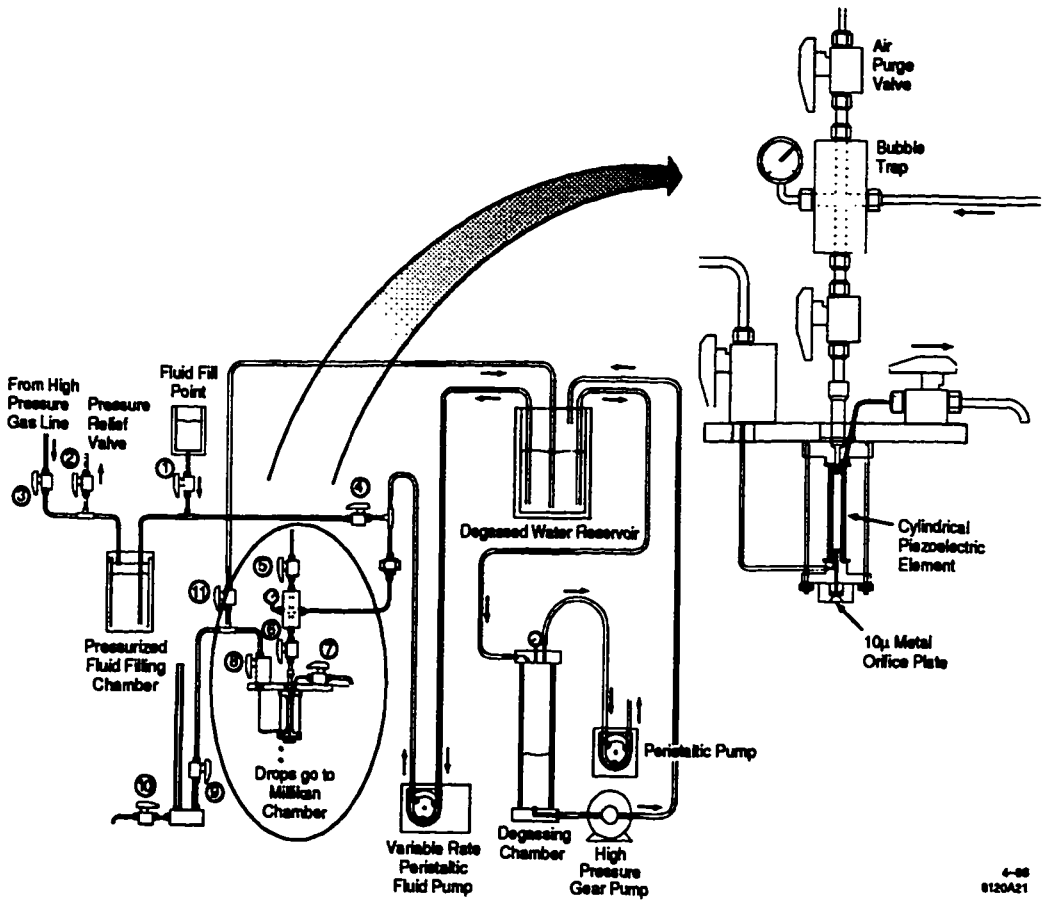

Figure D.1: The hydraulic system with a magnified image of the drop generator. The fill mode entailed first opening valves 1 and 2 with all other valves closed. Water was poured in at the reservoir at the top. Next, valves 1 and 2 were closed and 3, 4, 6, and 7 opened. Valve 5 was opened only if a bubble were observed in the transparent bubble trap. Opening valve 7 purged the top of the dropper. Closing 7 and opening 8 purged the bottom of the dropper. Valve 8 was left open and 9 opened to fill the manometer (10 was opened only when the manometer was too high). Valves 7 and 8 were alternately opened and closed to continue the purging process until we were satisfied that the system was completely purged. The drop production mode was in effect when all the valves were closed except for 8 and 9. To cycle the water through the vacuum degassing system, valves 4, 7 and 9 were closed and 6, 8, and 11 opened. Typically, we would operate in this mode for several hours to ensure that we had removed all the air bubbles from the water.

The dropper ensemble was then inserted into the experimental chamber by attaching the circular top plate to the rest of the chamber. This is the same chamber used by the oil phase of the experiment and is described in Chapter 3. Although the chamber shown in Fig. D.2 shows transparent acrylic walls, in the water phase of the experiment, it originally had aluminum walls, two of which had three rectangular holes (7.6 cm long and 5.1 cm wide) milled out for glass windows. One of these two windowed walls faced the lens and camera and the other was opposite. The centers of these windows were in the configuration of an isosceles triangle whose base was 12.7 cm and height was 3.8 cm. These windows were at least 45 cm above the bottom of the chamber. The existence of only three viewing ports, however, proved to be very disadvantageous in the early, troubleshooting phase of the experiment as we were unable to view most of the apparatus; it limited us to image only in the region of the windows. Therefore, all four walls were replaced by transparent acrylic ones and it was this modified chamber that was used in the oil phase of the experiment.

The convection shielding box containing the electric-field plates[1] (described in Chapter 3) was mounted on a nylon platform $23 \times 23\,\mathrm{cm}^2$ that was attached to an x-y stage. The x-y stage was in turn mounted on a height adjustable Delrin platform $22 \times 25\,\mathrm{cm}^2$ resting on a aluminum plate mounted 44 cm above the bottom of the large experimental chamber. The Delrin plate was varied in height by means of four base leveling screws. This setup enabled us to adjust the x-, y-, and z-positions of the electric-field plates so that we could align the holes in the plates to the drop stream.

Because of the small size of the water drops produced ($\sim 10-20\,\mu\mathrm{m}$) and because the fall path of the drops from the ejection orifice to the active region between the plates was approximately 5 cm, the drops would either evaporate before they reached the active region or visibly evaporate while we were taking measurements. Therefore, we placed a humidification assembly at the bottom of the experimental chamber. This consisted of a plastic container filled with water-soaked sponges. Small petri dishes

[1]The electric field plates were originally mounted on a nylon support frame that had about one centimeter long spacers situated in the region between the capacitor plates. This had two associated problems: 1) the nylon that protruded into the field region provided a tracking path along its surface for the high voltage and 2) the presence of the nylon distorted the electric field, leading to sharp field gradients that caused corona.

containing soaked sponges were also placed within the inner convection box that held the electric-field plates. The humidity within the large experimental chamber was measured by a hygrometer. Typically, we initiated drop production when the hygrometer measured over 90% humidity.

While the high humidity conditions were necessary to decrease the rate of evaporation of the drops, it had several drawbacks:

1. The transparent acrylic material of the chamber walls (both the outer and inner chambers) were highly hydrophilic and tended to deform over time. This affected how well we could image our drops since the geometrical path length varied. Furthermore, the nylon upon which the field plates were mounted was also hydrophilic, but to a lesser extent than the acrylic. This affected the plate separation.

2. Temperature changes overnight within the laboratory caused the entire chamber to fog up.

3. The moisture provided a tracking path for the high voltage and occasionally caused the electric field to arc.

4. The aluminum of the large experimental chamber corroded.

5. Opening up the experimental chamber for any reason, such as dropper maintenance or field plate positional adjustments, meant that we would have to rehumidify the chamber. Typically, this took over 6 hours.

This last problem was by far the most serious because in the early stages of this experiment, we were often making adjustments and modifications. The > 6 hours lag time necessary to rehumidify the chamber was, therefore, a constant time sink. We then devised a means of doing remote adjustments. We attached a wire loop on each of the micrometer knobs of the x-y stage on which sat the box containing the electric-field plates and placed ridged knobs on each of the four leveling screws in the Delrin platform. We then drilled stategically located $6.4 - 12.7$ mm holes in the acrylic wall opposite the wall facing the optics and the adjacent one that gave us

access to the x-knob. A hooked rod inserted through these holes enabled us to make positional adjustments with relative ease. When the adjustments were completed, the holes were plugged. To maintain the dropper, however, the top circular plate still had to be removed.

The hydraulic system necessary to operate this system is also shown in Fig. D.1. There were three modes of operation with this dropper system. They were the fluid fill mode, the drop production mode, and the degas mode. We had ascertained that air bubbles within the fluid of the dropper was giving us unreliable drop production and the degassing system became necessary. The caption of Fig. D.1 supplies detailed information on the operation of each mode.

In addition to the mechanical complexities of the system, there were problems arising from the water itself that made this phase of the experiment extremely difficult. Because the water was left in the system for weeks, it tended to stagnate. To prevent the growth of fungi and bacteria in this stagnant environment, we had to mix an antimicrobial agent [65, 66] to the water, $\sim 0.9\,\mathrm{ml}$ of antimicrobial agent per liter of distilled water. However, this had the effect of clogging up the $10\,\mu\mathrm{m}$ hole in the orifice plate because the antimicrobial agent had a very low vapor pressure compared with water. So while the water would evaporate from the orifice, the antimicrobial agent would not, thereby forming a clog that had to be flushed from the orifice.

Other contaminants within the water were removed by a filter [67] placed in series with the filling tubes (Fig. D.1). The pore size of the filters used ranged from $0.05\,\mu\mathrm{m}$ to $2\,\mu\mathrm{m}$. While the smaller pore size filters prevented more contaminants from clogging the ejection orifice, they also prevented the water from readily filling the dropper because the filtered contaminants clogged the pores. Therefore, we finally settled on the $2\,\mu\mathrm{m}$ filters. However, this filter had to be changed several times during each degassing cycle because of excessive clogging during this procedure.

Another problem we encountered with this system was high frequency vibration of the apparatus. Originally, the experiment was placed in the center of our second floor laboratory on two separate tables. The experimental chamber was centered on a wooden table and the optics were placed on another wooden table perpendicular to the chamber table. Seismic tests using a geophone showed that this was not a good

configuration because the seismic motion experienced by the optics were different from that experienced by the chamber. Although the CCD camera and the 135 mm lens were mounted on the same optical rail on one table, they, nevertheless, experienced different vibrational noise as they were located at opposite ends (Fig. D.2). Furthermore, the rail was mounted on two x-z stages that were in turn attached to pillars about 35 cm tall. This extra height was not conducive to a stable configuration for the optics.

Concurrent with the efforts to produce reliable water drops were studies into new and improved dropper designs. When we realized that we would have to dismantle the experiment in order to relocate it to a seismically quiet corner of the laboratory, we decided to take the experiment to the next phase with the new dropper described in the main body of the thesis. The new dropper was considerably less complicated and using oil enabled us to avoid the evaporation problem of water that was still not solved to our satisfaction. This also meant that all the hydraulics necessary for water was now obsolete and instead of humidifying the air, we dried it with dessicant.

The experiment was then relocated and reconfigured with the idea of minimizing vibrational noise. To that end, the experiment was rebuilt on one table, which was clamped down by aluminum I-beams, and the x-y stage upon which the small, inner box containing the electric-field plates rested was replaced by two solid aluminum bars. This inner box also sat much lower in the chamber, $\sim$ 18 cm above the bottom as opposed to the original $\sim$ 44 cm, because the new dropper was not attached to the top circular plate of the chamber and was, therefore, moved to a lower position within the large experimental chamber for greater stability. This allowed the optics to move down as well. The optical rail was then mounted on sturdier x-y-z stages. The strobe was also mounted on a more stable support structure.

With these modifications, the experiment moved easily into the oil phase, the results of which are in the thesis.

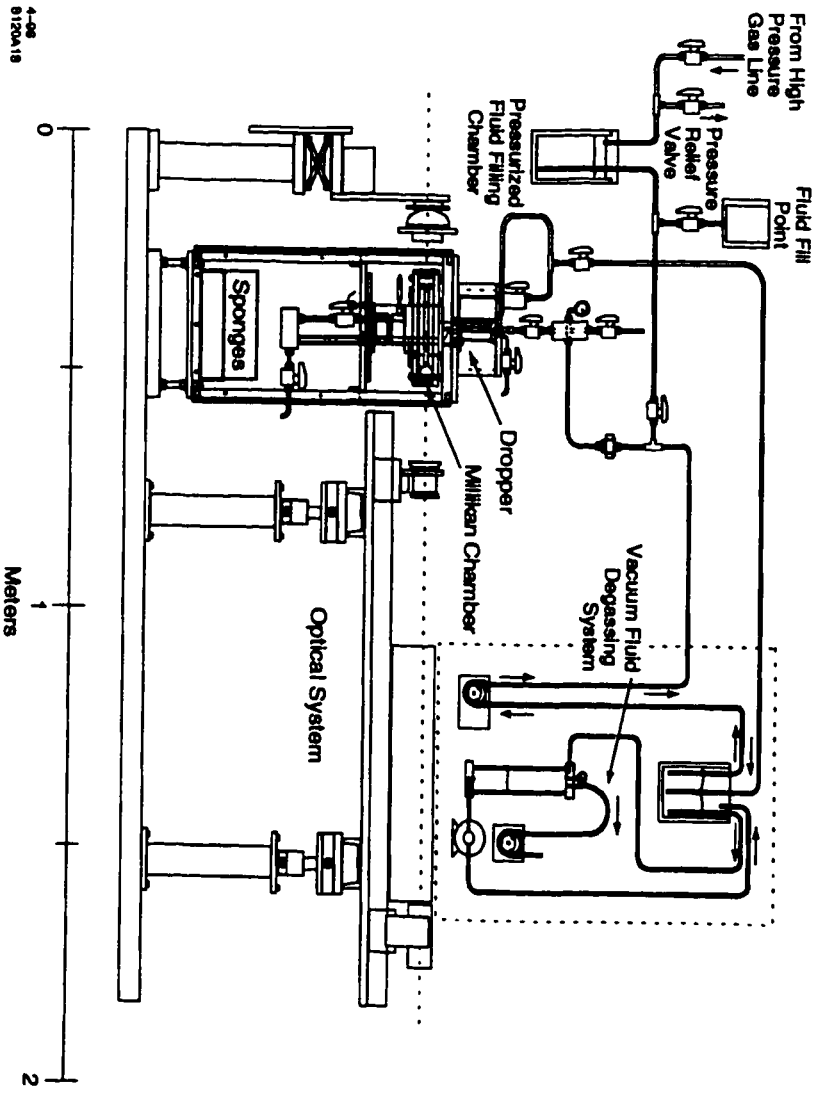

Figure D.2: General layout of the experiment showing chamber, optics and hydraulic system.

Appendix E

Changing Drop Charge with a UV Source

As discussed in [9], we had originally wanted to suspend any candidate drops by levitating them in an electric field so that we would be able to make further measurements. Charge changes would then be artificially induced on these events by an ultraviolet light source in order to obtain a consistency check on any anomalous charge measurements. Therefore, to test how easily we could suspend and induce a charge change, we developed a separate test chamber devoted to this endeavor.

The test chamber consisted of four transparent acrylic walls approximately $15 \times 20\,\mathrm{cm}^2$ (Fig. E.1). The top of the box was constructed from aluminum and had a removable lid so that we would have easy access to the dropper. The dropper used was the same type as the one used in the oil phase of the experiment. The dropper was put in a 2.5 cm diameter Delrin holder that fit snugly into a hole milled out of the center of an 2.5 cm thick aluminum slab $13 \times 18\,\mathrm{cm}^2$. Concentric with this 1.3 cm deep hole was a 1.6 mm through hole for the oil drops to emerge. The aluminum slab slid on two rails mounted onto the aluminum skeleton of the box and was used as the ground plate. The lower electric-field plate, $6.4 \times 6.4 \times 0.64\,\mathrm{cm}^3$, was approximately a centimeter away (the exact value of the plate separation was not important since these were feasibility tests) and was attached to the bottom of an inner convection

shielding box constructed from a 2.5 cm thick square piece of Delrin. The two side dimensions were 8.9 cm. A square cavity was bored out of the Delrin to a depth of 1.6 mm and had side dimensions of 8.3 cm. One window was milled out of each of the four walls of the Delrin box. Three of these windows, 2.5 cm long and 1.3 cm tall, were covered by glass and the fourth, 6.2 cm long and 1.3 cm tall, was covered by quartz. The quartz window was necessary because glass absorbs ultraviolet light while quartz has a $\sim$ 90% transmission in the ultraviolet region. The quartz window, therefore, faced the light source and was larger than the glass windows so as to admit a greater photon flux from the lamp. The Delrin box was pushed up against the ground plate by a pole to form a tight convection seal. The entire test chamber rested on a lab jack so its height could be varied in order to be collinear with the optics.

The ultraviolet source used emitted wavelengths of 366 nm and 254 nm [68]. A mechanical shutter was placed between the light source and the acrylic box to control the amount of ultraviolet exposure given to the drops. Showers of oil drops were ejected one at a time from the dropper in electronically controlled bursts. Occasionally a drop produced in the showers could be levitated by constantly adjusting the applied voltage in the lower electric-field plate. Once a drop was levitated, the shower bursts were stopped and the unlevitated drops were allowed to fall from the field of view. The mechanical shutter would then be raised, exposing the levitated drop to ultraviolet light. The shutter was lowered after observing a response; the drop would either move up or down depending on whether it became more positive or more negative. The drop was then relevitated with its new charge and the cycle begun again until the drop drifted out of the focal plane of the camera. At that point, we would try to levitate a new drop.

Tests with the longer wavelength did not show usable results: the levitated drops only responded to the 366 nm wavelength after a period of tens of seconds. This was too long. For our purposes, charge changes must occur in less than one second if a drop of about 7 μm were to be remeasured before it falls out of the field of view. Therefore, all the tests were conducted using the higher energy wavelength, which gave almost instantaneous results.

A suprising observation was that the levitated drops were always becoming more

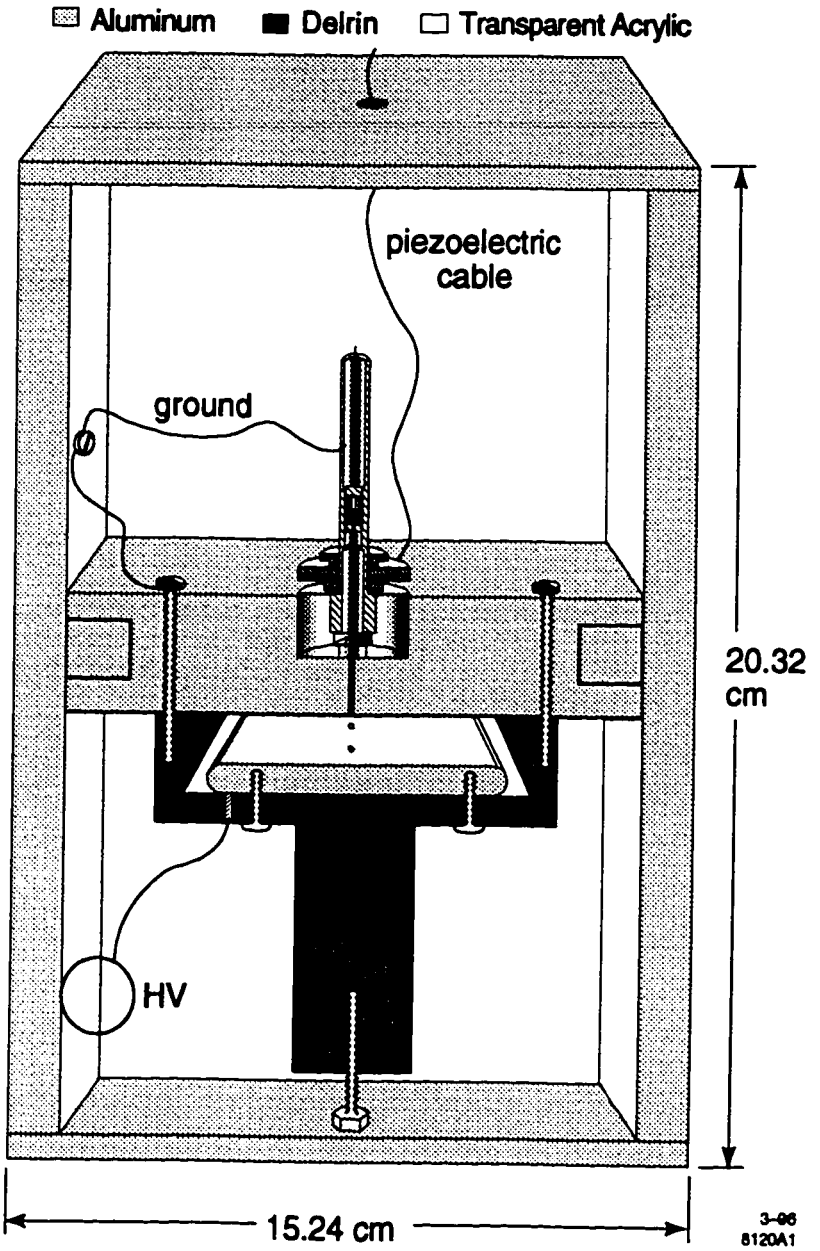

Figure E.1: Test chamber for studying artificially induced charge changes in levitated drops using an ultraviolet source.

negative. This was a clear indication that we were not photoionizing the drops as we had expected since that would mean the drops would become more positive. Our conclusion was that at 254 nm, we were operating at the work function of the aluminum oxide layer on the plates and electrons coming off the surface of the plates were attaching themselves to our drops. To prove this, we covered the lower electric-field plate with a sheet of quartz and aimed the ultraviolet lamp towards the bottom plate so that it would not photoionize the aluminum oxide layer on the top plate. With the quartz plate in place, the drops were unresponsive to the ultraviolet light.

We conducted further tests using a lower electric-field plate comprised of different metals. Using polished copper gave us positive results, but the charge change took place after about $1 - 2$ s of exposure. Oxidized copper took at least 5 s. Polished titanium produced very good results. Charge changes took place usually in < 1 s, but titanium oxidizes easily and oxidized titanium took about $4 - 9$ s to produce a charge change in the drops. Similarly, polished magnesium gave ideal results, but oxidized magnesium was unusable since metals that required constant polishing were impractical. Stainless steel plates produced null results.

Although the next phase of the experiment is oriented towards higher drop production rates, we have demonstrated that we can artificially induce charge changes in the drops using an ultraviolet source in our apparatus. As stated in the beginning of this appendix, this technique may be used in the future as a consistency check on anomalous charge measurements. This line of experimentation may be pursued again after we have achieved the higher rates.

Bibliography

[1] C. L. Hodges *et al.*, Phys. Rev. Lett. **47** 1651 (1981)

[2] D. C. Joyce *et al.*, Phys. Rev. Lett. **51** 731 (1983)

[3] M. A. Lindgren *et al.*, Phys. Rev. Lett. **51** 1621 (1983)

[4] M. L. Savage *et al.*, Phys. Lett. **167B** 481 (1986)

[5] R. A. Millikan, Phys. Rev. **32** 349 (1911)

[6] R. A. Millikan, Phil. Mag. **19** 209 (1910)

[7] R. A. Millikan *The Electron* (The University of Chicago Press, Chicago, IL, 1963)

[8] N. M. Mar *et al.* Accepted for publication by Phys. Rev. D for June 1996

[9] C. D. Hendricks *et al.* Meas. Sci. Technol. **5** 337 (1994)

[10] M. Gell-Mann, Phys.Lett. **8** 214 (1964)

[11] G. Zweig, CERN Report No. 8182 Th/401 (1964) unpublished

[12] D. Flamm and F. Schöberl *Introduction to the Quark Model of Elementary Particles* (Gordon and Breach Science Publishers, New York, NY, 1982)

[13] G. S. LaRue, W. M. Fairbank and A. F. Hebard, Phys. Rev. Lett. **38** 1011 (1977)

[14] G. S. LaRue, J. D. Phillips and W. M. Fairbank, Phys. Rev. Lett. **42** 142 (1979)

[15] G. S. LaRue, J. D. Phillips and W. M. Fairbank, Phys. Rev. Lett. **46** 967 (1981)

[16] G. S. LaRue "Measurement of the Residual Charge on Superconducting Niobium Spheres", Ph.D. dissertation (Stanford University, 1978)

[17] J. D. Phillips "Residual Charge on Niobium Spheres", Ph.D. dissertation (Stanford University, 1983)

[18] C. B. A. McCusker Aust. J. Phys. **36** 717 (1983)

[19] F. Halzen and A. D. Martin *Quarks and Leptons: An Introductory Course in Modern Particle Physics* (John Wiley & Sons, New York, 1984)

[20] R. Slansky *et al.* Phys. Rev. Lett. **47** 887 (1981)

[21] E. W. Kolb *et al.* Phys. Rev. Lett. **47** 1357 (1981)

[22] A. De Rújula *et al.* Phys. Rev. D **17** 285 (1978)

[23] Private communications with Professor Martin Perl.

[24] W. Bartel *et al.* Phys. Lett **88B** 171 (1979)

[25] W. Bartel *et al.* Z. Phys. C **6** 295 (1980)

[26] L. Lyons Phys. Rep. **129** 225 (1985)

[27] J. Weiss *et al.* Phys. Lett. **101B** 439 (1981)

[28] A. Marini *et al.* Phys. Rev. Lett. **48** 1649 (1982)

[29] M. C. Ross *et al.* Phys. Lett. **118B** 199 (1982)

[30] W. Guryn *et al.* Phys. Lett. **139B** 313 (1984)

[31] H. Aihara *et al.* Phys. Rev. Lett. **52** 2332 (1984)

[32] H. Aihara *et al.* Phys. Rev. Lett. **52** 168 (1984)

[33] D. Buskulic *et al.* Phys. Lett. B **303** 198 (1993)

[34] R. G. Roberts *The Structure of the Proton* (Cambridge University Press, Cambridge, 1990)

[35] J. J. Aubert *et al.* Phys. Lett. **133B** 461 (1983)

[36] F. Bergsma *et al.* Z. Phys. C **24** 217 (1984)

[37] A. N. Diddens *et al.* Nucl. Instr. Meth. **178** 27 (1980)

[38] M. Banner *et al.* Phys. Lett. **121B** 187 (1983)

[39] G. L. Shaw *et al.* Phys. Rev. Lett. **50** 1967 (1983)

[40] G. L. Shaw *et al.* Phys. Rev. D **36** 3533 (1987)

[41] D. Calloway *et al.* Phys. Lett. **232** 549 (1989)

[42] G. Gerbier *et al.* Phys. Rev. Lett. **59** 2535 (1987)

[43] A. Hoffman *et al.* Phys. Lett. **200B** 583 (1988)

[44] H. S. Matis *et al.* Phys. Rev. D **39** 1851 (1989)

[45] H. S. Matis *et al.* Nucl. Phys. **A525** 513c (1991)

[46] L. Jones Rev. Mod. Phys. **49** 717 (1977)

[47] M. Mori *et al.* Phys. Rev. D **43** 2843 (1991)

[48] M. Aglietta *et al.* Astropart. Phys. **2** 29 (1994)

[49] K. S. Lackner and G. Zweig, Lettere Al Nuovo Cimento **33** 65 (1982)

[50] K. S. Lackner and G. Zweig, Proc. AIP **93** (1982)

[51] K. S. Lackner and G. Zweig, Phys. Rev. D **28**, 1671 (1983)

[52] M. Marinelli and G. Morpurgo, Phys. Rep. **85** 161-258 (1982)

[53] P. F. Smith *et al.*, Phys. Lett. **153B** 188 (1985)

[54] D. Liebowitz, M. Binder and K. O. H. Ziock, Phys. Rev. Lett. **50** 1640 (1983)

[55] W. G. Jones *et al.*, Z. Phys. C, **43** 349 (1989)

[56] R. G. Milner *et al.* Phys. Rev. Lett. **54** 1472 (1985)

[57] Instrument Research Company Model 1k-30. Colombia, MD 21045 USA

[58] J. Heinzl and C. H. Hertz, *Advances in Electronics and Electron Physics* **65** (Academic Press, Inc., 1985)

[59] General Radio Stroboslave Type 1539-A. Quad Tech Inc. Marlboro, MA 01752 USA

[60] Cohu Model 6310. Cohu Inc. Danville, CA 94526 USA

[61] *CRC Handbook of Chemistry and Physics*, edited by R. C. Weast, M. J. Astle and W. H. Beyer (CRC Press, Inc., Boca Raton, FL 1986)

[62] A. Einstein *Investigations on the Theory of the Brownian Movement* edited by R. Fürth (Dover, New York, 1956)

[63] N. G. van Kampen *Stochastic Processes in Physics and Chemistry* (North-Holland, Amsterdam, 1981)

[64] WaveTek 859. WaveTek Corp. San Diego, CA 92123 USA

[65] Dowicil 75 or Dowicil 200 Preservative. Dow Chemical, Midland, MI 48674 USA

[66] Giv Gard DXN. Givaudan-Roure Corp. Clifton, NJ 07015 USA

[67] Millipore OM 043. Millipore Corp. Bedford, MA 01730 USA

[68] Model UVGL-58. UVP Inc. San Gabriel, CA 91778 USA

[69] D. H. Perkins *Introduction to High Energy Physics* (Addison-Wesley Publishing Company, Menlo Park, CA 1987)

[70] K. Kleinknecht *Detectors for Particle Radiation* (Cambridge University Press, Cambridge, 1990)

[71] F. E. Close *An Introduction to Quarks and Partons* (Academic Press, London 1979)

[72] T. Bowcock *et al.* Phys. Rev. D **40** 263 (1989)

[73] B. L. Ioffe, V. A. Khoze and L. N. Lipatov *Hard Processes* (North-Holland, Amsterdam 1984)

[74] C. B. A. McCusker *The Quest for Quarks* (Cambridge University Press, Cambridge, 1983)

[75] P. F. Smith *Ann. Rev. Nucl. Part. Sci.* **39** 73-111 (1989)

[76] M. Marinelli and G. Morpugo, Phys. Lett. **137B** 439 (1984)

[77] P. M. Morse *Thermal Physics* (W. A. Benjamin, Inc., New York, 1964)

[78] F. Wilczek and A. Zee Phys. Rev. D **16** 860 (1977)

[79] A. Zee Phys. Lett. **84B** 91 (1979)

[80] H. Harari Phys. Lett. **86B** 83 (1979)

[81] M. A. Shupe Phys. Lett. **86B** 87 (1979)

[82] H. Goldberg *et al.* Phys. Rev. Lett. **47** 1429 (1981)

[83] M. I. Strikman Phys. Lett. **105B** 230 (1981)

[84] L. F. Li and F. Wilczek Phys. Lett. **107B** 64 (1981)

[85] V. Gupta and P. Kabir Phys. Rev. D **25** 867 (1982)

[86] K. S. Lackner and G. Zweig Proc. Fifth Int. Conf. on Part. Phys. (May 1982)